# High Field Electrical Conduction And Breakdown In Insulating Polymers

by

**Dong Liu**

A Thesis Presented to

The University of Manitoba

in Partial Fulfillment of the Requirements for the Degree of

**Doctor of Philosophy**

in Electrical and Computer Engineering

Winnipeg, Manitoba, Canada 1992

ISBN 0-315-77759-1

# HIGH-FIELD ELECTRICAL CONDUCTION AND BREAKDOWN IN INSULATING POLYMERS

BY

DONG LIU

A Thesis submitted to the Faculty of Graduate Studies of the University of Manitoba in partial fulfillment of the requirements for the degree of

DOCTOR OF PHILOSOPHY

I hereby declare that I am the sole author of this thesis.

I authorize the University of Manitoba to lend this thesis to other institutions or individuals for the purpose of scholarly research.

**Dong Liu**

I further authorize the University of Manitoba to reproduce this thesis by photocopying or by other means, in total or in part, at the request of other institutions or individuals for the purpose of scholarly research.

**Dong Liu**

The University of Manitoba requires the signatures of all persons using or photocopying this thesis. Please sign below, and give address and date.

# Abstract

The current-voltage ($I$-$V$) characteristics of polyethylene films fabricated by plasma polymerization have been measured at very high electric fields using linear ramp voltages. Experimental results show that at average fields higher than 1 MV/cm, electrical conduction is mainly due to the Fowler-Nordheim type tunneling injection of holes from the anode and the high hole mobility. There is no evidence of impact ionization at fields close to the breakdown strength. High field conduction is filamentary and governed by the trapped hole space charge. Internal discharges such as electrical treeing and breakdown are initiated by thermal instability within high-current density regions of main conduction filaments (or channels), and then followed by the creation of low-density domains to provide large mean free paths for subsequent impact ionization which leads to an indefinite increase in carrier multiplication and final destruction of the material inside the filaments.

The same techniques have also been employed for the study of the effect of silicon incorporation in polyethylene. The results show that the incorporation of silicon in polyethylene creates hole traps, thus suppressing the conduction current and enhancing the breakdown strength. The amount of positive space charge resulting from the hole trapping increases with increasing magnitude and duration of the applied field for a fixed silicon content, and

increases with increasing silicon content for a fixed magnitude and duration of the applied field. This positive space charge tends to suppress the actual field at the hole-injecting contact and to enhance the actual field at the electron-injecting contact. For fields higher than a certain critical value, the rate of the current increase with field changes rapidly. This phenomenon is attributed to the onset of double injection. If a proper amount of silicon is incorporated in polyethylene, the overall effect would be to reduce the conduction and to increase its breakdown strength.

We have also studied the chemically polymerized polypropylene. The results show that the high field conduction in the polypropylene is also due to the hole tunneling injection. A thin SiPE, PE, or $SiO_2$ layer deposited on the injecting contact as an emission shield suppresses hole injection, and in turn, increases the breakdown strength of the polypropylene. These important new findings should lead to a better understanding of insulating polymers and a potential application in polymeric insulated systems.

The structure of plasma-polymerized polyethylene films with and without silicon incorporation has been studied on the basis of infrared spectroscopy. The structure of the films without silicon incorporation is similar to that of polyethylene but with CH and $CH_3$ elements. The incorporation of silicon introduces SiH, $SiH_2$ and $SiH_3$ elements into the structure.

# Acknowledgments

The author would like to thank his advisor, Prof. K.C. Kao, for his excellent guidance, endurable motivation, consistent and generous support throughout this research work.

The author would also like to thank Prof. H.C. Card, Prof. R.D. McLeod, Prof. R.S. Azad and Prof. D.J. Thomson for their constant help and cordial advice. Special thanks are given to Dr.V. Herak, Dr. G.C. McGonigal, S.R. Mejia, T.T. Chau, L. Kan and M. Jin for their endless patience in helping him with many practical difficulties encountered during this work.

The financial support from the Natural Sciences and Engineering Research Council of Canada (NSERC) and the Manitoba Hydro are gratefully acknowledged.

Finally the author is much obliged to his wife, Shauna Hui Wang, for her understanding and encouragement.

# Contents

# List of Figures

# List of Tables

# Chapter 1

# Introduction

## 1.1 The Background

Polymer films fabricated by plasma polymerization (or glow discharge polymerization) have been studied extensively in the past three decades. This technique was first used by Goodman[1] to produce insulating films. In the mid-1960's, a number of papers were published dealing either with the plasma polymerization process itself or with electrical properties of the films fabricated by this process. In the early days the plasma-polymerized materials were widely investigated in the hope that these materials may have potential applications in the areas used as microcapacitors, insulating or corrosion-protective coatings, etc.[2-12]. The thermal, electrical, and optical properties of plasma-polymerized polymers have been reviewed by several investigators [13-15]. However, most of the previous work is related to the dielectric behavior at low fields, and little has been devoted to high field electrical conduction and breakdown.

Recently, research on thin films fabricated by plasma polymerization is

concentrated in two directions; one is to study the material properties with the aim of using them for electronic applications, and another is to use the material in thin film form for studies of high field phenomena because for thin films high fields can be easily attained at relatively low applied voltages thus avoiding surface leakage and discharge problems associated with high voltages. The advantages of plasma polymerization over the conventional chemical polymerization are: (1) films produced by plasma polymerization can be made very pure because this process does not involve any catalysts or additives; (2) films can be made very thin, uniform and to contain low concentration of pin holes; and (3) foreign elements can be easily incorporated into polymers by means of plasma polymerization in a gas mixture containing molecules which form the monomers of the polymers and foreign elements; the incorporation of impurities into polymers enables the development of new polymers with some special properties for some particular applications. Furthermore, the chemical structure of formed polymers depends also on the properties of fragments of the forming materials, which are closely related to the fabrication parameters such as input-power, gas pressure, gas composition, and substrate temperature [16, 17]. Thus, the properties of a particular polymer can be tailored either by adjusting the fabrication parameters or by doping with suitable impurities.

The research and development in the field of the polymers have been rapidly growing, particularly after the discovery of polyethylene methacrylate in 1930 by Hill and Crawfood, and polyethylene in 1932 by Gibson and Swallow. Now polymeric insulating materials have been widely used as electrical insulators from microelectronic devices to power apparatus and cables. Polyethylene is the most used one among others because of its excellent dielec-

tric properties, easy processing as well as low cost. However, after many years in service, utilities have experienced a large number of failures in polyethylene insulated system and it is expected that these failures will continue to occur, and to even increase as the rated voltage of the insulating system is increased. The present trend towards the increase in the rated voltage and the reliability of polymeric insulated systems demands the improvement of the polymer material itself as well as the structure design. This serious problem has stimulated many researchers to study the mechanisms responsible for partial discharge (electrical treeing) and final breakdown. A great deal of work has been done on prebreakdown and breakdown phenomena in polyethylene and other insulating polymers.

Several theories have been put forward for high field conduction and breakdown in such insulating materials. The theories based on the classical concept of ionic conduction, electronic impact ionization and thermal breakdown have been reviewed by O'Dwyer[18], Klein[19] and Ieda[20], Recently, some new models have also been put forward. In Chapter 2, a brief review of these experimental and theoretical work will be given. However, considerable experimental evidence has confirmed that carrier injection from the electrical contacts and subsequent formation of homo-space charge near the contacts are the prelude for the partial discharge (electrical treeing), the ageing and the final breakdown. It should be noted that irregularities on the insulating polymer surfaces may make the effective field vary from domain to domain at the metallic contact-polymer interfaces. It is possible that the field at a particular asperity point is more than ten times the average field across the insulation. It is this extremely high field at one or more sharp asperity points

that initiate carrier injection and filamentary conduction, leading to the subsequent ageing and breakdown. In fact, the use of the conventional needle-plate (or point-plane) electrode configuration to study partial discharge or electrical treeing is mainly to simulate the surface irregularities at the interface between the metallic contact and the polymer.

## 1.2 Motivations and Objectives

Up to the present little has been reported about the dominant carrier species responsible for electrical conduction at very high fields and final breakdown in insulating polymers. An experimental method to determine the dominant carrier species at very high fields can be considered as the first step to study the high-field dielectric phenomena in polymers. This is in fact one of the objectives of this thesis project to carry out a series of experiments in order to determine the type of carrier species at very high fields. To do this, it is convenient to use polyethylene samples in thin film form so that very high fields can be easily attained at relatively low voltages. The plasma polymerization technique has been used to produce the polyethylene thin films for this investigation, because these films could be made very unform in thickness with a low concentration of pin holes as aforementioned. We also adopted the techniques already used for studies of thin silicon dioxide films to study the insulating properties of polymers in metal-insulator-semiconductor (MIS) structures, in our case, metal-polymer-semiconductor (MPS) structures. These techniques enable us to obtain the high fields at relatively low applied voltages and allow us to study the space charge accumulated in the material. To the best of our knowledge, our experiment results will be the first set of results obtained for

organic polymers using these techniques.

The foreign elements in polymers will introduce some changes in the chemical structure and the trapping parameters of the host materials. The effects of foreign elements incorporated in polymers have been studied in the past two decades. Many elements and monomers have been incorporated into polymers by various methods [21-26] in attempt to alter the the electrical properties of polymers and to create new functional materials.

Recently, much attention has been paid to the effects of foreign elements and monomers on high field dielectric behaviors in insulating polymers with the aim of improving their performance at high fields. The polyethylene incorporated with aromatic monomers such as styrene, allyl benzene, and 4-phenyl-l-butene, has a breakdown strength higher than the pure polyethylene. This may be due to the presence of benzene rings that decelerate electrons through the trapping or the scattering process, thus resulting in a reduction in conduction current and an increase in breakdown strength[27]. Our research group was the first to incorporate the silicon element into polyethylene by plasma implantation[28]. The incorporation of silicon introduces a large change in properties of polyethylene, but at that time, the electric field used was low because the films used were relatively thick (about 30$\mu$m). Therefore, another objective of this research is to study the effects of silicon incorporated in polyethylene on the high-field conduction and breakdown.

Many investigators have reported that the emission shields can be used to reduce the surface irregularities, to reduce injection, and to produce a space charge layer, which may indirectly result in some improvement of the dielectric properties of polymers insulting configurations. Bahder et al. have reported

that an insertion of an emission shield between the semiconductor coating and the polyethylene increases the ac breakdown strength by 30% [29]. An emission shield has also been used by Tu et. al. to increase the breakdown strength of polyethylene[30]. A plasma-polymerized film has been used by Nakano to reduce the leakage current through the polyethylene films[31]. Therefore, one of the objectives of this investigation is to study the effects of such a layer on the high field conduction and breakdowns.

## 1.3 Organization of The Thesis

In the preceding introduction we have described some background knowledges, the motivations and the objectives of this investigation.

Chapter 2 gives a brief review on electrical conduction and breakdown in insulating polymers with the emphasis on polyethylene.

Chapter 3 describes the RF plasma system, the sample fabrication, and the chemical structures of the plasma-polymerized polyethylene thin films with and without silicon incorporation.

Chapter 4 describes the high field electrical conduction and breakdown in plasma-polymerized polyethylene films.

Chapter 5 describes the high field electrical conduction and breakdown in silicon-incorporated polyethylene.

Chapter 6 describes the high field conduction in polypropylene and emission shield effects.

Chapter 7 summarizes significant findings which lead to the conclusions.

# Chapter 2

## Brief Review on Electrical Conduction and Breakdown in Insulating Polymers

A great deal of experimental work has been reported on electrical conduction and breakdown in insulating materials, especially, in insulating polymers. To elucidate these phenomena, a number of theories and models have been put forward. In this chapter we shall briefly review both the experimental and the theoretical work in this area, as well as the current approaches to the improvement of insulating materials.

A wide range of the insulating polymers have become available in today's electrical and electronic industry. Among the common ones are polyethylene (PE), polypropylene (PP), polystyrene (PS), polyethylene terphthalate (PET), polycarbonate (PC), and polytertrafluorethylene (PTFE or Teflon). They all can characteristically withstand an electric field in excess of several MV/cm, and also their electrical conductivities are very low at fields below a certain critical value. In general, the field dependence of the conductivity of

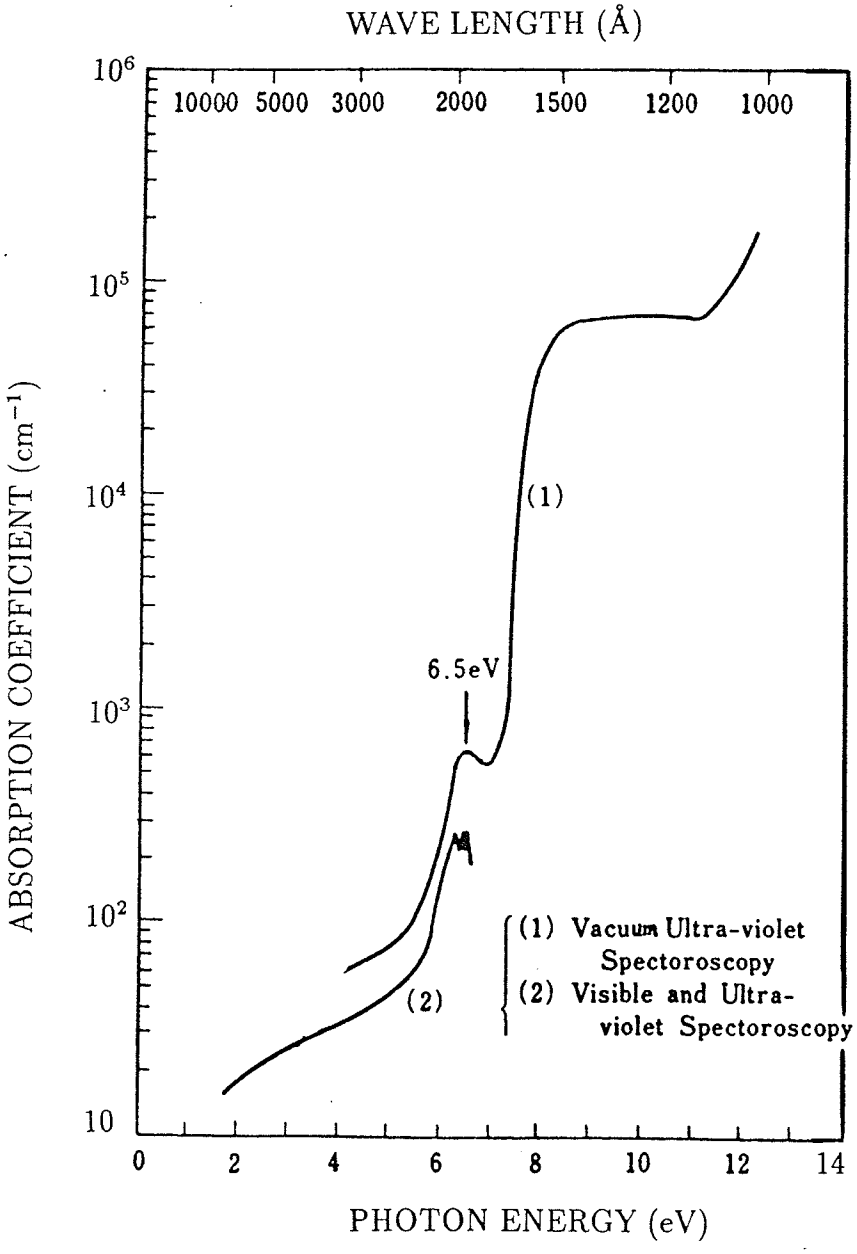


Figure 2.1: *Absorption coefficient of polyethylene as a function of photon energy. (After Tanaka,[33]).*

these polymers can be divided into three regions: low, medium, and high field regions. The current obeys Ohm's law in the low field region, but increases exponentially or superlinearly with the field in the medium field region, and very rapidly in the high field region prior to breakdown. It is likely that in these polymers the conduction process in each region is different and that the degradation and breakdown processes are often complex and unpredictable. In this review, the emphasis will be on polyethylene as it is the most widely used insulating polymer.

Polyethylene consists of macro-molecules with a main chain linked through $\sigma$ bonds. The molecules are weakly bonded by Van der Walls' forces to form a semicrystalline solid which is a mixture of crystalline and amorphous parts. The fluctuation of potentials and interatomic distances, and the absence of long-range order are some of the typical features of this material. Electronic states and electrical conduction in polymers have been analyzed on the basis of the theory of amorphous materials[32], and the assumption that the chain branching, impurities, dislocations, or broken bonds will generate localized states within the band gap, which will, in turn, act as trapping centers. Neutral acceptor or ionized donor (positive) states tend to trap electrons and neutral donor or ionized acceptor (negative) states tend to trap holes. These states can also act as recombination centers. Unlike the semiconductors with elemental impurities, the energy levels of such acceptor and donor states generally are not confined, respectively, to the neighborhoods of the valence band edge ($E_v$) and the conduction band edge ($E_c$). They may occur any where in the band gap.

Figure 2.1 shows the dependence of the optical absorption coefficients

on photon energy for polyethylene. There are two absorption peaks, the large peak at about 7eV and the small peak at 6.5eV [33]. A similar spectrum has also been reported by Partridge [34]. The large peak appears to be the fundamental absorption, implying that the optical band gap for polyethylene is around 7.4eV. This value is closed to that theoretically estimated by McCubbin and Gurney[35]. The tail of the fundamental absorption as clearly shown in Fig.2.1 indicates the formation of a band tail as predicted by theory of amorphous materials. Optical analysis has revealed that chemical double bonds such as C=C bands of vinylidene vinyl, and transvinylene might contribute to the shallow acceptor-like traps close to the conduction band edge; and Carbonyl radicals, p-terphenyl derivatives and hydroxyl derivatives of phenanthrene might contribute to the deep donor-like traps[33]. It has also been reported that the concentration of acceptor-like electron traps is higher than that of donor-like hole traps in polyethylene.

Thermally-stimulated current (TSC) technique has been much-used to determine the energy spectrum of trapping states in solids. However, the trapping levels in PE determined by the TSC technique varies from research group to group, possibly due to the difference in the morphology of the PE samples and in the experimental conditions used for the TSC measurements among different groups. Nevertheless, the results derived from the TSC measurements still provide some useful information about traps in polymers. Typical TSC spectra, with and without x-ray irradiation reported by Mizutani et al. [36, 37] are shown in Fig.2.2. With the x-ray irradiation, there are five TSC peaks which can be considered to be due to the release of trapped carriers introduced by x-ray irradiation. The peaks $P_1$ ($E_t$=0.1$\sim$0.3 eV), $P_2$ ($E_t$=0.2$\sim$0.3

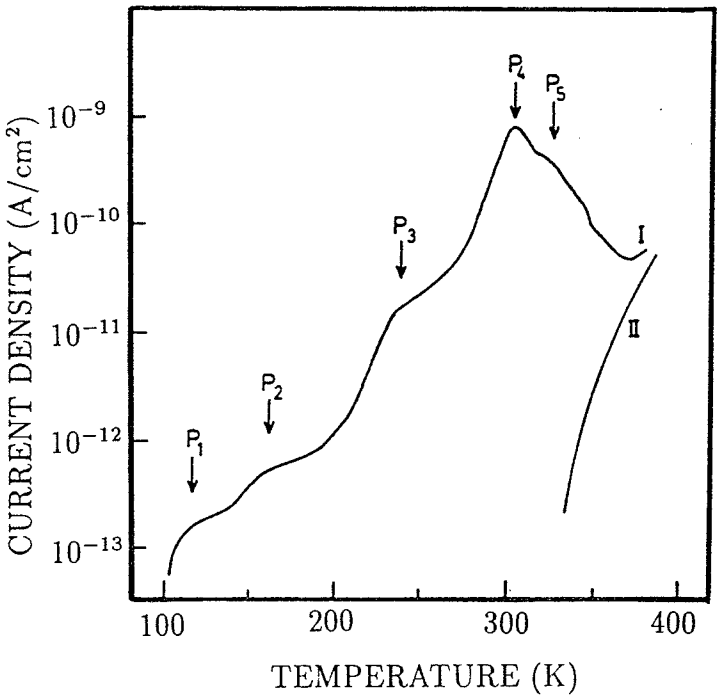


Figure 2.2: *TSC spectra for low density polyethylene under a bias voltage of 270 V. Curve I: TSC spectrum with x-ray irradiation; Curve II: TSC spectrum without x-ray irradiation. (After Mizutani, Suzuok, and Ieda,[36]).*

eV) and $P_3$ ($E_t$=0.8$\sim$1.0 eV) may be due to traps associated with molecular motions [36, 37]. The largest peak $P_4$ ($E_t$=0.9$\sim$1.4 eV) may be associated with traps in the boundary region between the crystalline and amorphous regions, and the peak $P_5$ ($E_t$=1.7eV) may be associated with traps in the crystalline region. Similar TSC spectra have also been reported by Lewis et al. [38],using the electron beam radiation to produce carrier in polyethylene. Obviously, these traps in the polyethylene play a decisive role in the conduction and the breakdown processes.

## 2.1 Electrical Conduction

### 2.1.1 Transient Current

The electrical conduction current, immediately after the application of a step-function dc voltage, decays with time, the rate of the decay depends on the magnitude of the applied field. In general, the decay follows approximately a power law time dependence, that is $\mathbf{i} \propto \mathbf{t}^{-n}$ with the index $\mathbf{n}$ in the order of unity as shown in Fig.2.3. This current transient phenomena can be ascribed to one or more of the following three basic processes: (1) dipolar relaxation, (2) electrode polarization, and (3) charge injection leading to formation of trapped space charge. A great deal of experimental work has revealed that the process (3) is the major cause for the current decay for both polar and non-polar insulating materials [39-41]. When a charge-injecting electrode is in contact with an insulator, charges will be injected from the electrode into the material, and be trapped near there to form a homo-space charge. An internal field built up due to this homo-space charge will be in the direction opposite to the applied field toward the injecting electrode, thus suppressing further injection, and this

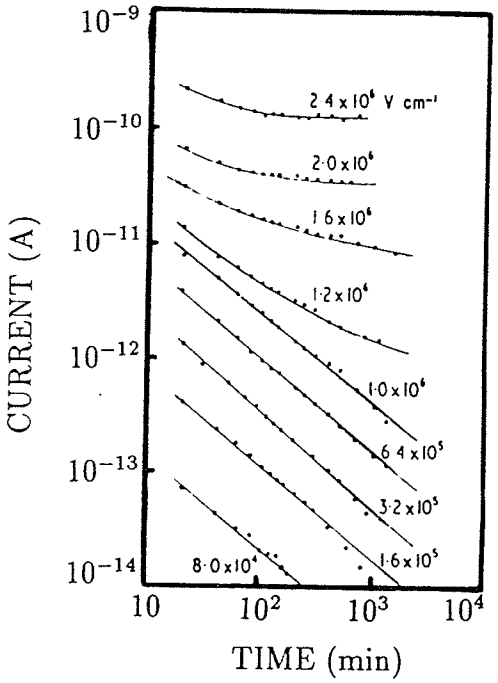


Figure 2.3: *Decay of current with time in polyethylene after the application of various fields at room temperature. (After Lewis, [38]).*

causes the current decay. With the metal-insulator(inorganic)-semiconductor (MIS) structure, Walden [42] have reported that the flat band voltage ($V_{fb}$) has a logarithmic dependence on the time interval during the application of the electric field, i.e., $V_{fb} \propto \ln(1+t/t_0)$, where $t_0$ is the characteristic time. The changes in the flat band voltage is directly related to the space charge accumulation and distribution inside the insulator. Based on the analysis of the charge distribution profile, he have concluded that the transient current is proportional to $(t^{-n})$. A similar finding for polyethylene has also been reported by Wintle et al [39]. Based on the decay of the pulsed photocurrent superimposed onto the dark current decay as shown in Fig.2.4, Tahira and kao[43] have concluded that the decay of the dark charging current is associated mainly with a time-dependent trap-filling process due to the elec-

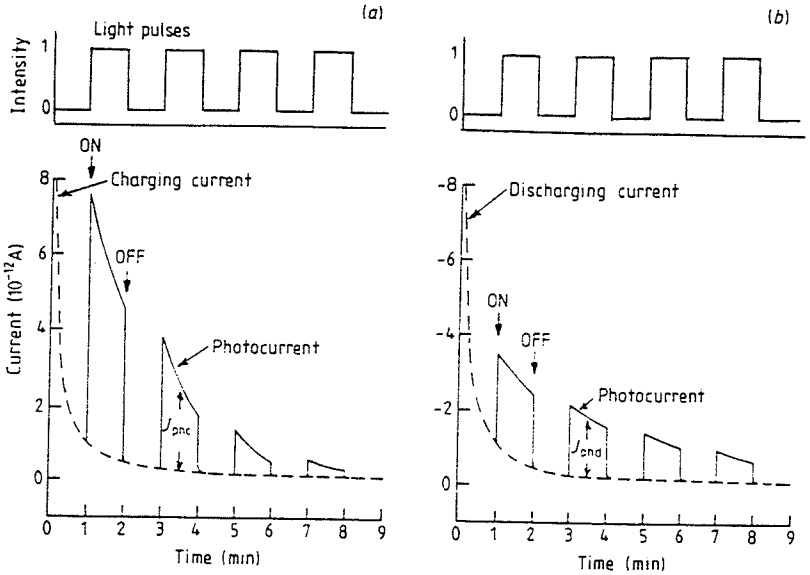


Illuminated electrode positively biased at 120V

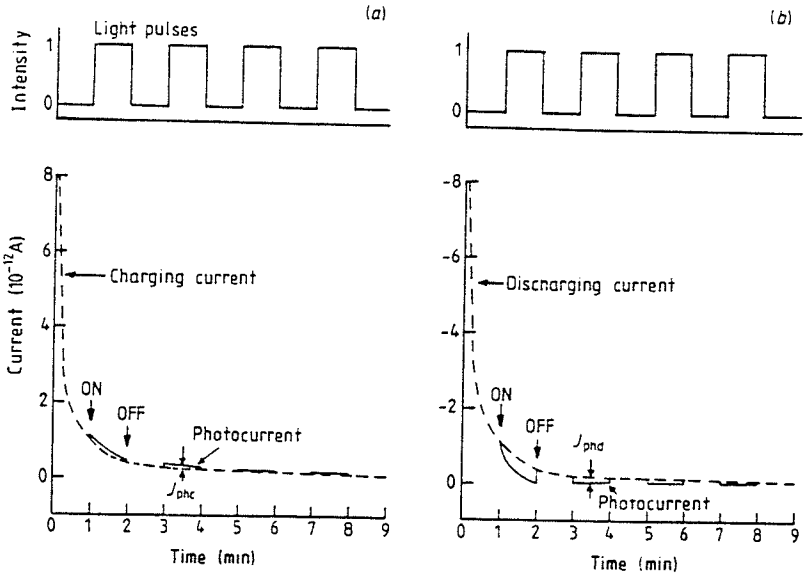


Illuminated electrode negatively biased at 120V

Figure 2.4: *(a) The photocurrent superimposed on to the charging current, and (b) the photocurrent superimposed on to the discharging current in polyethylene under exciting radiation by a series of rectangular UV light pulses for the illuminated electrode negatively biased and positively biased at 120V, respectively. (after Tahira and Kao, [43]).*

trons injection from the metal-polymer contact, while the decay of the dark discharging current is associated mainly with the time dependent detrapping process. The rate of the current decay, in general, increases with increasing applied field and with increasing temperature, indicating also that the current decay is mainly associated with the trapping and detrapping of injected carriers [44, 45].

Dipolar relaxation involves the reorientation of dipoles distributed throughout the material. This process can be accounted for $t^{-n}$ dependence of transient current if a sufficiently wide distribution of the relaxation time exists in the material[46]. However, the orientation of dipoles does not involve space charge and therefore the field inside the sample should be quite uniform between two parallel electrodes. This is definitely not the mechanism for polyethylene because it can not explain the pulsed photocurrent decay phenomenon observed by Tahira and Kao[43].

The electrode polarization process involves space charge separation. Under a electric field the positively charged species tend to move toward the cathode and the negatively charged species toward the anode, with the tendency of enhancing the field at the electrode surface and reducing the field in the bulk. This may explain the current decay at low fields within a short period of time. As time goes on, the hetero-space charge may enhance the field at the electrode.

### 2.1.2 Charge Injection

The charge injection or transfer at the electrical contacts is one of the important processes associated with the electrical conduction in polymers.

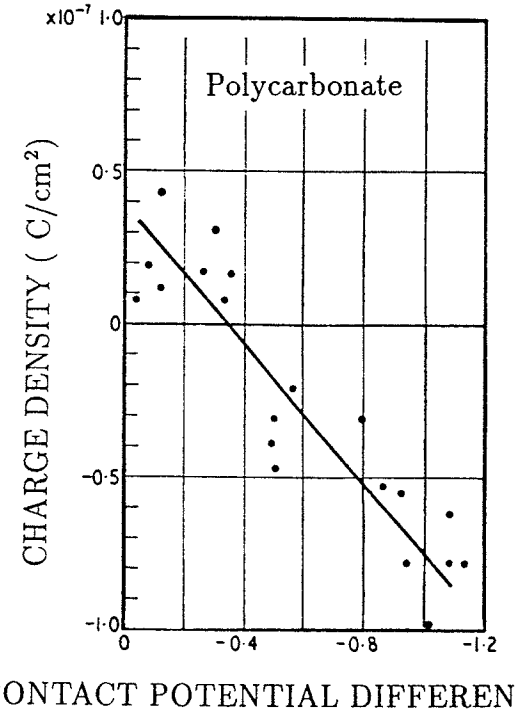


Figure 2.5: *Charge density as a function of metal contact potential difference for polycarbonate in absence of electric field. (After Davies, [51]).*

Studies of surface-charge transfer phenomena in polymers suggest that charge carriers can be easily injected from the electrodes into the bulk materials with or without applying electric fields [47-53]. Figure 2.5 shows that the amount of charges injected to the polymers at zero field depend on the work function of the contacting metals. The injected charge density increases with increasing field and also increases with increasing time interval of the applied field [49]. Electrons may be injected spontaneously into polyethylene from the metallic contact even at zero field. With a negative potential applied on the metal (cathode), the injection can be increased markedly, but with a positive potential (anode), a large potential is required for the natural negative charge to be annulled and the positive charge to appear at the interface[54, 55]. The surface condition of the material will affect the injection charge and, hence the

conduction current.

Using a non-uniform field electrode configuration such as point-plane configuration, the amount of injected positively charged carriers (with the point electrode at positive polarity) in polyethylene is higher than that of injected negatively charged carriers (with the point electrode at negative polarity), and negatively charged carriers are more readily to be trapped than positively charged ones [56]. Using a uniform field electrode configuration such as sphere-plane configuration (the so called uniform field means the field prior to the formation of space charge), the negative space charge begins to build-up near the cathode at an average field of about 0.2 MV/cm and its density increases with increasing applied field upto about 1 MV/cm, but beyond this field its density tends to decrease with the applied field; while the positive space charge begins to build-up at an average field higher than 0.8 MV/cm [31]. In polyethylene insulated cables, the amount of injected carriers is higher when the core is at the positive polarity than when it is at the negative polarity [57]. These findings imply that the threshold field for electron injection is much lower than that for hole injection. As the hole mobility is much larger than the electron mobility, for applied fields higher than the threshold field for hole injection, the conduction becomes controlled by holes rather than by electrons.

The charge injection phenomena have been interpreted in terms of charge injection through surface states or charge injection according to either Schottky or Fowler-Nordheim process. The polymers are characterized not only by an electron affinity $\chi$ and energy gap $E_g$, but also by a high density of surface states extending some distance into the polymer as shown in

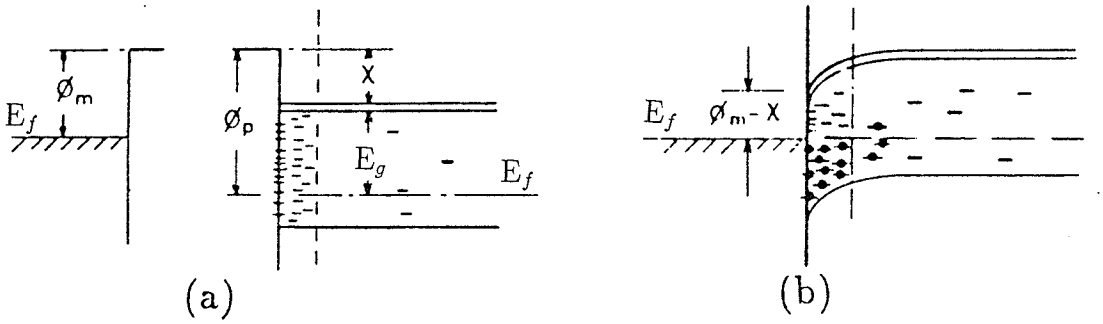


Figure 2.6: *Surface states in the interface region between the metal and the polymer (a) before contact, and (b) after contact.*

Fig.2.6. At points between the metal and the molecular dielectric solid, there are localized surface states formed within the tunneling range, which may act either as the the acceptor or as donor states, depending on their locations in the energy gap. The injection process is not instantaneous. The height of the barrier $\phi_m - \chi$, differences in work function $\phi_m - \phi_p$, and the concentration of trapping states at the surface and in the bulk determine the time required for the injection to reach a equilibrium condition. In general, the time is short if the equilibrium condition requires only the charge to inject into the surface states, otherwise, it could be a slow process [58]. The polarity of the charge injected into the surface states at zero field depends on the conditions of the surface states. For polyethylene in contact with a metal, the charge is negative, indicating that the surface states of polyethylene are acceptor-like. For polyethylene in contact with polypropylene, polyethylene is negatively charged, indicating that there is a large concentration of acceptor-like surface states as compared with polypropylene[52]. Such a charge injection across the

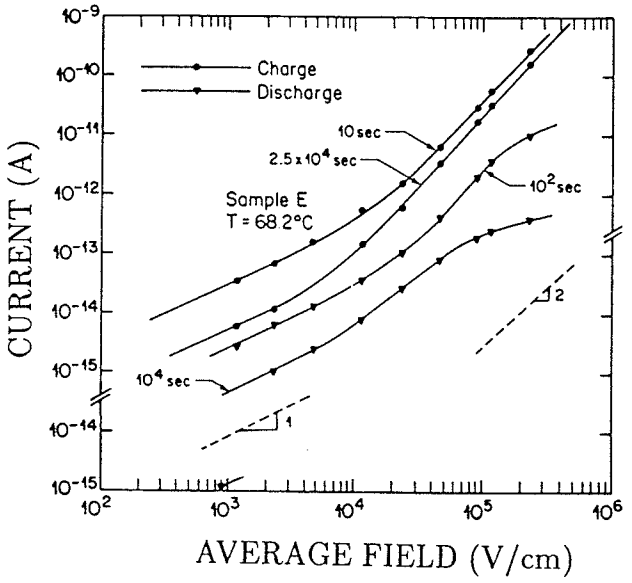


Figure 2.7: *Isochronal current-field characteristics of polyethylene. (After St-Onge, [60]).*

electrode/dielectric interfaces is enhanced by the applied electric field. The applied field tends also to cause the charge to move from the sites of injection into the bulk of the polymer. This charge will be trapped and form a homo-space charge which tends to reduce the further movement of the charges from the surface states into the bulk.

### 2.1.3 Electrical Conduction under Low and Medium Fields

Electrical conduction in polyethylene under low and medium fields is a bulk limited process. Figure 2.7 shows the typical isochronal current-field characteristics. For average fields less than $10^4$V/cm, the conduction follows Ohm's law. At low fields, the density of the conduction current is in order of $10^{-11}\sim10^{-8}$ A/cm$^2$, indicating a very low electron mobility for polyethylene, which is about $10^{-11}\sim10^{-8}$ cm$^2$/V s derived from the conduction currents[60].

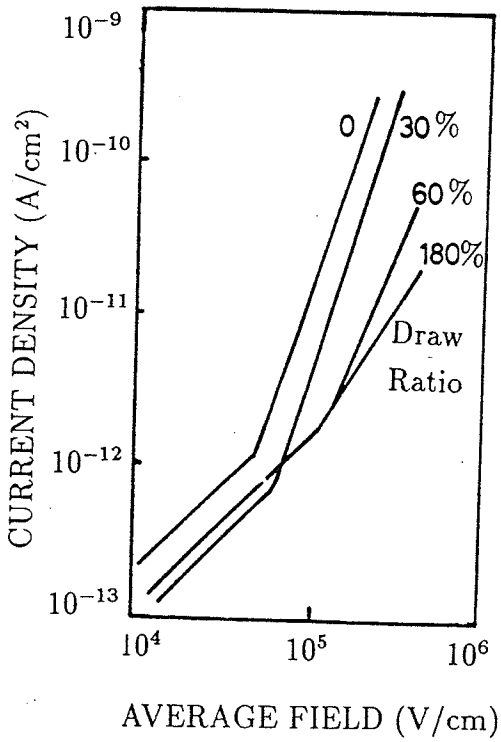


Figure 2.8: *Current density-field characteristics of stretched polyethylene at various draw ratios. (After Yahagi, [61]).*

Mechanical defects affect the conductivity of polyethylene. Figure 2.8 shows the conduction current as a function of applied electric field with various degrees of mechanical stretching ratio of the polyethylene. The stretching causes a change in the densities of the amorphous parts and crystalline parts in the material. The density of crystalline parts increases with increasing stretching ratio. The reduction of the conduction is due to the splitting of crystalline and the increasing trap sites[61]. Phase transitions also affect the conductivity of polyethylene. Temperature dependences of the conductivity in the temperature region of crystallization for both low and high density polyethylenes are shown in Fig.2.9. The reduction in conductivity is suggested to be associated with the reduction of amorphous parts in the material [62, 63]. The carrier

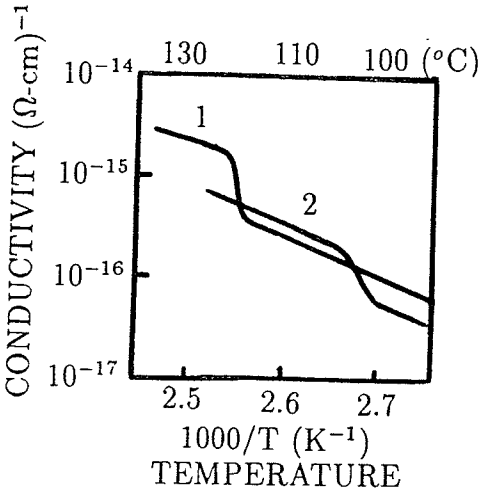


Figure 2.9: *Temperature dependence of conductivity of (1) high density polyethylene, and (2) low density polyethylene. (After Kosaki, Yoda, and Ieda, [62]).*

transport through the amorphous part plays an important role in the electrical conduction in the low field region.

The bulk limited conduction in insulating polymers under low and medium fields has been ascribed to one or more of the following mechanisms: (1) Pool-Frenkel effect, (2) hopping or Impurity conduction, and (3) space charge limited current. In the case of the Poole-Frenkel effect, the trapped charge carrier is thermally excited and assisted by the electric field into the conduction band. The conductivity due to this mechanism as functions of temperature and electric field is given by:

$$\sigma = \sigma_o exp(\beta_p F^{1/2}/2kT) \tag{2.1}$$

where $\beta_p = 2(e^3/4\pi\varepsilon_r\varepsilon_o)^{1/2}$, and $\sigma_o$ is the conductivity at zero field.
This mechanism gives values of $\beta_p$ nearly twice the experimental ones for some case and does not explain the ohmic trend observed at low fields. Several investigators have pointed out that the slope of the $\ln\sigma \sim F^{1/2}$ is a value between

$\beta_p$/kT and $\beta_p$/2kT depending on the energy levels and the distribution of donors and acceptor-like traps. For polyethylene, the experimental values of $\beta$ is about 0.5~0.9 $\beta_p$ [64, 65]. The discrepancies between the theory and the experiment have been attributed to the undimensional character of Poole-Frenkel relation, which ignores the electron emission in directions different from that of the applied field. Therefore, many models have been subsequently proposed considering the electron emission in all directions. Ieda et al. [66] have introduced a cut off state related to the phonon interaction and assumed that an electron in such a state behaves as a free carrier. Hill[67], Adamec and Calderwood[68, 69] have assumed an increase of the backward potential barrier in the same amount as that of the decrease in the applied field direction. After these modifications, the modified equation gives not only the usual Poole-Frenkel relation at medium field, but also Ohm's law at low field. Recently, Paracchini et al. [70] have taken the internal electric field into account with the Poole-Frenkel effect. Nath et al. [71] have suggested a new model, "Poole field lowering of the trap depth", in which the trapped charges are thermally excited to the conduction band of th crystalline regions and then hop through band tail states. All of above modification are in agreement with some experimental results, indicating the Poole-Frenkel conduction might be the closest mechanism to describe the electrical conduction in this field region.

In the hopping process, the charge carrier jumps from one site to another by tunneling. This process is due to the field induced reduction of the barrier width without involving a thermally activation process. However, thermal activation of the electron always promotes the tunneling process. Impurities in the polymer will form impurity states in the forbidden energy gap, which in

some cases act as steping stones in assisting the hopping process. When the localized electronic wave functions of the impurity states overlap, an electron bound to one impurity state can hop to an unoccupied impurity state, especially, when the impurities introduce both donor and acceptor centers in the material.

The space charge limited conduction (SCLC) usually occurs in medium field region. The space charge formed in the material produces a internal electric field which controls the conduction process and the injection process. However, the square law of the SCLC, i.e., $J \propto V^2/d^3$, is rarely observed, especially for polymers. This is due to the fact that the traps present in polymers are distributed both in space and in energy. In this case, the expression for space charge limited current is in a form of $J \propto V^n$ in which the index n will depend on trap distributions both in space and in energy[72-74].

### 2.1.4 Electrical Conduction under High Fields

Most high field conduction studies are on thin films since high fields in thin films can be easily attained at relatively low applied voltages [75-81]. The typical I−V characteristics in the high field region for plasma-polymerized poly (ethylene and trifluoromethance) are shown in Fig.2.10. It is clear that the current increases very rapidly with increasing field in the high field region. The current density is high, of the order of $10^{-8} \sim 10^{-5} A/cm^2$, for fields higher than 2MV/cm. The conduction current depends on electrode material. The current is larger for the anode made of Au than that made of Al, indicating the importance of hole injection at high fields[75]. A similar finding has also been reported for poly-p-xylylene (PPX) [76, 77]. For PPX films,

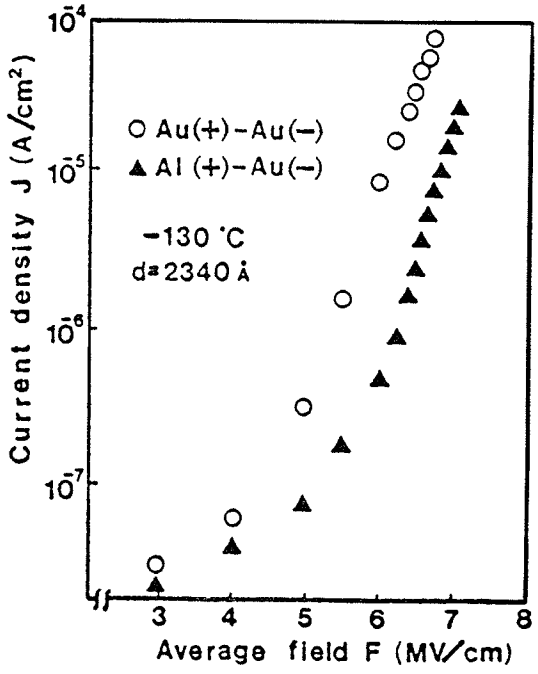


Figure 2.10: *Effect of electrode metal on current density-field characteristics of plasma-polymerized poly (ethylene and trifluoromethane). (After Ishii, Ohki, and Nakano, [75]).*

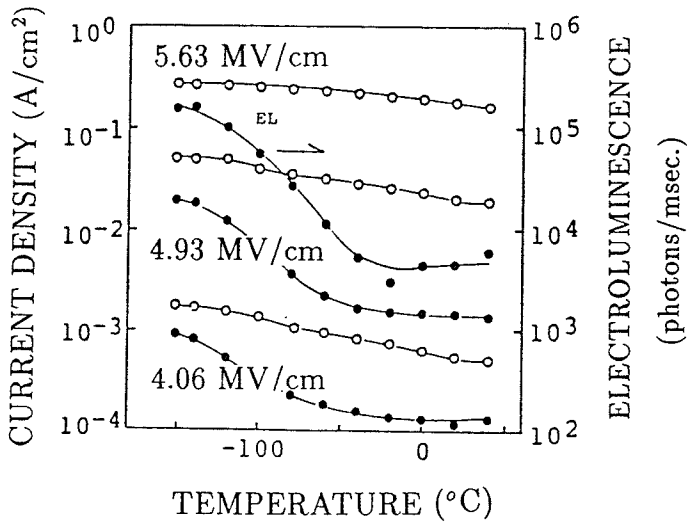


Figure 2.11: *Temperature dependences of current and the electroluminescence (EL) in PPX at various high fields. (After Mizutani, Mori, Takai, and Ieda, [76]).*

electroluminescence (EL) has also been observed at high fields. Both the conduction current and EL have the negative temperature dependences at high fields (F>3MV/cm) in the low temperature region as shown in Fig.2.11. It has been suggested that the hole injection, high hole mobility, and subsequent hole avalanche are responsible for the high field conduction and electroluminescence in PPX [76].

The transient photocurrent and the time constant in a polymer thin film as functions of applied field are shown in Fig.2.12. A small photocurrent and large time constant are obtained at low and medium fields. However, sharp changes in the photocurrent and the time constant occur above a critical field which is in order of 0.2~0.3 times the breakdown field. A "hot electron process" model has been used to explain this phenomenon. This model has suggested that the chemical structure of saturated polymers may provide band

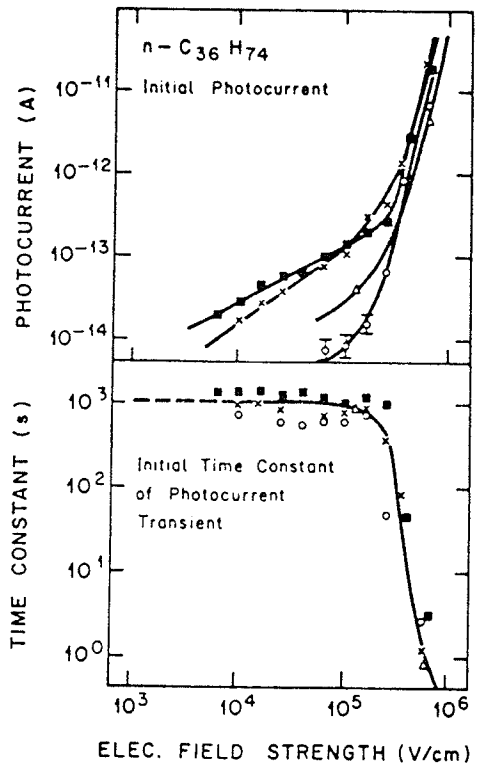


Figure 2.12: *The transient photocurrent and the time constant as functions of applied field in n-$C_{36}H_{74}$ films. There are sharp changes in the photocurrent and the time constant at a field of 3x10$^5$ V/cm. (After Pfluger, Cartier, and Dersch, [78]).*

mobilities of the order of $10cm^2/V\text{-}s$. Because of the disorder in polymers, a mobility edge is expected to exist in both the conduction band and valence band. The band mobilities are only expected at fields higher than a critical field ($F_c$) in order to keep the charge carriers hot above the mobility edge. Under the critical fields, injected carriers are quickly trapped, resulting a very small conduction current. Above the critical fields, injected carriers can be kept in high mobility states, resulting a large conduction current [78, 153]. In this model, the effect of electric fields is only to "heat up" the injected electrons. However, the sharp changes in the conductivity can also be attributed to another injection process (e.g., the hole injection process) becoming operative under the high fields.

## 2.2 Prebreakdown Phenomena

### 2.2.1 Filamentary Conduction

Electrical partial discharge and breakdown paths are always filamentary irrespective of the material phase such as dielectric gases, liquids, or solids under electric fields of any forms [82]. Mizutani et al. [83] have reported that the pre-breakdown current in polyimide thin films is filamentary, and that this current increases with time at a fixed field close to the breakdown strength within a short period prior to the occurrence of final breakdown, and is independent of the electrode area. This indicates that the conductivity of the filament increases with time, possibly due to Joule-heating which increases its temperature until the heat loss to the ambient balances the energy input. On the basis of such a thermal process, Mizutani et al.[83] have calculated the prebreakdown current as a function of time, and their theoretical predication

agrees well with the experimental results. Inuishi and Powers[84] have also observed the filamentary pre-breakdown current in polyethylene terephthalate (PET) films at -180°C. Nagao et al. [85] have reported that the temperature distribution on a polyethylene film surface after high field electrical stressing measured by a thermalgraphic technique is not uniform, and that the conduction current before breakdown is filamentary. The filamentary conduction implies that the carrier injection efficiency differs from domain to domain on the electrode surfaces, and that the material itself is non-homogeneous which leads to a non-uniform field distribution in the axial direction, and a non-uniform conductivity distribution in the transverse direction. The individual building blocks in organic insulating solids are the relatively large molecules rather than atoms. When such a solid is subjected to electrical stressing, the electrical force is acted on each charge in the structure. All of the charged components are not equally well anchored, and failures take place at the weakest spots. Failures always appear as small channels pierced from one electrode to the other, making the high field conduction filamentary, and the electrical breakdown a weak-link phenomenon.

### 2.2.2 Low Density Domains

Prebreakdown disturbance has been observed in liquefied polyethylene by Xie and Kao[86], using a schlieren technique at fields much lower than its breakdown value as shown in Fig. 2.13. The schlieren image, i.e., the low-density domain, always appears near the point electrode irrespective of the waveform and the polarity of the applied voltage. The low density domain tends to spread and gradually to disappear during its movement from the high

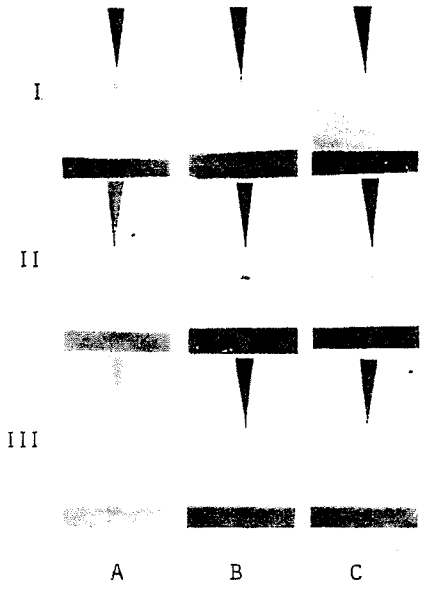


Figure 2.13: *Photographs of the low-density domains at 145° C taken at t after the first appearance of the disturbance, which occurs at t′ after the application of the stressing voltage. (A) 6.5 kV ac (60 Hz, rms), t′=31 min, (I) t=1 s, (II) t=3 s, and (III) t=5 s; (B) 10 kV dc (negative point), t′=25 min, (I) t=0.5 s, (II) t=4 s, (III) t=7 s; and (C) 10 kV dc (positive point) t′=25 min, (I) t=1 s, (II) t=5 s, (III) t=9 s. (After Xie, and Kao, [86]).*

field point electrode to the low field plane electrode. In solidified polyethylene, this low density domain does not move, but grows and the schlieren image becomes darker as the electrical stress time is increased. Time is required for the first appearance of the low-density domain after the application of a predetermined voltage. A similar phenomenon has also been reported by Sueda and Kao [87] in n-hexane, and by Murooka [88] in liquid nitrogen. The observation described above implies that electrical discharge and breakdown in dielectric liquids and solids involve the creation of low density domains or channels in the bulk by carrier injection from electrical contacts and subsequently dissociative trapping and recombination.

Electrical partial discharges in polyethylene at various hydrostatic pressures have been studied by Kao et al.[89]. Their results show that the internal discharge magnitude increases as electrical stressing time increases; the rate of this increase is enhanced when the stressing voltage is increased, but suppressed when the hydrostatic pressure is increased as shown in Fig. 2.14. The discharge magnitude measured within one minute of the application of the stressing voltage is very small, and the pressure dependence of the discharge magnitude is less pronounced if the samples are stressed for a short period of time (a few minutes after the application of the stressing voltage), indicating that the discharge is not due to presence of microcavities already existing in the polyethylene. They have suggested that considerable time is required for the development of low density domains or channels. The major portion of the discharge is due to the low density domains or channels created during the stressing period. The external pressure should not affect the carrier injection from the point tip. However, the external pressure does have two effects: (a) it

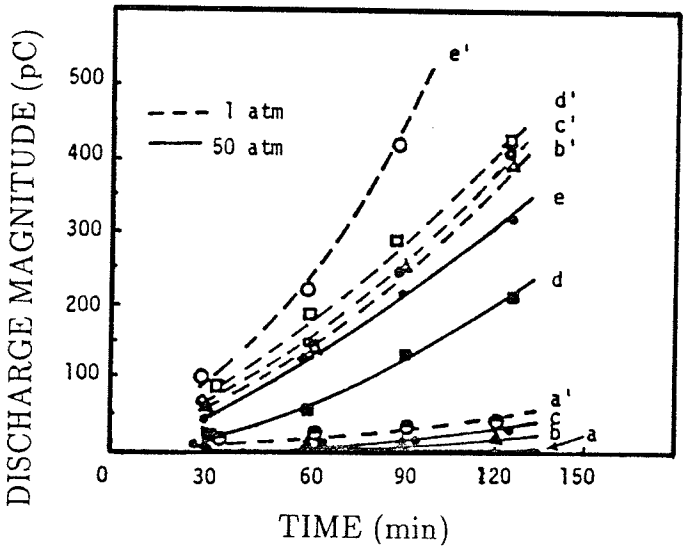


Figure 2.14: *Effect of hydrostatic pressure on the discharge magnitude-stressing time characteristics. a-a', 6.5 kV; b-b', 7.0 kV; c-c', 7.5 kV; d-d', 8.0 kV; e-e', 8.5 kV; a', b', c', d', e' at pressure of 1 atmosphere; a,b,c,d, and e at 50 atmospheres. (After Kao, Xie, and Tu, [89]).*

reduces the size of the existing microcavities, and in turn increases the internal pressure in them, resulting in a decrease of the mean free paths for carriers, and (b) it suppresses the formation and the development of low-density domains or channels due to electrical stressing under high fields, thus reducing the chances for the initiation of partial discharges. This is another experimental evidence that low-density domains have been developed in the material prior to breakdown.

### 2.2.3 Light Emission

Prebreakdown partial discharge is always accompanied with light emission. The light emission prior to the breakdown in condensed insulating materials was first observed in n-hexthin by Smith et al. [90], and then in KBr

by Cooper et al.[91]. Bamji et al. [92] have reported that the light emission at the semiconductor tips in polyethylene prior to the initiation of electrical trees. A similar phenomenon has also been observed at metallic points in polyethylene [93-97]. The light emitted from the material is mainly in visible region which involves an energy release of the order of 1.7~3.1 eV [90] and possibly upto 4 eV in some cases [92, 95]. Applied hydrostatic pressure can suppress almost completely the random light and the current burst, and reduce the light emission intensity to the nonburst level for n-hexane. These results indicate that the emitted light is associated with partial discharge after the formation of low-density domains[98]. Some investigators[92, 95, 97] have speculated that light emission may occur even prior to the creation of the low density region. In this case, the emitted light is considered to be the electroluminescence due to the radiative recombination of the injected electrons (or holes) with the trapped holes (or electrons).

## 2.3 Electrical Treeing

Another critical limitation of the polymeric insulated system is the electrical aging or gradual degradation of the material under high fields. Many investigators [99-108] have reported that tree-like discharging patterns, or electrical trees appear inside the buried power cables after their failure in service. Electrical trees always appear near the actual sites of failures and they start often at electric fields of one or two orders of magnitude smaller than the average breakdown strength of the polymers. Electrical treeing which is related to aging and gradual degradation, leads to final failure of the insulating systems even under the normal operating conditions. The most commonly used

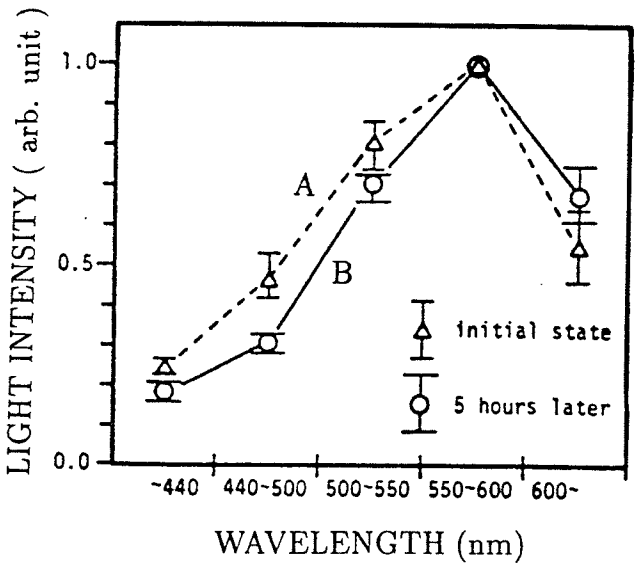


Figure 2.15: *Spectra of the light emitted from the polyethylene at the point tip with a point-plane electrode configuration. (A) At the beginning of the voltage application. (B) 5 hours after voltage application. (After Shimizu, Katsukawa, Miyauchi, Kosaki, and Horii, [95]).*

electrode configurations for the study of electrical treeing phenomena are the point-plane and point-point electrode configurations[107]. Some of the electrical treeing phenomena observed using these electrode configuration are briefly described below.

### 2.3.1 Experimental Observations

An electrical tree has two distinct phases. The first is the tree initiation phase during which no detectable partial discharges occur; and the second is the growth phase during which the tree propagates. It has been reported that luminescence occurs during initiation phase [92-97]. The spectra of this luminescence obtained by Shimizu et al. are shown in Fig.2.15. They have also reported that the light from a partial discharge in a sample with a de-

liberately introduced void is different from this luminescence in terms of the spectrum, the brightness, and the waveform of the light output. They considered this luminescence to be associated with the recombination between positive and negative charges injected from the point electrode under ac fields [95]. The light is emitted at 120 Hz under a 60 Hz ac applied voltage, and the brightness corresponding to the negative and the positive half cycle is almost equal, indicating that both injected electrons and injected holes play an equally important role in this phenomenon. The components of wavelengths shorter than 550 nm decrease, but those of wavelengths longer than 600 nm increase at the time of 5 hours after voltage application, as compared with the initial spectrum. They have suggested that the scission of molecular chains may occur during trapping and recombination, which may, in turn, cause the change in the energy level and the concentration of deep traps as the luminescence centers, leading to the change in the emitted light spectrum. A special dark region in the polymer was also observed at the needle tip after prolonged ac voltage application which may be associated with the decomposition of the polymer caused by the bombardment of the injected carriers. The tree channels start in the dark region and time is required for the creation of the dark region and for the transition from it to the formation of electrical trees[95]. The time required for the initiation of electrical trees decreases significantly with increasing temperature which may be associated with a lowering of the breakdown strength of the polyethylene at higher temperatures. All of these results indicate that the electrical treeing is a process to cause gradual degradation of the material.

Recently, a very sharp point electrode with radius of about 0.1 $\mu$m has

been employed to study the tree initiation at relatively low voltages in order to enable the measurement of the charge flowing during each cycle of the applied ac voltage in polymer, i.e., the cumulative charge during the tree initiation phase [109]. Using such a sharp piont electrode, it has been observed that the cumulative charge flowing through the polyethylene increases linearly with time after voltage application. The speeds of the charge growth in normal, degassed and cross-linked polyethylene, are respectively, 16, 13, and 10 pC per 10 min, revealing that the tree initiation process requires some definite energy depending on the material and its treatment. More time is required for tree initiation in degassed polyethylene than that in the normal polyethylene. Normal polyethylene contains oxygen while the degassed polyethylene has a much lower concentration of oxygen. Oxygen present in free volumes inside the polymer may be responsible for the rapid degradation of the material. A similar phenomenon has also been reported by other investigators [92, 110]. The tree initiation voltage of normal polyethylene is lower than that of degassed, $N_2$- and $SF_6$- impregnated polyethylene[92]. The tree initiation voltage decreases with the voltage rising speed for applied linearly ramp voltages [111-113] as shown in Fig.2.16. This dependence is due to the fact that time is required for the accumulation of homo-space charge to reach a certain level to lower with tends to lower the effective fields for carrier injection. For the point electrode at the positive polarity, the tree initiation voltage is lower than that for point electrode at the negative polarity, indicating that the injected hole can travel a longer distance before being trapped. Figure 2.17 shows that the pattern of electrical tree is highly ramified for the point electrode baised negatively, indicating that the process has a strong stochastic nature. However, for the

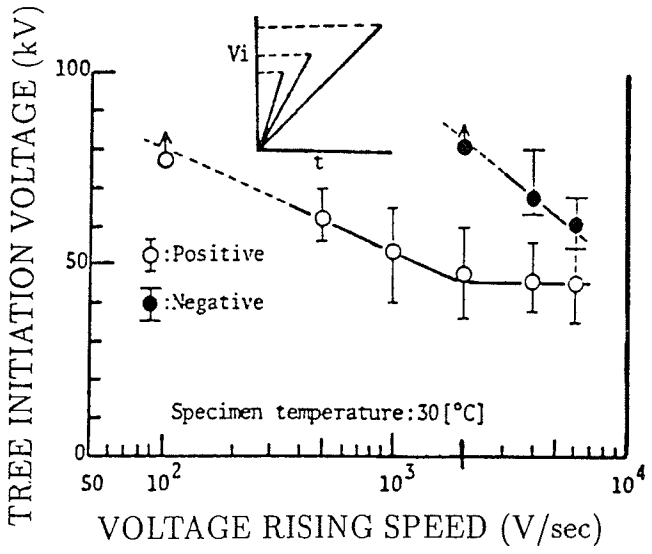


Figure 2.16: *Tree-initiation voltage as a function of voltage rising speed for linearly ramp voltages. (After Ieda, and Nawata, [113]).*

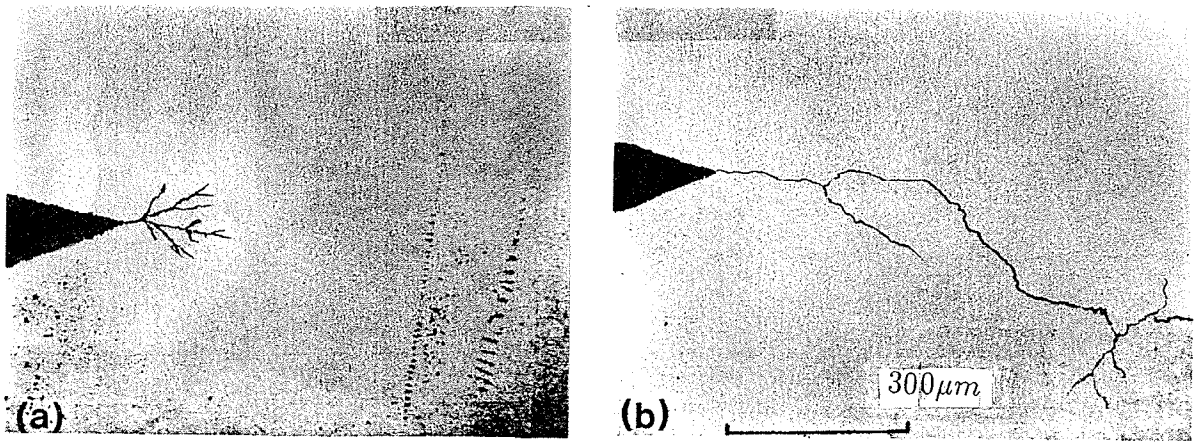


Figure 2.17: *Patterns of the electrical trees: (A) for the point in negative polarity; (B) for the point in positive polarity. (After* McLeod, *Liu, Pries, Kao, and Card, [115]).*

point electrode biased positively, the pattern has a strong tendency to extend the tree to a longer distance possibly due to the higher mobility for holes [114, 115].

### 2.3.2 Tree Initiation Mechanisms

#### (A) Trees initiated by charge injection

It is generally believed that electrical trees are initiated by charge carrier injection. Obviously the injected charge carriers can perform the following functions:

(a) The injected charge carriers may gain sufficient energy from electric fields to bombard the molecules causing decomposition to form lower molecular products or gases, which may result in the formation of low density domains in which discharges may occur to form trees[56]. Since the ionization energy of hydrocarbons is about 10 eV, it is unlikely that the injected electrons can gain sufficient energy from the fields to cause ionization even at at a field of the order of 10MV/cm, thus the formation of low density domain may be one of important steps for tree initiation.

(b) The injected carriers may cause the light emission and, in turn, photodegradation of the polymer by photo-physical and the photo-chemical processes, the former produces the light or heat and the latter causes the formation of free radicals leading to material degradation or the initiation and the formation of electrical trees [92, 116, 117].

(c) The injected carriers may release an energy of several eV due to the trapping and recombination processes. The released energy of an injected carrier, if not converted to radiative luminescence, may be transferred to another

electron by an Auger-type process, and this second electron may have sufficient energy to break the chemical bond of the polymer chain[119]. Many injected electrons which follow this bond-breaking process may create low-density domains, then impact ionization may take place inside such domains to initiate the electrical trees [118, 119].

**(B) Trees initiated by partial discharges**

Electrical trees may be initiated by partial discharges in small cavities existing in the polymers because small cavities may be created at the tips of foreign particles or asperities of electrode surface due to differential thermal expansion coefficients of the polymer and the metal, or due to adsorbed or occluded gases on the surface[120]. But careful preparation of the point electrodes can eliminate the formation of cavities and in that case the trees may not be initiated by cavities[95].

**(C) Trees initiated by mechanical forces**

The high Maxwell compression force on the dielectric caused by the high electric fields at the point electrode can induce a mechanical force perpendicular to the direction of the electric fields in the polymer. When such a force exceeds a certain critical value, it may cause crushing in the polymer and lead to the initiation of electrical trees[20, 153]. A compression force applied uniaxially perpendicular to the axis of a point-plane electrode configuration suppresses the growth of the electrical tree, but a tensile force applied in the same manner enhances the growth of the tree[153]. It is possible that the electrostatic energy applied to the polymer at high fields may exceed the formation energy of the material.

### 2.3.3 Propagation of Electrical Trees

The propagation of the electrical trees is due to discharges or impact ionizations, and the material corrosions resulting from these discharges inside the tree channels. The variations of the discharge conditions, such as the waveform and the magnitude of the applied voltage, the material, and the temperature, affect the pattern of the electrical tree. The most common patterns are often branch-like and bush-like patterns. The bush-like tree consists of a number of interconnected channels and the maximum discharge magnitude of the bush-like tree is much larger than that of the branch-like tree. The light emitted from discharge in a branch-like tree is concentrated in the branch extremities, while all channels are bright in a bush-like tree[123]. The main difference between these two patterns of trees is the density of the channels, bush-like tree has more channels than the branch-like tree. Several investigators [124-126] have reported that the action of discharges produces CO, $CO_2$, and $H_2$ in the tree channels. Low molecular weight products such as methane($CH_4$), acetylene ($C_2H_2$), or ethylene($C_2H_4$) may also be produced. All of these decomposition products indicate the degradation of the polyethylene. An important factor in the growth of the trees is their access to the free air or water surroundings. Trees starting at the surfaces with an unlimited supply of air or water may grow and extend through the material to bridge the electrodes. Trees starting at an internal void or inclusion can rarely grow to a very large size. An increase in void pressure due to ionization may extinguish the discharge in the void. When the gas pressure in the tree is reduced sufficiently by permeation outwards, ionization may occur again, resulting in

a pulsive discharge in the tree channels[104, 106].

### 2.3.4 Effect of Additives

Many additives can, to some degrees, suppress the electrical treeing and improve the breakdown strength [106,127-129]. One of the major group of the additives are called the voltage stabilizers which are mainly aromatic organic compounds, such as O-nitrotoluene, 2-nitrotrodiphenylamine, siloxane oligomers, etc. These aromatic additives are thought to operate as electron traps tending to capture energetic electrons without causing any permanent changes in the host materials[106]. Tu et al. [127] have reported that the ac tree initiation voltage of polyethylene and XLPE increases by four times from 10 to 40 kV by adding 6% acetophenone in the polyethylene. McMahon [129] et al. have also reported that dodecanol can suppress electrical tree growing, even after the tree initiation. This effect may be attributed to the field-dependent conductivity leading to the field-grading. The main mechanism is to relieve the electrical stress at sites of high electric fields due to the increase in conductivity at high fields. The field-dependent conductivity may be caused by either field-enhanced dissociation or field-enhanced ionization, or both.

## 2.4 Electrical Breakdown

### 2.4.1 Temperature Dependence

Figure 2.18 shows the breakdown strength as a function of temperature for polymethy methacrylate, polyethylene, polystyrene and polyisobutylene. In general, the temperature dependence of breakdown strength of non-polar polymers can be divided into the low temperature region in which the break-

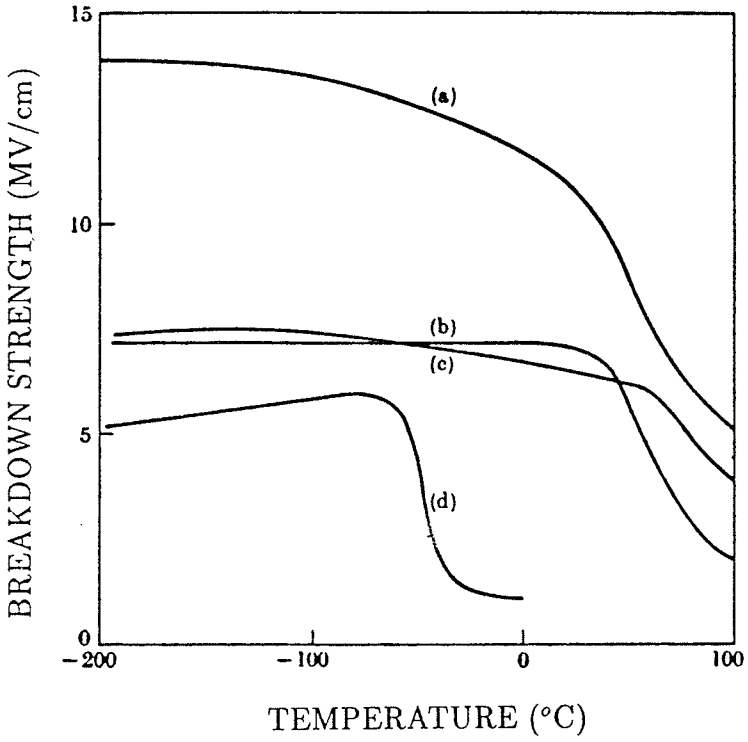


Figure 2.18: *The breakdown strength of some polymers as a function of temperature. (a) Polymethyl methacrylate, (b) polyethylene, (c) Polystyrene, and (d) Polyisobutylene. (After Oakes, [130]).*

down strength is insensitive to temperature, and the high temperature region in which the breakdown strength decreases with increasing temperature. For polar polymers the breakdown strength decreases slowly with increasing temperature from the low temperature to some critical temperature, and beyond this critical temperature it falls steeply. For polyethylene there clearly exist both the low and the high temperature regions. The breakdown strength of polyethylene is insensitive to the temperature from the liquid helium temperature to 50°C. From 50°C to the melting point the breakdown strength falls steeply[131]. The critical temperature ($T_c$) to separate the low and the high temperature regions for polyethylene is related to the glass transition temperature ($T_g$)[132]. In the low temperature region, breakdown may be mainly associated with the electronic processes in the material, while in the high temperature region breakdown may be dominated by the thermal heating or electrochemical processes.

### 2.4.2 Morphology Effects

In general, the breakdown strength of polymers increases with increasing crosslinking, especially in the high temperature region, partly because the crosslinking results in an increase of the melting point. Polyethylene consists a mixture of the crystalline and the amorphous phases. Breakdown strength depends on the structure of crystalline region and the degree of crystallinity as well as the properties of amorphous region. Figure 2.19. shows the dependence of the breakdown strength of polyethylene on the degree of crystallinity. Below 80°C, the breakdown strength increases with the decrease of crystallinity, but above 80° this dependence is reversed[133]. The higher the crystallinity,

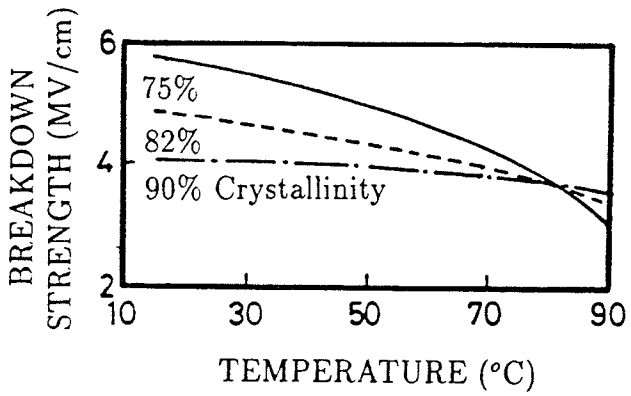


Figure 2.19: *Effect of crystallinity on the breakdown strength of high-density polyethylene. (After Miyauchi, and Yahagi, [133]).*

the higher is the melting point. This may be the reason why the breakdown strength increases with increasing temperature above 80°C. However, higher crystallinity may introduce more defects or traps between the crystalline and the amorphous regions; and enhance the accereration of hole in the crystalline regions; leading to a lower breakdown strength in the low temperature region. Yahagi [61] have reported that breakdown strength is higher for the polyethylene with less difference in density between crystalline lamellae and amorphous parts, and that the polyethylene consisting of smaller crystal and dense amorphous parts may be better than larger crystal and coarse amorphous parts.

In spherulite structure, the amorphous part exists in both the spherulite boundaries and inter-lamellar region. It has been observed that discharge channels always run along the spherulite boundaries [134]. Breakdown occurs most frequently at the spherulite boundaries and the breakdown strength is much lower than that of polyethylene without such boundaries[135]. The crystalline or spherulite part has a higher density than the amorphous part, thus the breakdown path tends to run through the low density domain.

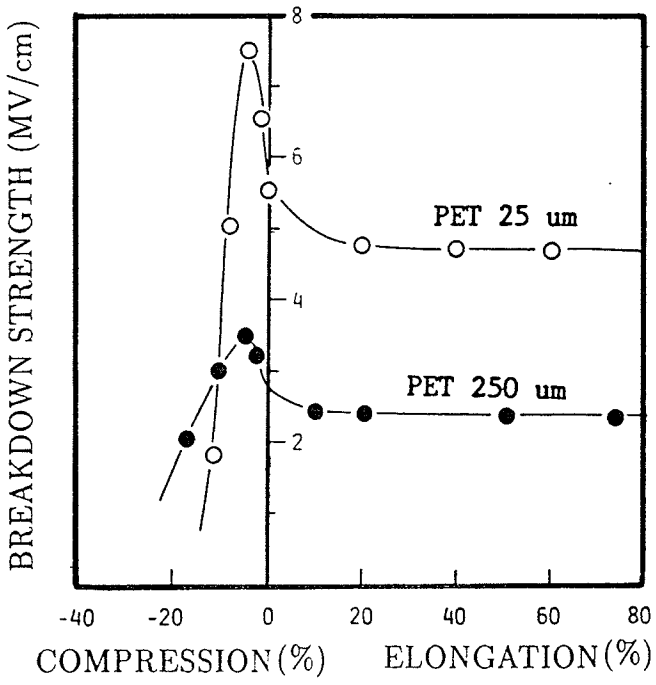


Figure 2.20: *Effects of mechanical compression and elongation on the breakdown strength of PET. (After Park, Hara, and Akazaki, [136]).*

### 2.4.3 Effects of Elongation and Compression

Several investigators [136-139] have studied the breakdown strength of the polymers after the samples being subjected to elongation and compression. Some typical results are shown in Fig.2.20. An increase in breakdown strength of the compressed polymer is caused by a decrease in the free volume, and a decrease in the breakdown strength when the compressed stress higher than a critical pressure (eg. 100 MPa) is due to the formation of submicroscopic cracks by chain rupture of the molecules in amorphous regions. Compression improves the dc and impulse breakdown strength of polyethylene, possibly due to partial removal of defects and free volumes[139].

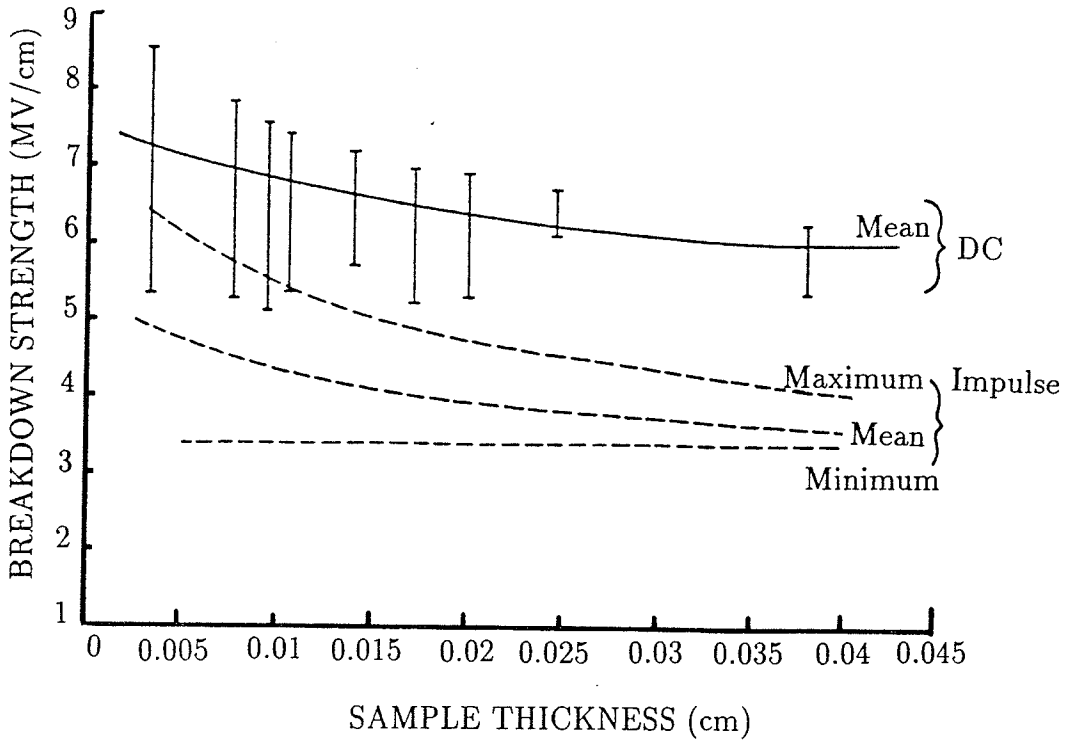


Figure 2.21: *Effect of thickness on the breakdown strength of polyethylene. (A) the dc breakdown strength; and (B) the impulse breakdown strength. (After Watson, Heyes, Kao, and Calderwood,[82]).*

### 2.4.4 Effects of Sample Thickness and Electrical Prestressing

The breakdown strength of polyethylene depends on the sample thickness as shown in Fig.2.21. The impulse breakdown strength of polyethylene is generally smaller than the dc breakdown strength. This may be due to the effect of homo-space charge in the vicinity of the carrier-injecting electrodes during the period of the application of slowly rising voltage or dc voltage. The effect of the homo-space charge may be greater for a thin sample than for a thick one, thus resulting in the thickness dependence of breakdown strength. The effect of prestressing with direct voltage on the impulse breakdown strength

of polyethylene is shown in Fig.2.22. When prestress and impulse are of the opposite polarity, the breakdown strength dramatically decreases with the increase of the prestressing fields. When prestress and impulse are of the same polarity, the breakdown strength is approximately equal to the dc breakdown strength. This effect can also be attributed to the effect of homo-space charge accumulated during the prestressing period.

### 2.4.5 Effects of Incorporated Foreign Elements

Mizutani et al.[141] have reported that the incorporation into polyethylene with halogen comonomers such as PBPM (penta bromo phenyl methacrylate) and TFMM (trifluoro methly methacrylate) increases the breakdown strength of polyethylene, while BM (benzi methacrylate; including no halogen atom) does not as shown in Fig.2.23. The incorporation of Br-halogen monomers into polyethylene suppresses markedly the high field conduction. Other halogen comonomers such as TEMM with F atoms also exhibits similar effects[141]. The halogen comonomers act as traps in polyethylene whose trapping and/or scattering prevents free carriers from being accelerated in the fields and thus increases the breakdown strength. The incorporation of other organic impurities such as styrene, allyl-benzene, and 4-phenyl-1-butene, [27], and nitrogen[28, 142] also increase the breakdown strength of polyethylene. Foreign elements may also introduce shallow traps into the polymer thus reducing the energy released from the trapping and recombination processes, and indirectly increasing the breakdown strength, according to Kao's breakdown model[119]. The experimental results suggest that the incorporation into polyethylene with appropriate monomers or foreign elements is one of methods

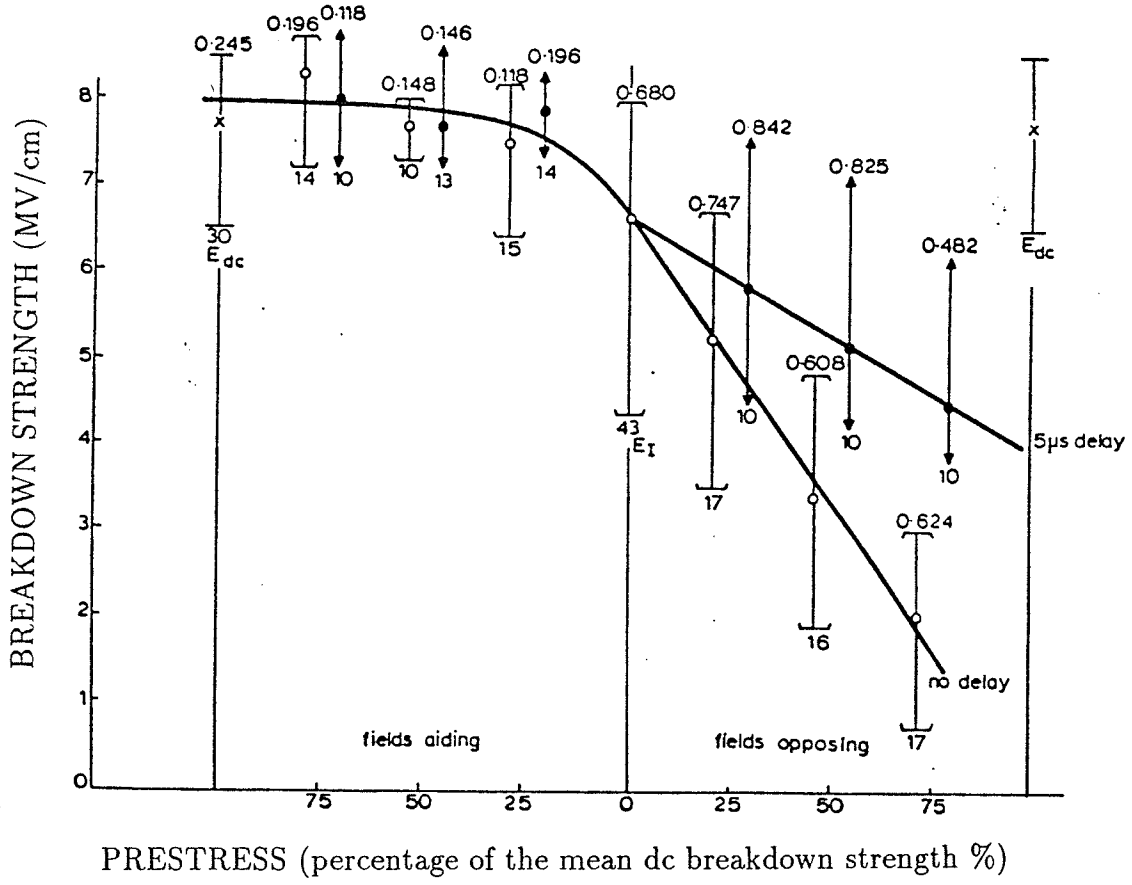


Figure 2.22: *Effect of dc prestressing on the impulse breakdown strength of high purity polyethylene at 20° C. The vertical bars represent the spread of breakdown strength; the figure below a bar is the number of tests and the figure above is the variance. Open circles correspond to application of the impulse voltage immediately after pre-stressing, and full circles correspond to a 5 μsec. delay. (After Bradwell, Cooper, Varlow, [140]).*

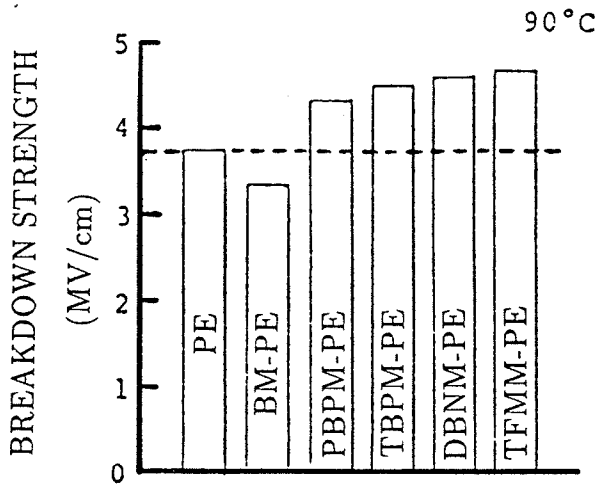


Figure 2.23: *Breakdown strength for polyethylene without and with various monomers incorporation. (After Mizutani, Suzuoki, Hikita, Yoo, and Ieda, [141]).*

to improve its breakdown strength. Moreover, the incorporation by copolymerization or plasma polymerization has the advantage of achieving chemical bonding and avoiding bleed-out of foreign elements.

### 2.4.6 Emission Shields

An emission shield inserted between the semiconductor coating and the polyethylene insulator in cables increases ac breakdown strength of the cable by 30% [29, 143]. The permittivity of the material used for emission shield should be higher than that of the polymer so that the electric fields near the semiconducting coating can be reduced, thus reducing the carrier injection[30, 144]. Tu et al.[30] have used a mixture of $BaTiO_3$ (90%) and chlorinated (10%) polyviylchloride as emission shield and found that the breakdown strength for polyethylene with such emission shield coated on both sample surfaces is higher than that without under various voltage conditions, indicating that the emis-

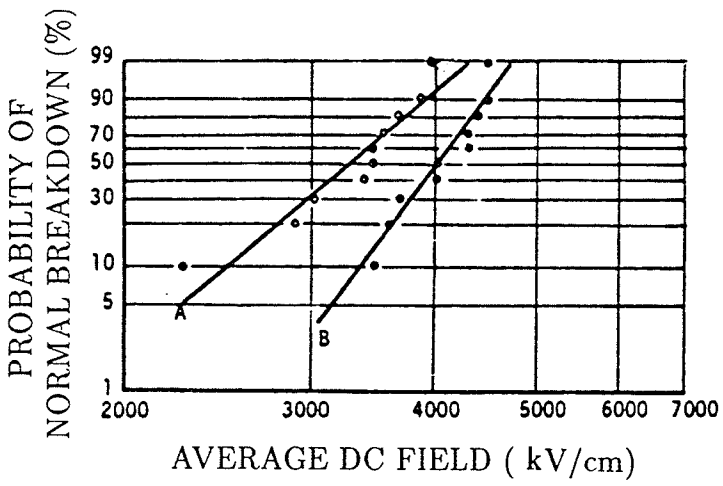


Figure 2.24: *Percent cumulative probability of normal breakdown as a function of dc field for one electrode with emission shield: (A) the electrode with emission shield at negative polarity, (B) the electrode with emission shield at positive polarity, based on apparent thickness* $d = d_{PE} + d_{ES}$, *where* $d_{PE} = 80\mu m$ *and* $d_{ES} = 30\mu m$. *(After Tu, Liu, Zhuang, Liu, and Kao,[30]).*

sion shield acts as a barrier to suppress carrier injection as shown in Fig.2.24. They suggested that an emission shield should be so chosen that its potential barrier height is not lower than the polymer with respect to the injecting contact and its relative permittivity is higher than that of the polymer. Liu et al.[114] have reported that the tree initiation voltage is markedly increased when point electrode is coated with an oxide layer. These two findings are consistent with each other since the relative permittivity of the oxide layer is larger than that of polyethylene and therefore the oxide layer acts as an emission shield. It is interesting to note that emission shield is more effective for it coated on the positive electrode than on the negative electrode[30, 57, 114], indicating polyethylene may have a density of electron traps higher than that of hole traps, but the energy level of the latter is deeper than the former as reported by several investigators [33, 43].

A plasma-polymerized polyethylene deposited on the polyethylene surface can also act as an emission shield [31], but in this case, its function is to provide a trapping layer to form a homo-space charge region to suppress carrier emission.

## 2.5 Breakdown Theories

Several electrical breakdown theories have been put forward in the early days, which are considered as the classical breakdown theories[18]. Among them the important ones are (a) the theory based on the collapse of the energy balance, i.e., the transfer of the energy of hot electrons gained from the electric fields to the lattice (electron-phonon interaction) so as to increase the lattice temperature to a critical value at which a permanent change in lattice may occur; (b) the theory based on the high fields induced impact ionization leading to avalanche breakdown; and (c) the thermal breakdown theory based on the Joule heating of the material. The most common one is (b) which involves the creation of a local high conduction path through the dielectric by electron impact ionization. The classical theories are not able to explain many breakdown phenomena, possibly, due to the fact that the assumed conditions used for the development of these theories are ideal and, in most cases, they are quite different from the practical ones, particularly in polymers. Thus, many new models have been developed, taking into account some experimental aspects. In the following we shall review briefly some important ones.

### 2.5.1 Modification of the Avalanche Theory

One of the shortcomings of the classical avalanche breakdown theory is that it does not take into account the effects of the space charges which are produced either by impact ionization or by carrier injection from the electrodes. O'Dwyer [145] has pointed out that a theory that considers impact ionization as an important process and at the same time retains the assumption of a uniform field is not realistic when there are many generations of ionizing collisions. By considering impact ionization with subsequent separation of electrons and holes as the major mechanism responsible for the field distortion in the electrically stressed insulating material, he has developed a modified avalanche breakdown model by assuming that the mobility of one type of carriers (e.g., electrons, $\mu_n$) is much higher than that of the other type (e.g., holes, $\mu_p$). If $\mu_n > \mu_p$ and electron injection from the cathode play also an important role in the breakdown process, then it can be imagined that the positive hole space charge (free and trapped holes) will enhance the fields toward the cathode and hence the electron injection. Both the impact ionization and the electron injection tends to promote each other resulting in a large distortion of the field, i.e., the local field near the cathode may be many times higher than the average field. It is this local field which leads to final breakdown. This modified avalanche breakdown model may explain the thickness dependence as shown in Fig.2.21, because the thicker the sample the more is the hetero-space charge and hence the lower is the average breakdown strength, but it cannot explain the decrease of the tree-initiation voltage with increase of the voltage rising speed as shown in Fig.2.16 and the prestressing

effects shown in Fig. 2.22. Although some investigators [146, 147] have attempted to further modify this avalanche breakdown theory by including the effects of electron and hole traps, the modification does not alter the sameness of the general tendency, that is, the polarity of the net space charge is always heterogeneous to that of the carrier-injecting electrode, and it always tends to enhance the carrier injection and to lower the average breakdown strength if the impact ionization is the basic process leading to avalanche breakdown.

To develop a breakdown model the following facts must be considered: (1) the heating effects due to prebreakdown current and dielectric losses, (2) the compression force due to charges on the surfaces of the insulating material, (3) the low-carrier mobilities and the small mean free paths, (For most insulating polymers, the electrons or holes may not be able to attain an energy high enough to cause impact ionization even at a field of $10^7$ V/cm.), and (4) the electrochemical reactions with the environment. The following models do take into account some of the above facts.

### 2.5.2 Electromechanical Breakdown

Stark and Garton [148] were the first to suggest that the breakdown strength of polyethylene can be estimated by

$$\frac{1}{2}\varepsilon F^2 = Y ln\frac{d_o}{d} \tag{2.2}$$

where $\varepsilon$ is the permittivity, $d_o$ is the initial sample thickness, Y is the Young's modulus, F is the applied field, and d is the strained sample thickness under electrical stress, i.e., under compression. For $\ln(d_o/d)=1/2$ or $(d_o/d) > (1/0.6)$, the sample will collapse. Thus the average breakdown strength ($F_b$) can be

expressed as

$$F_b = (\frac{Y}{\varepsilon})^{1/2}. \tag{2.3}$$

Electromechanical breakdown may occur in polyethylene at high temperatures or in cross-linked polyethylene. However, electromechanical breakdown of polyethylene can be prevented by encapsulation [149, 150]. Although this breakdown mechanism explains well the temperature dependence for the breakdown strength in the high temperature region of polyethylene, and polyisobutylene, it cannot explain many temperature-dependent breakdown features. For example, it cannot explain the temperature dependence of breakdown strength below 80°C for polystyrene and polyethylene methacrylate (PMMA) [18]. Dynamic mechanical losses occur in all polymers and vary due to the variation of the temperature-dependent mobility in different parts of the molecular chain resulting in an increase of "free volumes" between molecular chains and a change in the specific heat and thermal expansion coefficient. These factors have not been included in the approach by Stark and Garton.

### 2.5.3 Budenstein's Model

Budenstein considered the breakdown process consisting of four stages: a formative stage, a tree initiation stage, a tree growth stage and a return streamer stage[151]. During the formative stage, the energy is added to the dielectric from the field of external sources. Energy is stored by local rearrangement of the charge distribution in the solid via polarization, collision ionization, trapping and atomic displacement. The end result is to alter the charge balance locally so that molecular bonds are broken. The transition from the solid to the gas phase is hypothesized to occur at this stage if the local

charge density increases to the point where non-bonding orbitals are formed. This formation of the gas phase will lead to the tree initiation stage. The tree growth is due to the energy transferred from the field to the gases in the form of electric discharge which then further erodes the solid, and/or in the same way as it is in the formative stage at the tip of the tree channels. The return streamer occurs when a tree extends from one electrode to the other; then current through the highly conducting streamer forms the breakdown channel.

This model is very similar to the gaseous discharge process and can explain that the anode is the preferred surface for the initiation of trees in PMMA. The localized levels in the material are assumed to be the favorable paths energetically for injected electrons to move through the material towards the anode end. The electrons tend to leave their sites at the cathode end on a distributed basis and, in tune, to pile up at the well-defined anode end. This makes the field required for bond breaking at the cathode end higher than that at the anode end[152]. However, a great deal of experimental results reveals that the hole injection process plays an important role in the breakdown process. The tree initiated at the anode point may also be due to the hole injection and followed by the material degradation.

### 2.5.4 Zeller's Model

The basic concept of Zeller's model is the "hot electron process"[153]. He has suggested that the chemical structure of saturated polymers may provide band mobilities of the order of $10cm^2/V\text{-}s$. Because of the disorder in polymers, a mobility edge is expected to exist in both the conduction band

and the valence band. According to his model, band mobilities are only expected at fields higher than a critical field ($F_c$) in order to keep the charge carriers hot above the mobility edge. Thus, at fields higher than $F_c$, most electrons (or holes) can be considered as hot electrons (or hot holes), moving in the extended states with a relatively high mobility in a manner similar to electronic conduction in amorphous semiconductors [32]. If the field is sufficiently high, the electrons injected from the electrode can become hot and subsequently bombard the material causing either impact ionization or chemical damage of the material. Zeller has also considered that the mechanical stress created at high fields at the tip of the point-plane electrode configuration is responsible for the initiation and the growth of electrical trees. At the voltage for the onset of the tree initiation, the mechanical stress developed at the tip is larger than the bonding strength of the material. However, the charge injected at low fields may also lead to material degradation, which have been indicated in many prebreakdown phenomena, e.g., the cumulative charges measured before tree initiation. This indicates that the tree initiation could be due to low mobility carriers.

### 2.5.5 Kao's Model

In general, insulating polymers have the following features: (1) low carrier mobilities; (2) large energy band gap Eg, (larger than 4 eV); (3) higher localized gap state concentration (much larger than the thermal equilibrium carrier concentration); and (4) small mean free paths. For these materials it is almost impossible for carriers to gain enough energy from the field to become sufficiently hot to cause structural changes in the materials, which means that

impact ionization is impossible prior to breakdown. Also the Zener process is impossible since the tunneling probability for electrons is negligibly small in large band gap materials. Based on these facts, Kao[119] has proposed a new theory of electrical breakdown in insulating materials. According to his theory, the electrons (or holes) injected from the electrode will be trapped or recombined after one or a few scatterings because of a small mean free path and a large localized gap state concentration. In the transition from an upper to a lower energy state, an energy equal to the energy difference between the two states will be evolved either radiatively or nonradiatively. In non-crystalline insulators such a transition is mainly non-radiative. Since low mobility materials always have a high energy gap, this released energy will be in the order of 4 eV $\sim$ 5 eV. Taking electrons as the major carriers, this released energy can be transferred to another electron and transform it into a hot electron via an Auger-type process as shown in Fig.2.25. This second electron can then have sufficient energy to bombard a molecule and break its bonds. Furthermore, the energy released from the second electron will be transferred to a third electron and make it in turn into another hot electron. The bonding energies are in the order of 3.5 eV to 4 eV for polymers. The processes will create a low density region in the polymer, then the impact ionization may occur in this low density region when the field, the mean free path, and the ionization energy of the radicals in the region are at appropriate values. Internal discharge such as electrical treeing and breakdown are initiated by impact ionization within such low-density domains or channels and followed by an indefinite increase in carrier multiplication in the conduction level that extends the channels and finally destroys the material inside them.

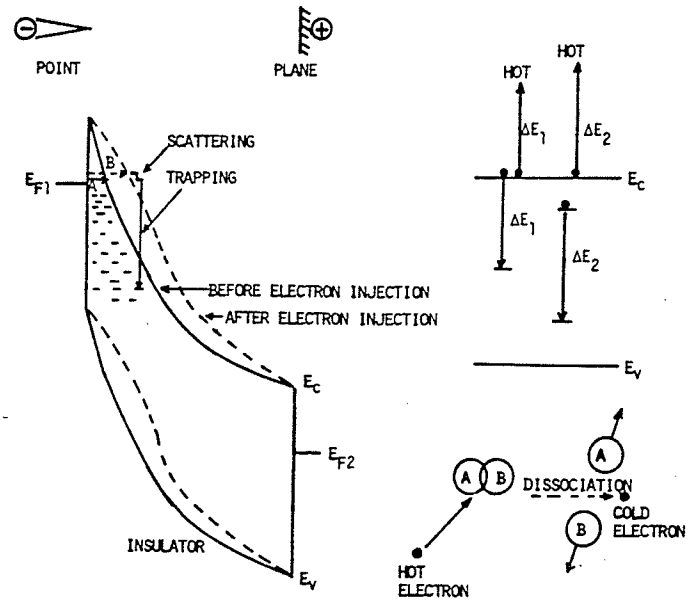


Figure 2.25(a): *Illustrating electron injection, electron trapping, build-up of homo-space charge modifying internal field distribution, hot electron generation process, and dissociation of molecule into radicals by hot electron bombardment for the point electrode at negative polarity. (After Kao, [119]).*

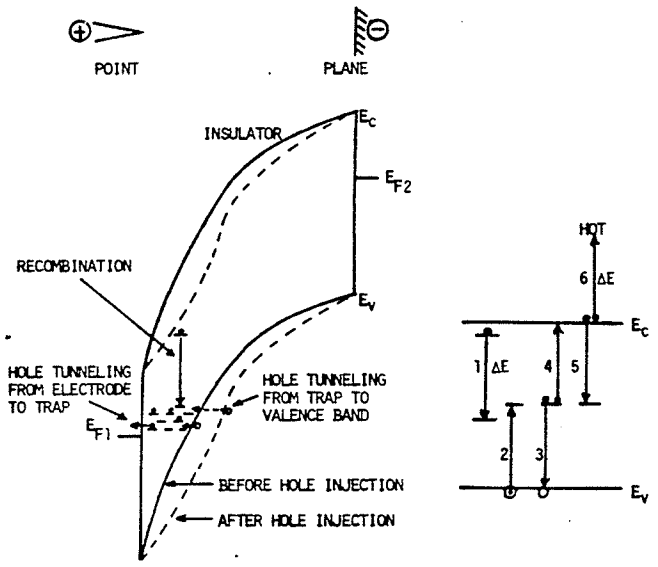


Figure 2.25(b): *Illustrating hole injection, trapped electron–trapped hole recombination, build-up of homo-space charge modifying internal field distribution, and hot electron generation process for the point electrode at positive polarity. (After Kao, [119]).*

The main differences between Kao's model and the conventional ones are: (a) the energy of the hot electron is generated by an Auger type process and is not gained from the field; and (b) the impact ionization takes place only in the low-density domains and not in the material itself. It is the first model which takes the energy released from the trapping and recombination processes into account. This model can explain many experimental phenomena, especially, the low-density domain formed before breakdown[86, 89]. Based on his theory, the incorporation of appropriate impurities into polymers will improve the breakdown strength if the impurities can introduce shallow traps.

# Chapter 3

## Chemical Structure of Plasma Polymerized Polyethylene Films with and without Silicon Incorporation[1]

There are many techniques to fabricate thin organic films, such as solvent casting, vacuum evaporation, sputtering, plasma polymerization etc. So far, the plasma enhanced chemical vapor deposition technique is the one widely used because of its extended applicability to various monomers. Such plasma-polymerized films can be made of high purity source materials. Polymer films fabricated by plasma polymerization have been studied extensively in the past three decades [11-17]. So far, most studies have been concerned with the fabrication techniques, film properties and possible applications. Little has been reported on the chemical structure of such films. In this chapter we should describe the radio frequency plasma system for plasma polymerization of the polyethylene films with and without incorporation of silicon and discuss the

[1]Part of the material presented in this chapter has been published in Polymer Communication Vol. 32, No.11, pp.329-331, (1991) [185].

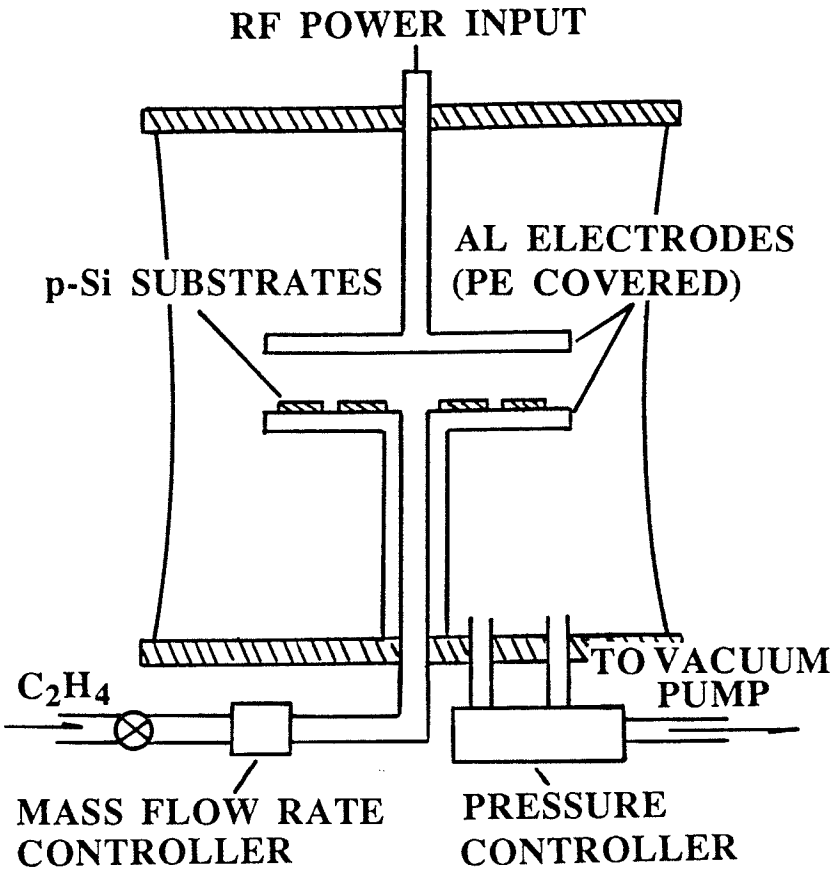


Figure 3.1: *Simplified schematic diagram of the radio-frequency (RF) plasma polymerization chamber.*

chemical structure of these films based on their infrared (IR) spectraoscopy.

## 3.1 The Radio Frequency Plasma System and Thin Film Deposition

The radio frequency (RF) glow-discharge chamber shown in Fig. 3.1 operating at 13.56 MHz was employed for the fabrication of polyethylene films by plasma polymerization of ethylene. The chamber consisted of a pair of

parallel disc electrodes of 15 cm in diameter, 0.5 cm in thickness and 3 cm in separation. The electrodes were aluminum discs covered with a polyethylene film. To produce the plasma-polymerized polyethylene films, pure ethylene gas was used. To produce silicon-incorporated polyethylene thin films, both ethylene and silane gases were used, the content of silicon element in the films was controlled by adjusting the volume ratio of $SiH_4/C_2H_4$ in the gas mixture. *p*-type, <100> oriented, 30-60 Ω-cm silicon wafers were used as substrates because they are transparent to IR light. All substrates were carefully cleaned using the RCA method [155, 156] with $1.7x10^6$ Ω-cm deionized water. Prior to loading, substrates were dipped in a reduced $HF/H_2O$ solution (1/100ccm) to remove the nature oxide on the surface. The chamber was evacuated to about $10^{-6}$ Torr for about 4 hours and then high purity ethylene (99.999%) or a predetermined gas mixture was led into the chamber, the operating pressure being about 1 Torr. The gas flow rate and the operating pressure were automatically controlled by a mass flow rate controller in conjunction with a feedback exhaust valve controller to maintain a constant gas flow and operating pressure during film deposition. Thermocouples and a resistance heater were embedded beneath the bottom electrode to control and to monitor the temperature of the substrates. The substrate temperature used for the fabrication of the films for this investigation was maintained constant at 25°C during film deposition. The deposition rate was about 33Å/min for pure polyethylene. The deposition rate varies with the ratio of the gas mixtures in the case of the foreign element involved depositions. After deposition the films were kept in the same vacuum chamber under a vacuum $10^{-6}$ Torr for heat treatment at 100°C for about 2 hours in order to anneal out any nonequilibrium structural stresses.

Table 3.1: Deposition Parameters For Plasma Polymerized Polyethylene Films with and without Silicon Incorporation.

| Volume ratio of $SiH_4/GH_4$ | Gas flow rate ($cm^3\ min^{-1}$) | | Deposition pressure (Torr) | rf power input (W) | Deposition rate (Å/min) |
|---|---|---|---|---|---|
| | $SiH_4$ | $C_2H_4$ | | | |
| 0 | 0 | 50 | 1.00 | 20 | 34 |
| 0.022 | 1.1 | 50 | 1.00 | 20 | 77 |
| 0.066 | 3.3 | 50 | 1.00 | 20 | 133 |
| 0.110 | 5.5 | 50 | 1.00 | 20 | 300 |

The film thickness was measured with a Varian $\AA$-scope interferometer (model 980-4000/4006) and checked by ellipsometry. The deposition parameters for plasma-polymerized films are listed in Table 3.1.

## 3.2 Plasma Polymerized Polyethylene (PE)

All films used for the study of the chemical structure were $3000\AA$ in thickness, which was thick enough to produce a good IR response. The absorption spectra were measured using a Bomem Michelson-100 infrared spectrometer. Figure 3.2 shows the IR spectra of PE films with and without various concentrations of incorporated silicon. Table 3.2 lists the assignments of the absorption bands based on these spectra.

By comparing the IR spectrum of the plasma-polymerized polyethylene (PE) films with those of conventional polyethylene and polypropylene shown in Fig.3.3, we can see that the PE films have some absorption peaks similar to those of the conventional polyethylene and polypropylene such as the $CH_2$

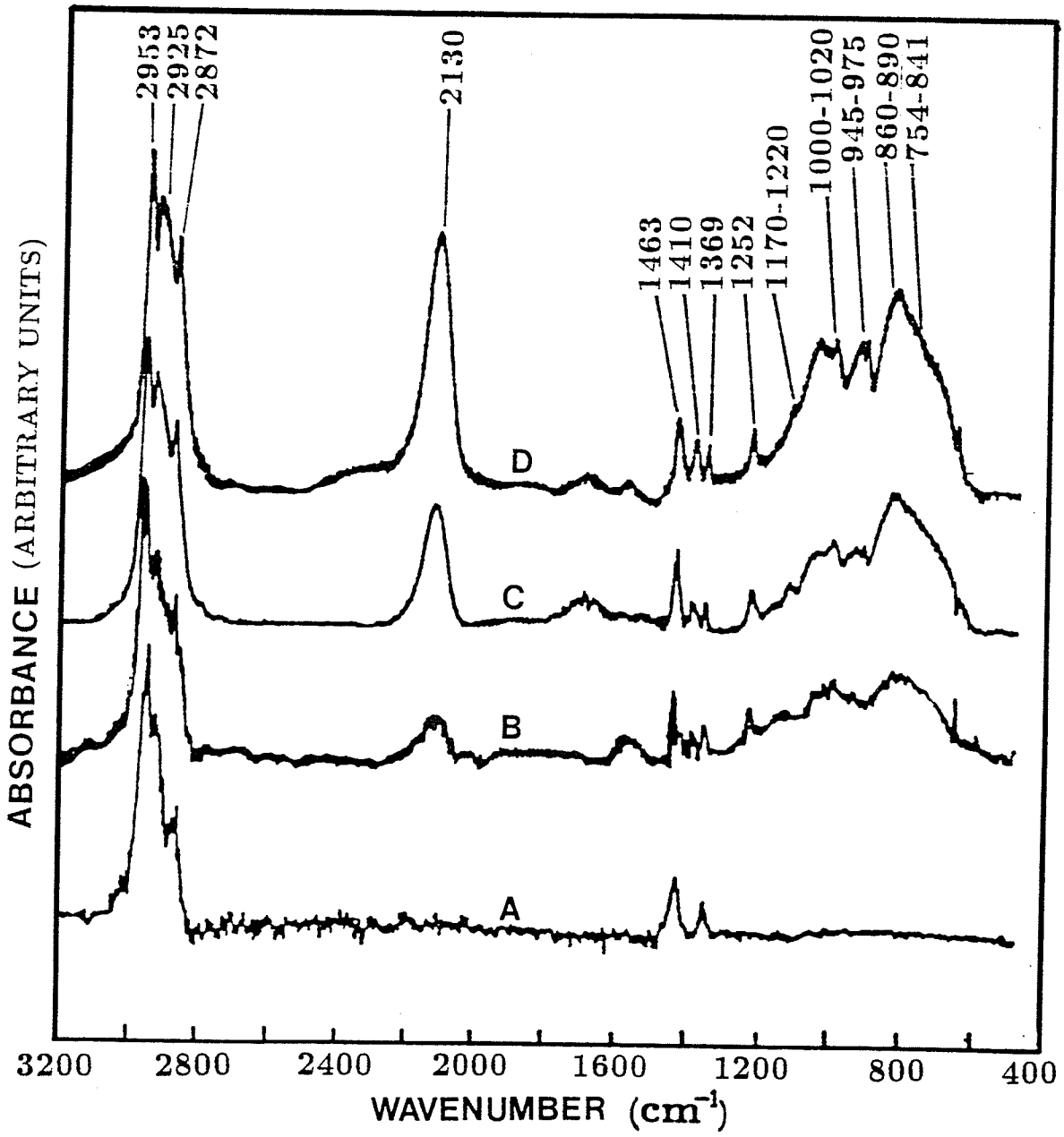


Figure 3.2: *Infra-red spectra of plasma-polymerized films: (A) ethylene only; (B) ethylene + 2.2% silane ($SiH_4/C_2H_4$=0.022); (C) ethylene + 6.6% silane ($SiH_4/C_2H_4$=0.066); and (D) ethylene + 11% silane ($SiH_4/C_2H_4$=0.11).*

Table 3.2: Assignments of Infra-red Absorption Bands

| Wave Number ( $cm^{-1}$) | Peak Assignments | References |
|---|---|---|
| 3025 | C-H stretching on $CH = CH$ | [157, 159] |
| 2953 | $CH_3$ stretching (antisymmetric) | [157, 159] |
| 2925 | $CH_2$ stretching (antisymmetric) | [157, 159] |
| 2916 | CH stretching | [159] |
| 2872 | $CH_3$ stretching (symmetric) | [157, 159] |
| 2853 | $CH_2$ stretching (symmetric) | [157, 159] |
| 2130 | $SiH_n$ stretching | [160] |
| 1463 | $CH_2$ bending | [157, 159] |
| 1410 with 960 and 1010 | $Si-CH=CH_2$ | [161] |
| 1369 | $CH_3$ bending | [157] |
| 1252 with 754-841 | $Si-CH_3$ rocking or wagging or stretching | [158, 161, 163, 165] |
| 1170-1220 | $Si - CH_2(CH_2)_xCH_3$ | [161] |
| 1000-1020 with 945-975 | $Si - CH_2 - CH_3$ | [161] |
| 860-890 | $SiH_2$ bending | [166] |

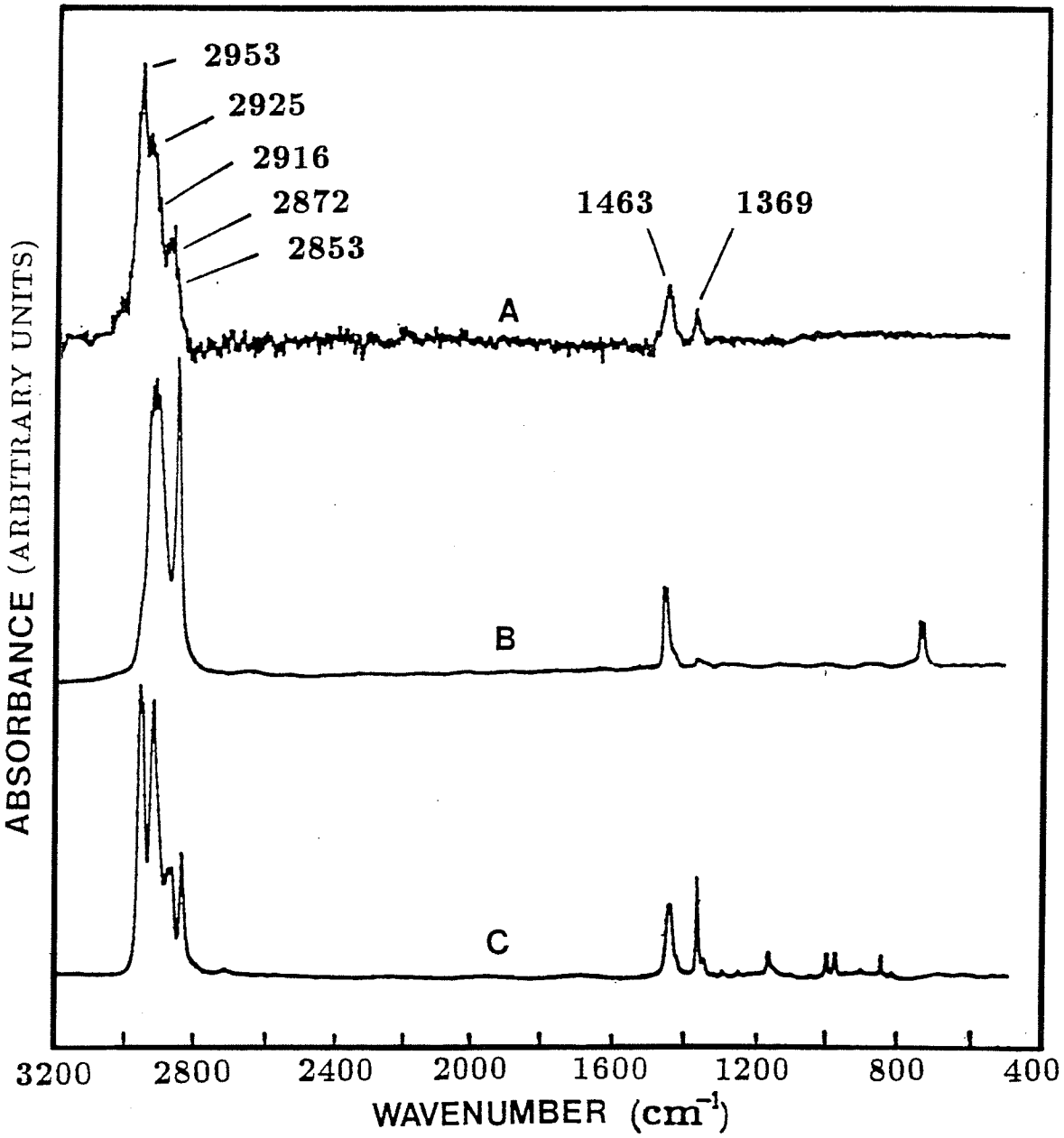


Figure 3.3: *Infra-red spectra for: (A) plasma-polymerized polyethylene; (B) conventional polyethylene; and (C) conventional polypropylene.*

antisymmetric stretching band at 2925 $cm^{-1}$, the $CH_2$ symmetric stretching band at 2853 $cm^{-1}$, the $CH_2$ bending band at 1463 $cm^{-1}$, and the $CH_3$ bending band at 1369 $cm^{-1}$. However, on a closer inspection of these spectra for wavenumbers between 2800 $cm^{-1}$ and 3000 $cm^{-1}$, and between 1300 $cm^{-1}$ and 1500 $cm^{-1}$, the relative magnitudes of the absorption peaks of the PE films are quite different from those of conventional polyethylene and polypropylene. Furthermore, the peaks at 2953 $cm^{-1}$ due to C−H stretching vibration on $CH_3$ and the peak at 2916 $cm^{-1}$ due to C−H stretching vibration on $CH_2$ appear in the spectra of the PE films and conventional polypropylene but not in conventional polyethylene, indicating that the structure of the PE films involves $CH_3$ and CH elements. It is likely that PE films have branches of $CH_3$ similar to those 2,4-dimethylpentane, 2,4,4-trimethyl-2-pentane,and 3,3-dimethylheptane. A small peak at $\sim$ 3025 $cm^{-1}$ which appears in the PE spectra is due to C−H stretching vibration, implying that the structure may also consist of double bonds (−CH=CH−) [157, 159].

The structure of the PE films definitely does not involve the saturated or unsaturated cycle alkenes and alkanes because the characteristic peaks for these elements ($\sim$ 650-1000, 1650 and 3300 $cm^{-1}$) do not appear in the spectra shown in Fig.3.3. It is most likely that the structure of these films is similar to that of the paraffin polymers in saturated hydrocarbons with normal and branched alkanes.

Unlike the conventional polyethylene produced by molecular polymerization, the PE films are formed by atomic or elemental polymerization in which the molecular structure of ethylene is not retained and the ethylene molecules serve as a source of elements used for the construction of large

molecules. This is why the structure of PE films is strongly dependent on the plasma parameters and the fabrication conditions [17, 154]. Plasma polymerization is a thermally activated chemical reaction process. Apart from the normal polymerization of $C_2H_4$ molecules to form $(CH_2)_n$, $C_2H_4$ may also be dissociated and transformed to other elements by the exothermic reaction as follows:

$$C_2H_4+H \longrightarrow C_2H_5$$
$$C_2H_5+H \longrightarrow 2CH_3$$

or dissociated by the endothermic reaction as follows:

$$C_2H_4 \longrightarrow 2CH_2$$

The exothermic reaction may occur more easily than the endothermic reactions since hydrogen atoms are usually very active chemically and react easily with hydrocarbon elements, and this is why the PE films have a high concentration of $CH_3$ elements. The absorption peak ratio $A_{1369}/A_{1463}$ (directly related to $CH_3/CH_2$ concentration ratio) for the conventional polyethylene is $\sim 0.1$ and that for the conventional polypropylene is $\sim 1.3$, as expected because an ideal polyethylene structure should not have $CH_3$ side groups, and an ideal polypropylene structure should have an $CH_3$ branch in each monomer. In PE films the $A_{1369}/A_{1463}$ ratio is $\sim 0.6$ indicating that their structure is between those of conventional polyethylene and polypropylene. Conventional polyethylene is a nonpolar material having a dielectric constant of $\sim 2.2$ and dissipation factor of $\sim 10^{-4}$ independent of frequency in the frequency range from $10^2$Hz to $10^6$Hz. The PE film have a dielectric constant of $\sim 2.8$ and a dissipation factor strongly dependent on frequency [154], in support of the fact

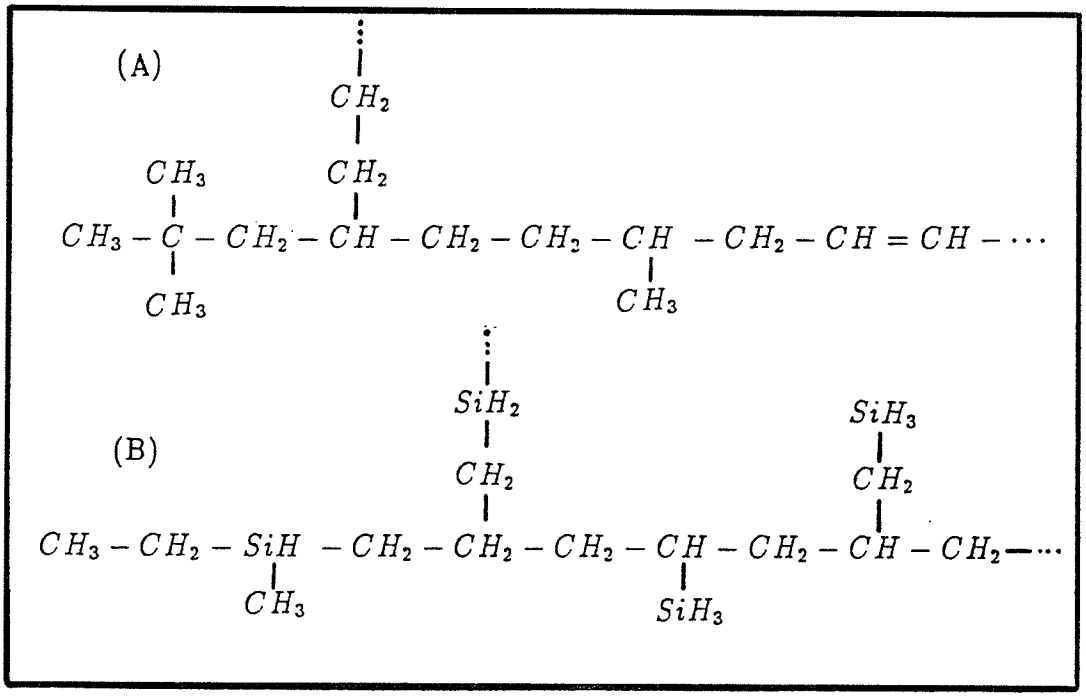


Figure 3.4: *Proposed chemical structures for: (A) plasma-polymerized polyethylene and (B) plasma-polymerized polyethylene with silicon incorporation.*

that the structure of PE films consists of antisymmetric $CH_3$ branches making it behave as a slightly polar material. On the basis of all the experimental facts we have proposed a structure for PE films and it is shown in Fig.3.4.

## 3.3 Silicon-Incorporated Polyethylene

The incorporation of silicon in plasma-polymerized polyethylene gives rise to some new absorption bands at 2130 $cm^{-1}$, 1252 $cm^{-1}$(with 750–841 $cm^{-1}$), 1170-1220 $cm^{-1}$, and 1000-1020 $cm^{-1}$ (with 945–975 $cm^{-1}$) corresponding to the band absorption of $SiH_n$, Si–$CH_3$, Si–$(CH_2)_n$ and Si–$CH_2$–$CH_3$, respectively, as shown in Fig.3.2. It can be seen that the absorption peak ratios

$A_{2950}/A_{2850}$ ($CH_3/CH_2$) and $A_{1369}/A_{1463}$ ($CH_3/CH_2$) decrease with increasing Si concentration, implying that the introduction of Si into the films enhances the formation of the $CH_2$ chains, and promotes the replacement of $CH_2$ elements with $SiH_2$ elements in the chain, and $CH_3$ elements with $SiH_3$ elements in the side groups. The bonding energies of the C−C, C−Si, C−H, Si−Si, and Si−H bonds are, respectively, 145, 104, 80, 78, and 74 Kcal/mol [162]. The higher the bonding energy, the easier the bond is formed. Comparing these elements the baning strength of C−Si bond is only second to that of C−C bonds, indicating that Si will be incorporated not only in the chain but also in the side groups. Silicon is the element that has a high tendency to stay in the solid phase. Silicon-containing compounds such as silane have a relatively high molecular weight and a relatively high vapor pressure. All these factors lead to an increase of the deposition rate with increase in the volume ratio of $SiH_4/C_2H_4$ as shown in Table 3.1.

The total absorption of an absorption band can be estimated based on its stretching mode by the following relation:

$$I = \int_{\omega} (\frac{\alpha}{\omega}) d\omega \tag{3.1}$$

where $\alpha$ is the absorption coefficient and $\omega$ the wavenumber. Obviously, I is directly related to the number of that particular bond in the film. The content of C−H bonds can be written as [163, 164]

$$N_{C-H} = K^{Str}_{C-H} I_{C-H} \tag{3.2}$$

and that of Si−H bonds as

$$N_{Si-H} = K^{Str}_{Si-H} I_{Si-H} \tag{3.3}$$

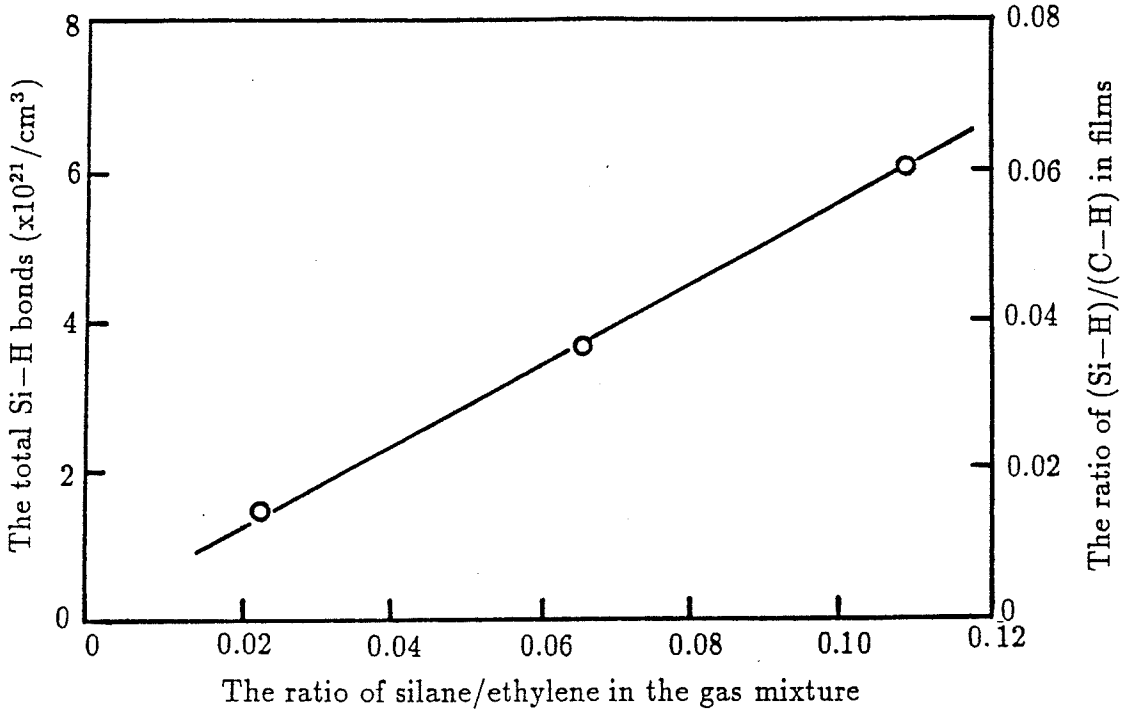


Figure 3.5: *Concentration ratio of Si−H/C−H and the total Si−H bonds in the films as functions of the ratio of silane/ethylene in the gas mixture.*

where $K^{Str}_{C-H}$=1.7×10$^{21}$cm$^{-2}$ and $K^{Str}_{Si-H}$=1.4×10$^{20}$cm$^{-2}$. The constant K for any bond can be determined using a nuclear reaction method [163], nuclear magnetic resonance and IR methods[164]. We have used equation (3.1)−(3.3) to calculate the ratio of Si−H to C−H contents and the total Si−H bonds as functions of the ratio of silane/ethylene in the gas mixture. The results are shown in Fig.3.5. The volume ratios of $SiH_4/C_2H_4$ of 0.022, 0.066, and 0.11 correspond to the ratio of Si-H/C-H bonds of 0.015, 0.035, and 0.06, respectively, in the films. On the basis of the above simple analysis and argument we have also proposed a structure for PE film with silicon incorporation as

shown in Fig.3.4.

In summary, the structure of the plasma-polymerized polyethylene films is similar to that of polyethylene with long $CH_2$ chains but also with some CH and $CH_3$ elements. The incorporation of silicon into the plasma-polymerized polyethylene introduces SiH, $SiH_2$ and $SiH_3$ elements into the structure.

# Chapter 4

## High Field Electrical Conduction and Breakdown in Pure Polyethylene[1]

A great deal of work has been done on prebreakdown and breakdown phenomena in polyethylene and other insulating polymers in bulk or film form as reviewed in Chapter 2, but little has been reported about the carrier species which leads to ageing, partial discharge and final breakdown at high fields. In the past most experiments on high-field conduction and breakdown were performed under dc, ac or impulse voltages with a metal-insulator-metal (MIM) electrode structure. In order to enable the determination of carrier species responsible for high field phenomena, we used thin polyethylene films fabricated by plasma polymerization because these films could be made very unform in thickness with a low concentration of pin holes. We adopted the techniques already used for studies of thin silicon dioxide films which are inorganic but have dielectric properties similar to organic insulating polymers. These

[1]Part of the material presented in this chapter has been published in Journal of Applied Physics, Vol.69, No.4, pp.2489-2496, (1991) [186].

techniques involve the measurements of current-voltage ($I$-$V$) characteristics using linear ramp voltages of various ramp rates, and also the measurements of the high-frequency capacitance-voltage ($C$-$V$) characteristics with a metal-polymer-semiconductor (MPS) structure. The advantages of using these techniques coupled with thin film samples are that the high electrical fields can be easily obtained at relatively low applied voltages; the surface leakage or discharge problems associated with high voltages can be avoided; and the space charge accumulated in the material can be studied.

## 4.1 Experimental Techniques

The method for the fabrication of polyethylene films on silicon substrates has been described in Chapter 3. For electrical measurements, aluminum (or gold, or silver) counter electrodes of 1000$\AA$ in thickness and each of 1.13x10$^{-2}$ cm$^2$ in area were vacuum-deposited on the polyethylene film surface through a shadow mask to form metal-polymer-semiconductor (MPS) capacitors. For current-voltage ($I$-$V$) characteristics measurements, a Hewlett Packard 4140B linear ramp voltage source with a logarithmic picoammeter was used; while for capacitance-voltage ($C$-$V$) characteristics measurements, a Boonton capacitance meter operating at 1 MHz and a Keithley 601 electrometer were used in conjunction with a linear ramp voltage souse as shown in Fig. 4.1. All $I$-$V$and $C$-$V$measurements were performed at room temperature (22°C). The thickness of the polyethylene films used for this investigation was 1000$\AA$. The film thickness was measured with a Varian $\AA$-scope interferometer (model 980-4000/4006) and checked by ellipsometry.

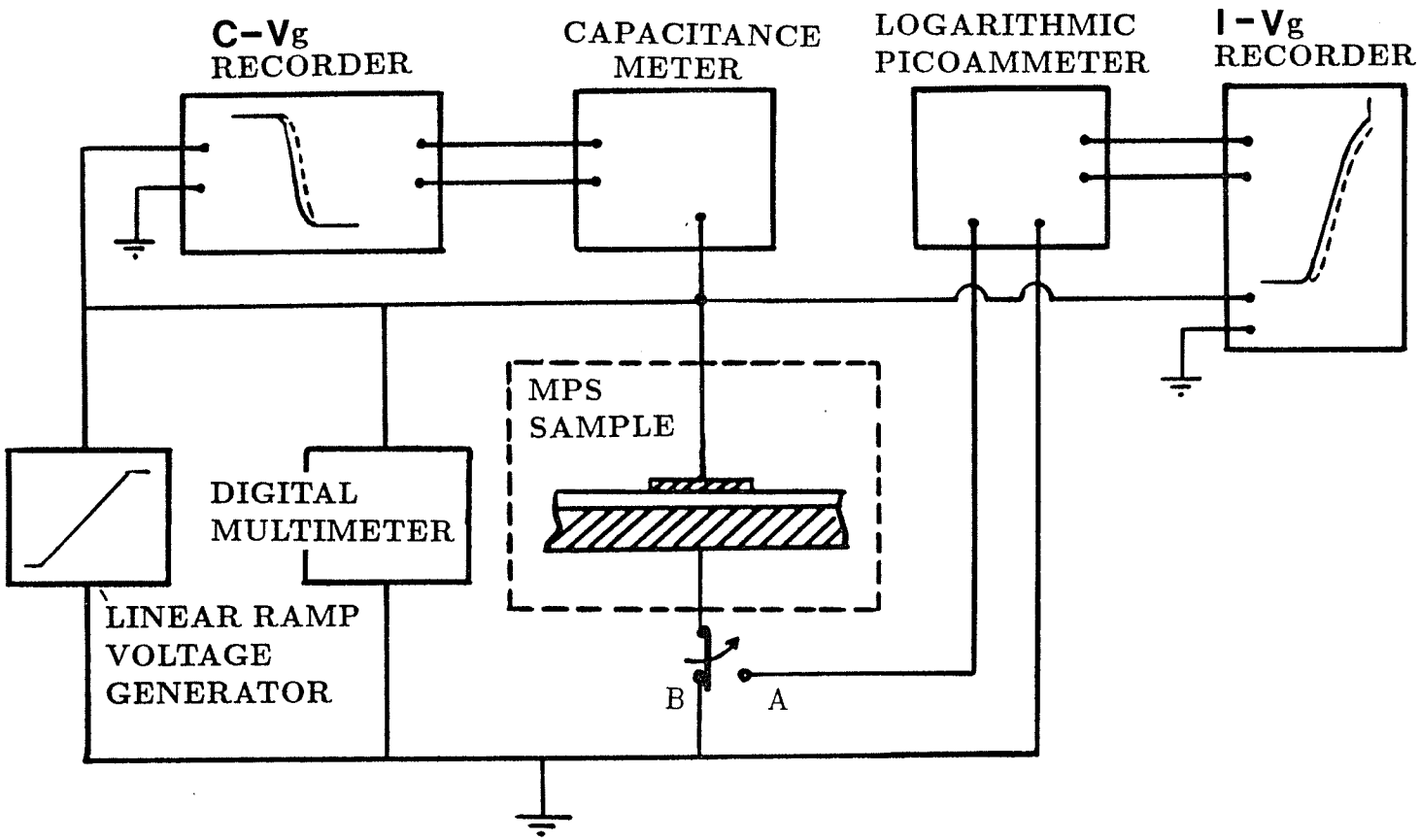


Figure 4.1: *Experimental setup for the measurements of the ramp current-voltage (I-V) and capacitance-voltage (C-V) characteristics. Switch at A for I-V and switch at B for C-V measurements.*

## 4.2 High Field Conduction Model

To study electrical transport in any material, it is important to consider first the chemical structure of the material. Polymers, in general, can be classified into two major categories, namely the conjuncted polymers and the saturated (or paraffin) polymers. For the former the overlap integral between adjacent chains (or molecules) is about 0.01 eV [35], while for the latter it is about 0.001 eV [35]. This implies that the intermolecular bonding or interaction for these materials is weak and the bandwidth is less than kT [167]. In other words, the usual concept of the band theory cannot be applied to these materials for at least electron transport in the conduction band. However, for saturated polymers such as polyethylene the intramolecular interaction within a chain (or a molecule) is strong and the bonding is covalent with monomers regularly arranged. In this case the overlap integral between monomers in a chain (or a molecule) is sufficiently extensive for the valence band to acquire an appreciable width. The band structure of an ideal polyethylene chain has been calculated by several investigators [35,167-170]. McCubbin and Gurnay [35] have reported that on the basis of their calculation the upper edge of the valence band of an ideal polyethylene chain is located at about $-10$ eV and the bandwidth is about 10 eV. They have also estimated the hole effective mass and the hole mobility to be about $0.1m_o$ and 50 $cm^2/V$ s, respectively, for an infinite ideal polyethylene chain, where $m_o$ is the rest electron mass. The chemical structure of our plasma-polymerized polyethylene films is not exactly the same as that of the ideal polyethylene, but the major parts are similar as discussed in Chapter 3. In fact, chemically polymerized and plasma-

get 0.92 probability of accretive recall even when $P_e$=0.2. BAM's error correction performance did not show much difference in both accretive and interpolative recall cases compared with the Hopfield network.

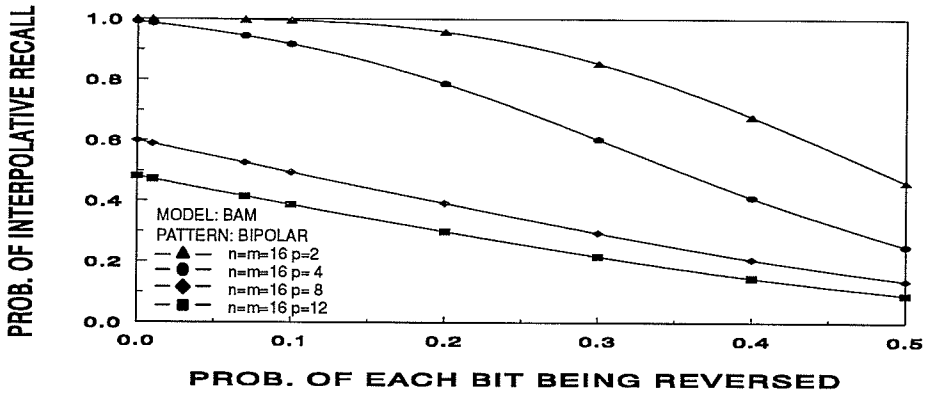


**Fig. 3.15** The error correction capability of BAM (interpolative recall). Memory configuration: $n$=16 and $m$=16. Memory load: $p$ = 2, 4, 8, and 12.

(3) *The effect of input and output pattern dimensions on accretive recall*

In order to test this property, one more BAM model was added. This model contained eight neurons in both input/output ports. Test results show that the input and output pattern dimensions only affects accretive recall. The effect of input and output pattern dimensions on other aspects is not obvious. Those results are omitted here. The effect on accretive recall was quantitatively calculated according to Eqn. (2.7) (refer to section 2.2.3 in chapter 2 for details) and the corresponding results are shown in Fig. 3.16.

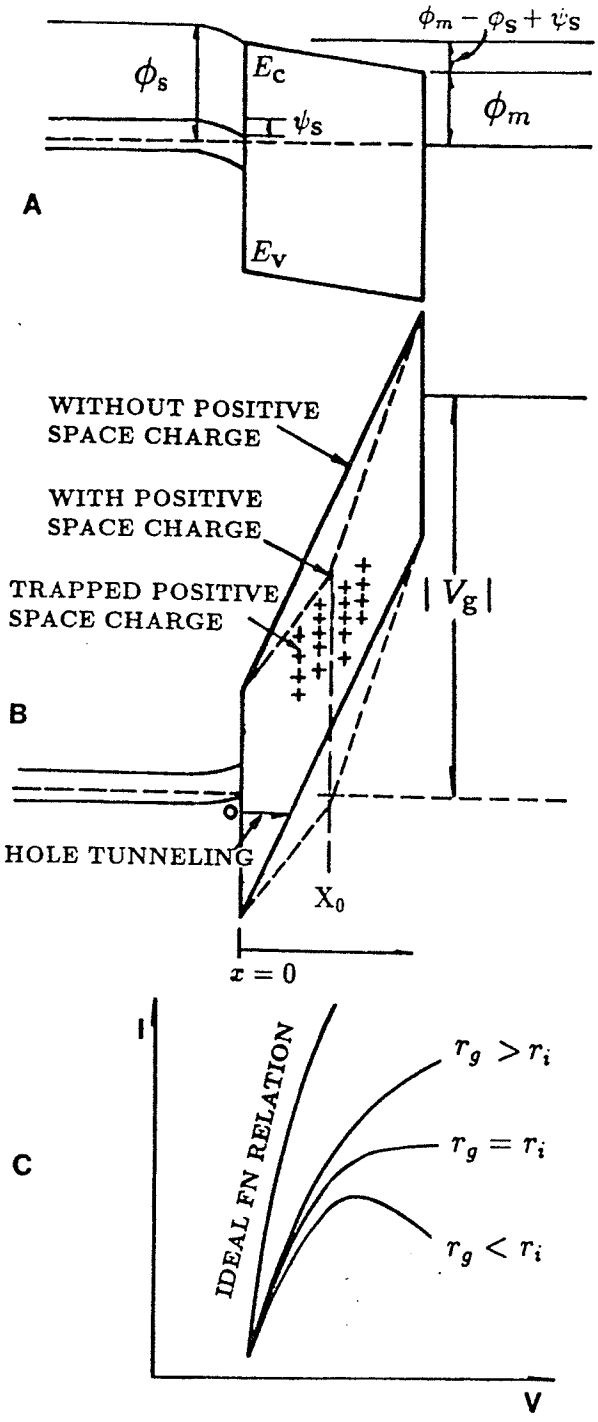


Figure 4.2: *Schematic diagrams illustrating: (A) the energy-band diagram in the absence of applied bias; (B) the build-up of trapped hole space charge and its effect on potential distribution; and (C) the I–$V_g$ characteristics under various trapping conditions.*

than the threshold field for hole injection, electrons are the dominant carriers contributing to dark conduction. But due to the low mobility of electrons, the conductivity is very small as generally reported in the literature.

It should be noted that unlike the injected electrons which may be immediately trapped near the cathode to form a homo-space charge suppressing further electron injection, the injected holes may travel quite a distance before being effectively trapped because they travel in a wide valence band with a relatively high mobility. In practical cases, the polyethylene chains are not long enough to bridge the electrodes. Therefore, holes moving as free carriers in the chains have to tunnel from chain to chain to maintain a continuous current flow from the anode to the cathode.

All polymers contain various kinds of unavoidable impurities and structural defects which form traps located in the energy band gap. Also, the electrode surfaces in contact with the polymer have unavoidable asperities and possible contamination. Thus, the effects of trapped carrier space charge and electrode surface conditions can not be ignored. It is most likely that at fields higher than the threshold field for hole injection, the conduction is filamentary because the electrode surface is not microscopically identical in asperity and surface condition from domain to domain. There may be one or more microregions in which the potential barrier has a barrier profile more favorable for carrier injection than that in other regions. Furthermore, the polymer sample itself is never homogeneous. Because of all these unavoidable nonuniformities the field, F, is not uniform longitudinally due to the space charge effects and the current density is not uniform radially due to the filamentary current flow. Filamentary conduction has been fully discussed by Mizutani et

al.[83], Barnett and Milnes [171] and Kao[172].

In a filament the current density is highest at the center and decreases with radial distance. For simplicity we assume that the hole current $I$ in one major filament can be written as:

$$I = \pi r^2 J_o, \tag{4.1}$$

where $J_o$ is the maximum current density at the center of the filament and $r$ is the effective radius of the filament so chosen that the total current in the filament is equivalent to a current flowing uniformly through the filament with a cross section area of $\pi r^2$.

In the following, we shall present our simple analysis for the ramp $I$-$V$characteristics for polyethylene films. For the case with the gate biased at a negative voltage and the $p$-silicon grounded as shown in Fig. 4.2, the MPS capacitor is in the accumulation mode. In the absence of trapped space charge and with the image effect ignored, the field at the hole-injecting contact (the anode), $F_a$, is given by [173-175]

$$F_a = \frac{\mid V_g \mid + \phi_{ms} + \psi_s}{d}, \tag{4.2}$$

where d is the thickness of the polyethylene film, $\phi_{ms}$ is the work function difference between the metal and $p$-silicon ($\phi_m - \phi_s$) which is always negative because $\phi_s$ is always larger than $\phi_m$, $\psi_s$ is the surface potential which should be very small as compared with $\mid \phi_{ms} \mid$ and practically independent of the magnitude of the negative gate voltage. In this case $F_a$ is generally smaller than the apparent average field $F_g = \mid V_g \mid /d$. Considering one major current filament, at fields ($F_a$) higher than the threshold fields for hole injection at

the injecting contact, the current should follow the Fowler-Nordheim (FN) relation

$$J_o = aF_a^2 exp(-\frac{b}{F_a}), \tag{4.3}$$

where $a$ and $b$ are the constants depending on the potential barrier profile at the hole-injecting contact. However, as soon as the hole injection starts, some holes will be trapped in traps inside the polyethylene forming a positive trapped space charge which creates an internal field, $F_i$, opposite to the applied field, thus reducing the effective field at the injecting contact.

For simplicity, we use a simple first order trapping model to describe the effects of the trapped space charge. The trapping rate can be written as [176]

$$\frac{dp_t}{dt} = \frac{\sigma J_o}{q}(N_t - p_t), \tag{4.4}$$

where $p_t$ and $N_t$ are the filled and the total hole traps densities, respectively, $\sigma$ is the trap cross section, and $q$ is the electronic charge. Using the boundary condition, $p_t$=0 at t=0, the solution of Eq.(4.4) gives

$$p_t = N_t \left[1 - exp\left(-\frac{\sigma}{q}\int_0^t J_o dt\right)\right]. \tag{4.5}$$

The internal field $F_i$ can be obtained by solving the Poisson equation, which is given by [177, 178]

$$F_i = \frac{Q_t}{\varepsilon_p}\left(1 - \frac{X_0}{d}\right), \tag{4.6}$$

where $\varepsilon_p$ is the permittivity of the polyethylene film, $X_o$ is the centroid of the trapped space charge distributed in the polyethylene film measured from the injecting contact as shown in Fig. 4.2, and $Q_t$ is the total trapped charge

which is given by

$$Q_t = q\int_o^d p_t dx = qN_t d\left[1 - exp\left(-\frac{\sigma}{q}\int_o^t J_o dt\right)\right]. \tag{4.7}$$

Once the trapped space charge is formed, the effective field at the injecting contact becomes

$$F_a = \frac{\mid V_g \mid + \phi_{ms} + \psi_s}{d} - F_i. \tag{4.8}$$

The rate of the change of $F_a$ is

$$\frac{dF_a}{dt} = \frac{dF_g}{dt} - \frac{F_i}{dt}. \tag{4.9}$$

For linear ramp voltages

$$\frac{dF_g}{dt} = r_g. \tag{4.10}$$

Eq.(4.9) can be written as

$$\frac{dF_a}{dt} = r_g - r_i, \tag{4.11}$$

where $r_i$ can be written as

$$r_i = \frac{dF_i}{dt} = \frac{d}{dt}\left[\frac{Q_t}{\varepsilon_p}\left(1 - \frac{X_0}{d}\right)\right] = \frac{1}{\varepsilon_p}\left(1 - \frac{X_0}{d}\right)\frac{dQ_t}{dt} - \frac{Q_t}{\varepsilon_p d}\frac{dX_0}{dt}. \tag{4.12}$$

The first term on the right-hand side of Eq.(4.12) is always larger than the second term. Thus $r_i$ is always positive and $dF_a/dt < r_g$, always holds. This is why the experimental ramp $I$-$V$curve deviates from the trap-free FN $I$-$V$curve if $I$ is plotted versus $F_g$ $(= V_g/d)$. Since

$$\frac{dQ_t}{dt} = N_t d\sigma J_o exp\left(-\frac{\sigma}{q}\int_o^t J_o dt\right), \tag{4.13}$$

Eg.(4.12) can be simplified to

$$r_i = \frac{dF_i}{dt} = \frac{qN_f}{\varepsilon_p}\left\{\left[\frac{\sigma J_o}{q}(d - X_0) + \frac{dX_0}{dt}\right] exp\left(-\frac{\sigma}{q}\int_o^t J_o dt\right) - \frac{dX_0}{dt}\right\}. \tag{4.14}$$

There are three cases

(i) $r_g > r_i$, the injection current, $I$, always increases with increasing $F_g$.

(ii) $r_g = r_i$, the injection current, $I$, becomes saturated since $r_i$ is a function of $J_0$. If $r_i$ does not change very much after it reaches the value equal to $r_g$, then $I$ would remain constant or not change very much, forming a ledge of the $I$-$V$curve within a certain range of $F_g$.

(iii) $r_g < r_i$, if both $N_t$ and $\sigma$ are large, $X_0$ may move toward the injecting contact as $t$ is increased. In this case, $I$, after reaching its peak value, may decrease with increasing $F_g$, forming a negative differential resistance region.

These three cases are depicted schematically in Fig. 4.2(c). However, as can been seen from Eq.(4.14), $r_i$ is controlled by many parameters. We shall further discuss the implication of $r_i$ on the $I$-$V$characteristics in the following section. If $N_t$ is uniformly distributed in space, it is likely that the first group of holes moving toward the metallic cathode will be trapped somewhere forming a first sheet of space charge which then tends to retard the on-coming subsequent groups of holes, thus enhancing gradually their interaction with bulk traps. In other words, the bulk traps are gradually filled starting from the first sheet of trapped hole space charge toward the injecting contact as shown in Fig. 4.2. We believe that the centroid of the trapping charge $X_o$ is not constant, but moves toward the injecting contact as the applied gate voltage is increased. For linear ramp voltages, $dX_0/dt$ should be always negative. This makes $r_i$ increase with increasing injection current level.

It should be noted that an increase in applied field not only enhances hole injection and trap filling but also creates new traps [119, 179]. It can be

imagined that each hole trapping event will evolve an energy of the order of 2~5 eV depending on the trap energy levels. This energy, if not converted to light emission, will be dissipated in the material in the form of breaking bonds and hence creating defects or traps[119]. As has been mentioned, the conduction is filamentary, and the current density in the filament is definitely much higher than the average density taken as the total current divided by the electrode area. Depending on the material and the concentration of traps, the current density in the major filament in many materials, particularly in polymers, may reach a level to cause thermal instability prior to the complete filling of all traps. In this case destructive breakdown is initiated by thermal instability which then creates low-density regions to provide long mean free paths for subsequent impact ionization leading to an abrupt increase in conduction current and final breakdown along the major filament.

## 4.3 Results and Discussion

At average fields $F_g$ lower than 1 MV/cm hole injection may be considered to be negligibly small as compared with electron injection in polyethylene because of the big difference between the electron and the hole injection barriers. However, as $F_g > 1$ MV/cm the injected hole current becomes dominant because $\mu_p p \gg \mu_n n$, where $n$, $p$, $\mu_n$ and $\mu_p$ are, respectively, electron and hole concentrations and electron and hole mobilities. Typical $I - V_g$ (plotted in $I - F_g$, where $F_g$ is the average field equal to $V_g/d$) characteristics are shown in Fig. 4.3. It can be seen that the $I - F_g$ curve is smooth and repeatable if there is no internal discharge or pin holes are tiny and their concentration is low so that they are not operative. For those samples containing defects,

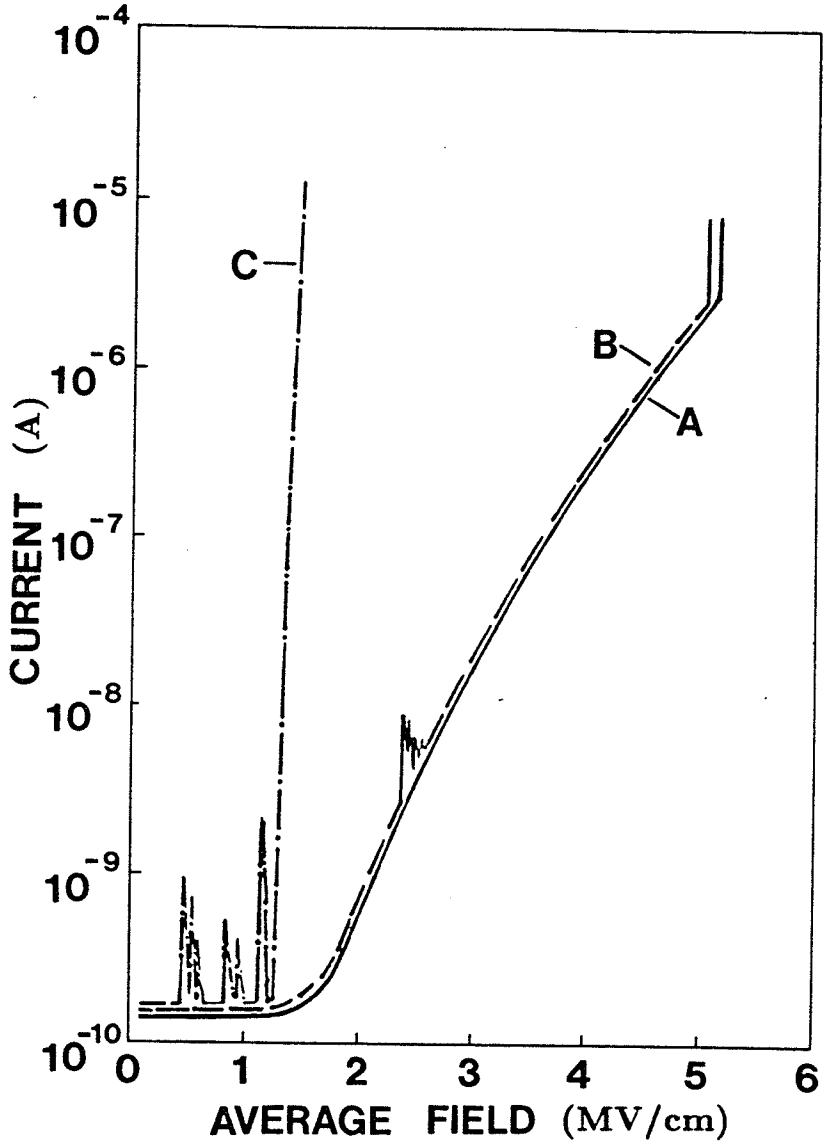


Figure 4.3: *Typical current-average field ($I$-$F_g$) characteristics for polyethylene films: (A)without internal discharge, (B)with some self-healing points, and (C)with internal discharge. Gate electrode: Al; gate bias:$-V_g$; ramp rate: 0.06 MV/cm s.*

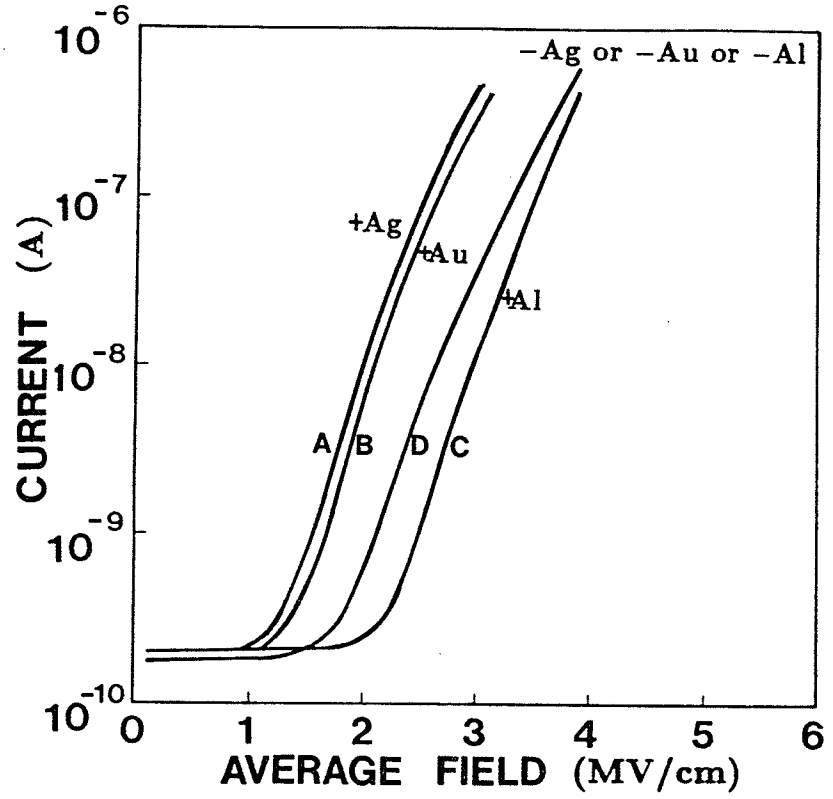


Figure 4.4: *Current-average field ($I$-$F_g$) characteristics as functions of gate electrode material. (A) +Ag gate electrode, p-Si substrate; (B) +Au gate electrode, p-Si substrate; (C) +Al gate electrode, p-Si substrate; and (D) −Ag, or−Au, or −Al gate electrode, p-Si substrate. Ramp rate: 0.06 MV/cm-s.*

current jumps occur on the $I - F_g$ as shown in Fig. 4.3. To determine the type of the dominant injected carriers, we used type A sample and various gate electrode materials deposited on the same polyethylene film to form MPS capacitors, so that all capacitors were practically identical except the gate electrode material. Figure 4.4 shows that the $I - F_g$ curve depends on the gate electrode material if the gate is biased at the positive polarity but it is independent of electrode material if the gate is biased at the negative polarity, indicating that the current is mainly hole current and controlled by the

efficiency of hole injection from the injecting contact. The dependence of the threshold field for hole injection on the gate electrode material agrees qualitatively with the barrier height for hole injection to polyethylene. The barrier heights for electron injection are 3.1 eV, 4.1 eV and 4.2 eV for Al, Au and Ag, respectively, determined by photoemission [180-182]. It should be noted that for hole injection the barrier height should be approximately equal to the energy gap minus the barrier height for electron injection; the latter is proportional to the work function.

When a linear voltage ramp is applied to the gate, the current is constant up to the threshold field for hole injection. This current is the displacement current due to $C(dV_g/dt)$ where $C$ is the total capacitance of the MPS capacitor. At field higher than the threshold field for hole injection, the conduction current is due mainly to hole injection following the Fowler-Nordheim (FN) type of $I - F_a$ relation. As has been mentioned in the last section, the field at the injection contact $F_a$ for the ideal case without traps is approximately equal to the average applied field $F_g$, and the $I - F_g$ current follows closely the FN relation as shown in Fig. 4.5. However, for the practical case with traps, $F_a < F_g$ because of the internal field $F_i$ created by the trapped hole space charge which is opposite to $F_g$. The effective field at the injecting contact is equal to $F_a = F_g - F_i$. According to Eqs.(4.6) and (4.14), $F_i$ increases with increasing time since $F_g = r_g t$. Our experimental results agree semi-quantitatively with the theory as shown in Fig. 4.5. At a given $F_g$, the lower the ramp rate, the higher the internal field is created, because more carriers are trapped. This ramp-rate effect is also shown in Fig. 4.5.

In order to study the hole trapping process in some detail, we have

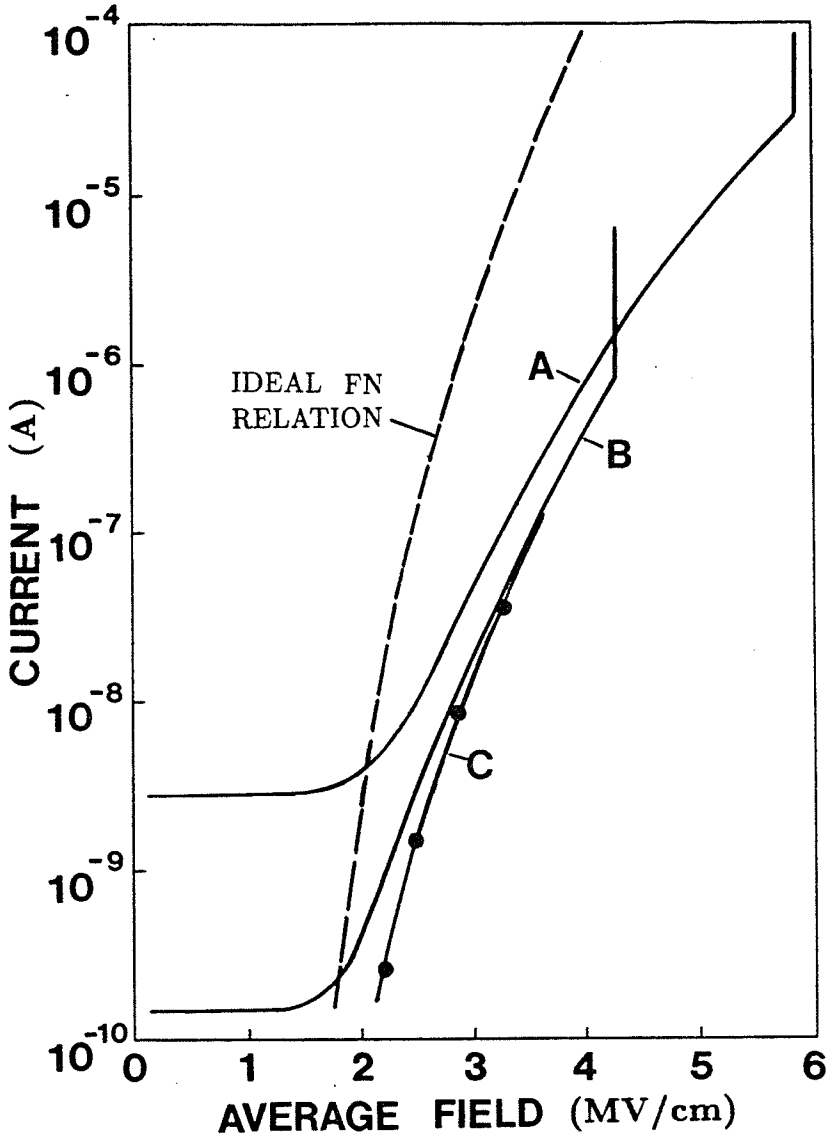


Figure 4.5: *Current-average field ($I$-$F_g$) characteristics for (A) ramp rate: 0.6 MV/cm s; (B) ramp rate: 0.06 MV/cm s; and (C) dc voltage. Gate electrode: Al; gate bias:$-V_g$.*

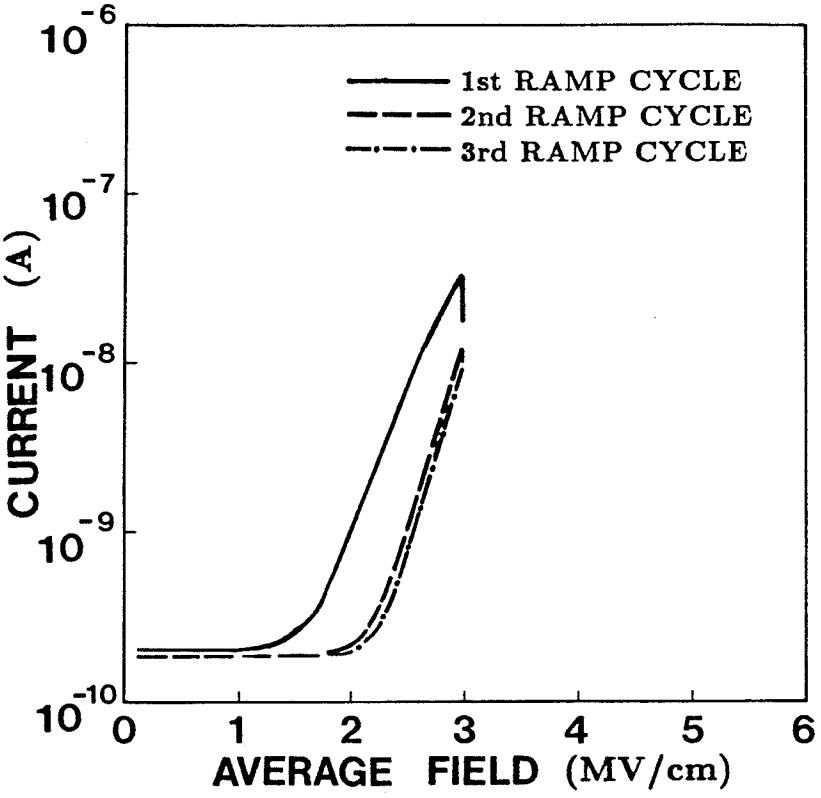


Figure 4.6: *Change of the I-$F_g$ curves when the ramp is stopped at 3 MV/cm and this field is kept constant for 20 seconds. Gate electrode: Al; gate bias:$-V_g$; ramp rate: 0.06 MV/cm s.*

used the following experimental procedure to reveal the effect of the electrical stressing time on the $I - F_g$ and $C - F_g$ characteristics. After a virgin MPS capacitor is stressed with a first cycle of linear voltage ramp at 0.06 MV/cm s until it reacher 3 MV/cm and then held there for 20 seconds, the current decreases with time during this time as shown in Fig. 4.6, indicating that the trapped charge and hence the internal field build-up at 3 MV/cm with time. However, in the second cycle of the voltage ramp stressing, the $I - F_g$ curve shifts to the right-hand side of the first one, indicating that most traps

may have been filled so that $F_a = F_g - F_i$ decreases very little with time at $F_g$=3MV/cm and so does the current. In the third and the fourth cycle $I$-$F_g$curves are almost identical, indicating that the trap filling may have reached a dynamic equilibrium. In this case $F_a = F_g - F_i$ is constant and the current remains unchanged with time at $F_g$=3 MV/cm as shown in Fig. 4.6. If the ramp rate during the first cycle of stressing to a virgin MPS capacitor is suddenly changed from 0.06MV/cm s to 0.0006 MV/cm s when $F_g$ reaches 2 MV/cm, the current decreases with increasing $F_g$ for $F_g$ >2 MV/cm because of the low ramp rate as shown in Fig. 4.7. In the second cycle with the change of the ramp rate made at 2.5 MV/cm, the current still decreases with increasing $F_g$ for $F_g$ >2.5 MV/cm, but the rate of this current decrease is smaller than that in the first cycle. In the third cycle with the change of the ramp rate made at 3.5 MV/cm, the rate of the current decrease is much smaller than that in the first and the second cycle. These results indicate clearly that the amount of holes being trapped and the build-up of the internal field increase with increasing electrical stress and stressing time.

We have also measured the high frequency (1MHz) $C - F_g$ characteristics using the voltage ramp to sweep from accumulation mode to inversion mode (between $F_g = 2MV/cm$ to $F_g = -2MV/cm$) at the ramp rate of 0.06 MV/cm s. Typical $C - F_g$ curves on a virgin MPS capacitor sweeping from $F_g$=0.5 MV/cm to $F_g$=−1.5 MV/cm and then from $F_g = -1.5MV/cm$ back to $F_g$=0.5 MV/cm are shown in Fig. 4.8(b). In the first cycle of sweeping the $C - F_g$ curves (branch 1 and 2) form a hysteresis loop, indicating that there must be some positive charge introduced in the bulk of the polyethylene film during the branch 1 of the sweeping cycle. In polyethylene films the field

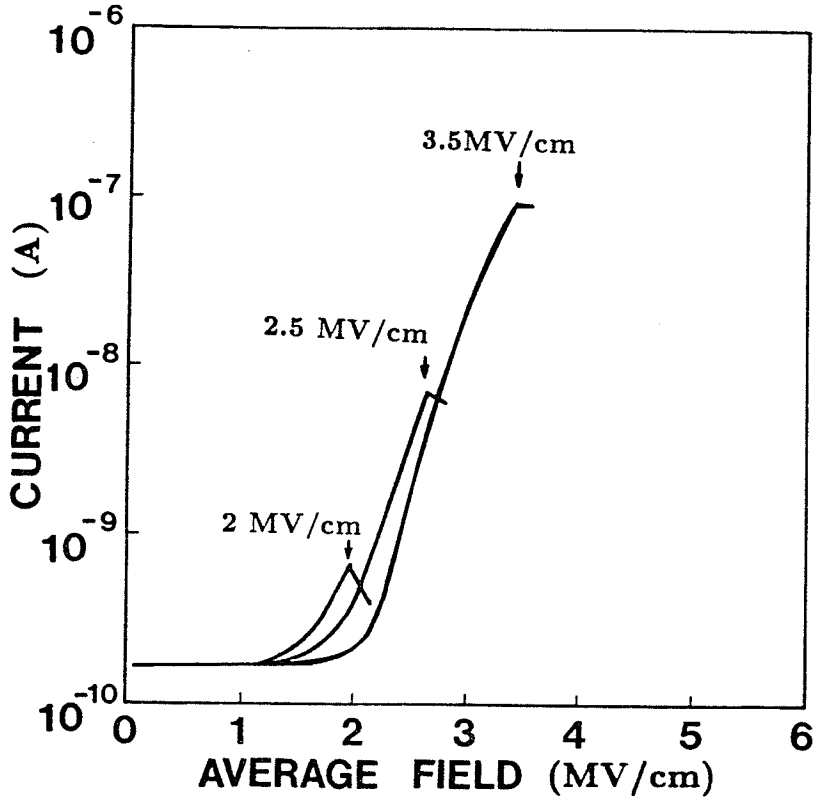


Figure 4.7: *Change of the I-$F_g$curves when the ramp rate of 0.06 MV/cm-s is suddenly changed to 0.0006 MV/cm-s at 2MV/cm in the first cycle, at 2.5 MV/cm in the second cycle and at 3.5 MV/cm in the third cycle. Gate electrode: Al; gate bias:$-V_g$; ramp rate: 0.06 MV/cm-s.*

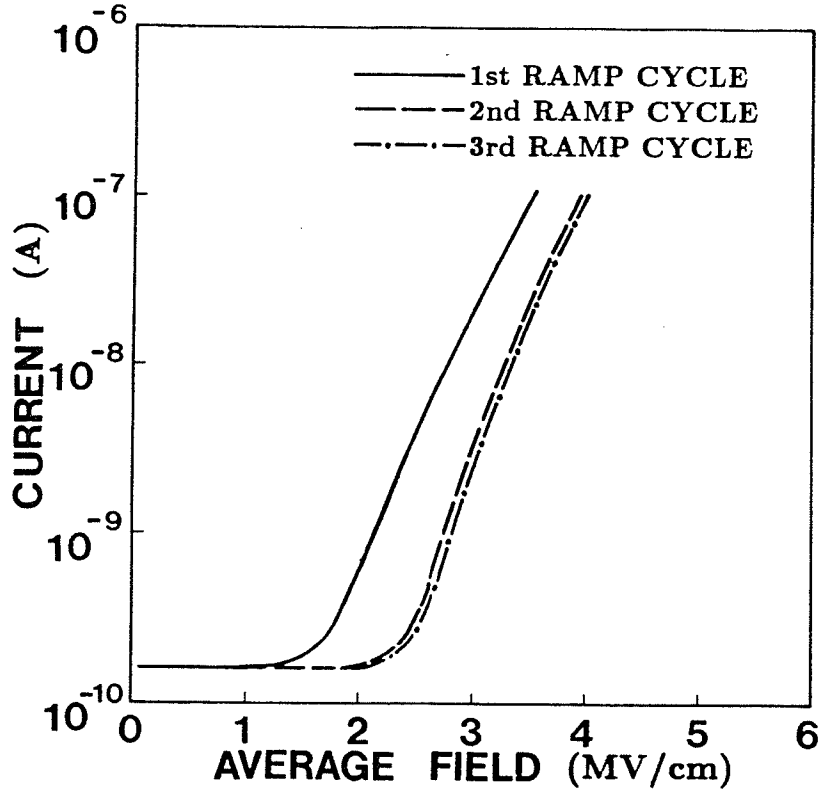


Figure 4.8(a)

Figure 4.8: *Effects of the ramp voltage stressing on (a) the current-average field ($I - F_g$) characteristics and (b) the corresponding capacitance-average field ($C - F_g$) characteristics. Gate electrode: Al; gate bias:$-V_g$; ramp rate: 0.06 MV/cm s.*

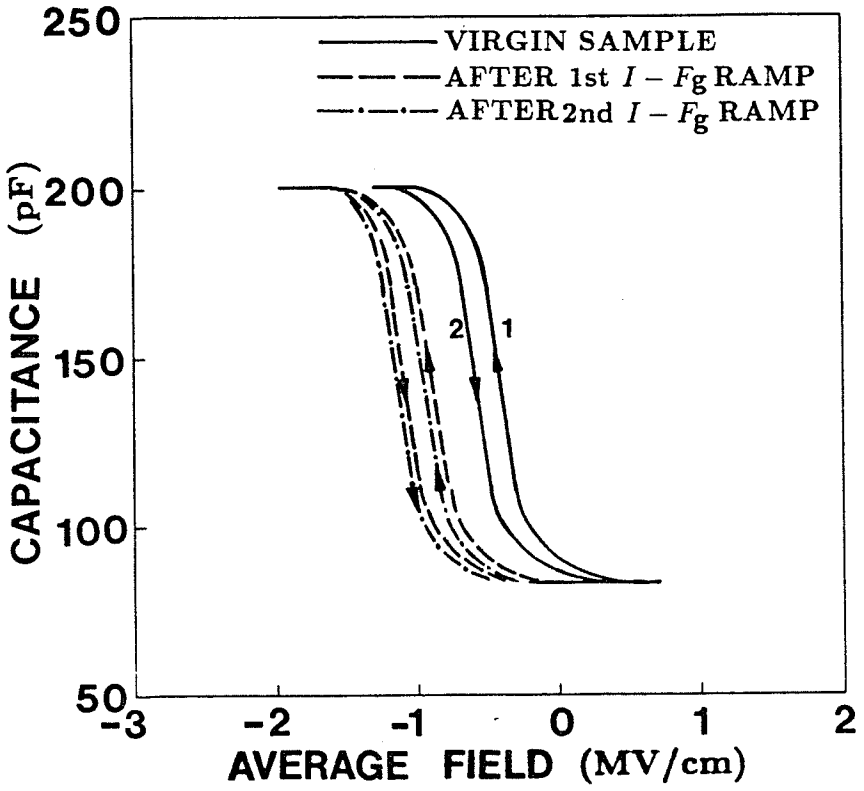


Figure 4.8(b)

required to make the MPS capacitor in the accumulation mode is about the same as the threshold field for the hole injection. This is why some holes will be injected in the film and trapped there at $F_g \geq -1.5$ MV/cm. After the first cycle of $C - F_g$ measurements, the MPS capacitor was then stressed with a first cycle of voltage ramp at 0.06 MV/cm s. Then second $C - F_g$ hysteresis loop was immediately measured right after that, and also immediately followed with a second cycle of voltage ramp stressing. This procedure was repeated several times. The $I - F_g$ and the corresponding $C - F_g$ characteristics are shown in Fig. 4.8. It can be seen that there is a shift in both the $I - F_g$ and $C - F_g$ curves after the first stress cycle, but this shift gradually diminishes in the second and further cycles, indicating that the filling of bulk traps may

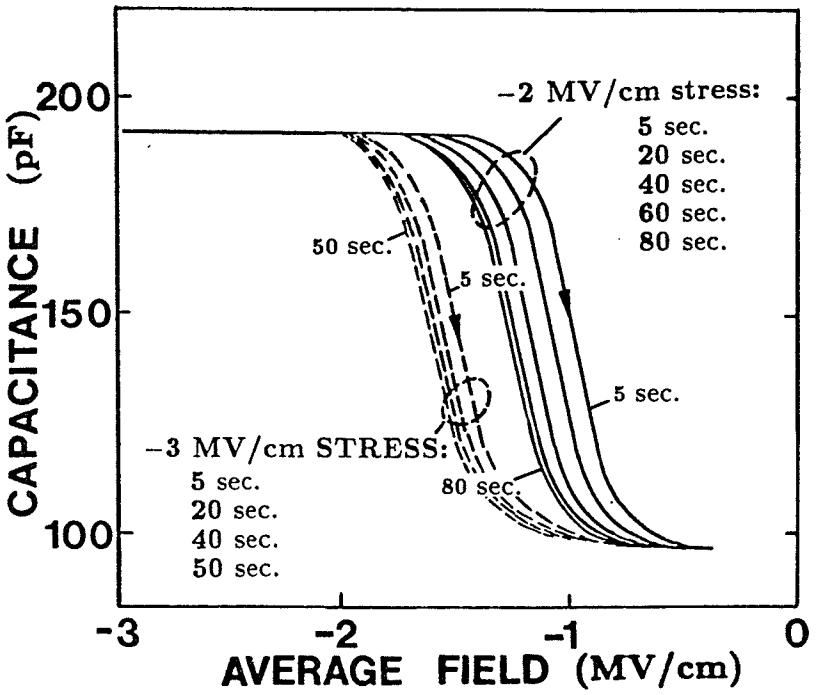


Figure 4.9: *Effects of prestressing field and duration on the C–$F_g$ characteristics. Gate electrode: Al; gate bias:–$V_g$; ramp rate: 0.06 MV/cm-s.*

have reached a dynamic equilibrium unless the stressing field or the stressing time is increased. Figure 4.9 shows clearly that the amount of holes being trapped to form a positive space charge depends on both the prestressing field and the prestressing time. In this case only the sweep direction from the negative to the positive gate voltage was used. It should be noted that the sweep of the gate voltage from the negative to the positive may introduce positive trapped charge in the bulk by hole injection from *p*-Si at the field in the accumulation mode, and the sweep in the reverse direction will reduce the positive trapped charge in the bulk near the polymer-semiconductor interface at the

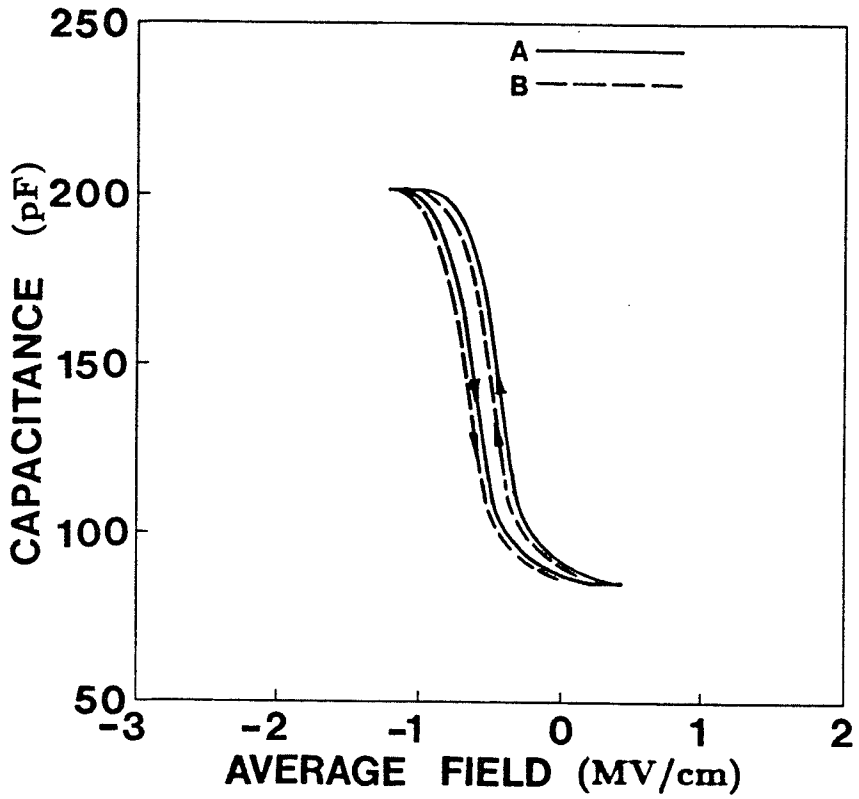


Figure 4.10: *Counterclockwise hysteresis loop of C-$F_g$ curves: (A) sweeping from the +gate voltage to the −gate voltage and then back to the +gate voltage; (B) sweeping from the −gate voltage to the +gate voltage and then back to the −gate voltage. Gate electrode: Al; ramp rate 0.06 MV/cm s.*

gate voltage in the inversion mode at which some positive trapped charge may be neutralized by electrons injected from the p−Si. This is why the hysteresis loops overlap between the second and the third cycles of prestressing as shown in Fig. 4.8(b), and this is also why the hysteresis loop always runs counter-clock wise regardless of the sweep direction, i.e., sweep direction staring either from the positive gate voltage or from the negative gate voltage, as shown in Fig. 4.10.

There are two basic mechanisms which may lead to the hysteretic be-

havior of the $C$-$V$curves, and they are the charge injection from the injecting contact and the mobile charge movement in the bulk. For the case due to the charge injection, the negative gate voltage ($V_g$) will introduce the positive charges at the polymer-semiconductor interface, shifting the $C$-$V$curve to the left in the $C$-$V$plot (see branch 2 in Fig. 4.8(b)); and positive $V_g$will introduce the negative charges (or neutralize some positive charges) at the polymer-semiconductor interface, shifting the $C$-$V$curve to the right (see branch 1 in Fig. 4.8(b)). Thus, these two branchs will form a counterclockwise hysteresis loop. For the case due to mobile charge movement, the negative gate voltage ($V_g$) will attract the positive charges away from the polymer-semiconductor interface, shifting the $C$-$V$curve to the right; and positive $V_g$will push the positive charges towards the polymer-semiconductor interface, shifting the $C$-$V$curve to the left. Thus, these two branchs will form a clockwise hysteresis loop. The present results indicate that the hole injection process is the dominant process under high fields in polyethylene.

The average breakdown strength depends on the ramp rate of the applied voltage ramp. The slower the ramp rate, the lower is the breakdown strength as shown in Fig. 4.5. Figure 4.11 shows the breakdown site on the polyethylene film surface at the gate after the removal of the aluminum gate electrode under a microscope of magnification X400. The average size of the breakdown channel has been estimated to be about 10 $\mu$m in diameter. This can be considered as an indirect evidence that high-field conduction is filamentary. Supposing that the current filament which leads to final destructive breakdown is the filament carrying the majority of the total current, then we can estimate roughly the current density of this filament. For the filament size

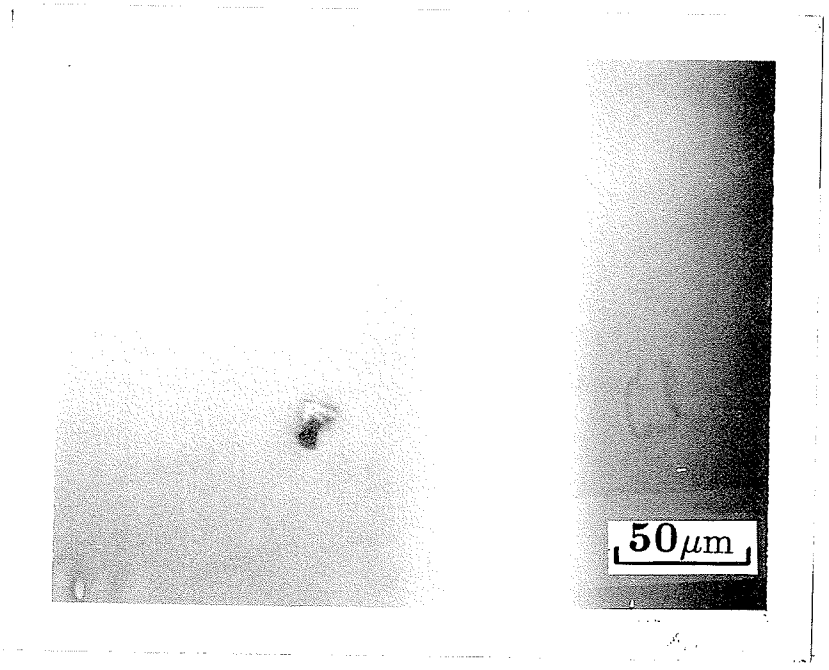


Figure 4.11: *Photograph illustrating the size of the breakdown channel on the polyethylene film surface.*

of 10 $\mu$m in diameter, the current density may reach 1 A/cm$^2$. The energy stored in the filament at the current corresponding to an average field of 4 MV/cm is approximately equal to 4MW/cm$^3$. This energy is much more than the energy required to cause thermal instability. We believe that destructive breakdown is initiated by thermal destruction and followed by the creation of low-density regions which provide large mean free paths for subsequent impact ionization leading to a sharp increase in current at the breakdown field. There is no evidence of impact ionization prior to the occurrence of thermal instability. That the breakdown strength decreases with the decrease of the applied voltage ramp rate as shown in Fig. 4.5 is consistent with the above argument.

In summary, the high-field conduction in polyethylene is due to holes injected by Fowler-Nordheim type of tunneling from the injecting contact to the polyethylene through a potential barrier. The deviation of the experimental $I$-$V$ characteristics from the trap-free FN relation is due to the trapped hole space charge which creates an internal field opposite to the applied field. The experimental results agree well with theoretical predication. The high hole current density at high fields implies that the valence band is wide and the hole mobility is high in the chains, and that holes migrate from chain to chain by tunneling. The high-field conduction is filamentary. Electrical breakdown is initiated by thermal instability caused by local high current density, and followed with the provision of large mean free paths for subsequent impact ionization, leading to a rapid increase of the current and final breakdown.

# Chapter 5

# High Field Electrical Conduction and Breakdown in Silicon-Incorporated Polyethylene[1]

Polymer films incorporated with foreign elements prepared by plasma polymerization in a gas mixture containing polymer monomer molecules and foreign elements have been studied in the past two decades. In our previous work [142, 154], we have found that the incorporation of silicon element in polyethylene films causes some changes in the properties of polyethylene. At that time, the silicon was incorporated into polyethylene by a plasma implantation process[142] and the electric fields used were low because the films used were relatively thick (about 30$\mu$m). In Chapter 4, we have mentioned that the use of samples in thin film form (about 1000$\AA$) for the study of high field phenomena in dielectric polymers can reduce the surface leakage current

[1]Part of the material in this chapter has been published in Journal of Applied Physics Vol.70, pp.919-924, (1991) [187] and Proceedings of ICPADM-91 held in Tokyo, on July 8-12, (1991)[188].

or discharge problems associated with high voltages because with thin films very high fields can be easily attained at relatively low applied voltages. In the investigation into high-field electrical conduction and breakdown in silicon-incorporated polyethylene, we also used thin film samples and adopted the same techniques for the measurements of current-voltage ($I$-$V$) and capacitance-voltage ($C$-$V$) characteristics as those described in Chapter 4. In addition, we have also measured the photoconduction and the photo-released current as functions of photon energy with the aim of studying the trapping parameters.

## 5.1 Experimental Procedures

The technique for the fabrication of silicon-incorporated polyethylene films has been described in Chapter 3. The deposition parameters for plasma-polymerized Si-incorporated polyethylene films are given in Table 3.1 of Chapter 3. The techniques used for preparation of the metal-polymer-semiconductor (MPS) capacitors and electrical measurements are the same as those described in Chapter 4. The thickness of all the films used for this investigation was 1000$\mathring{A}$ unless otherwise stated.

In order to study the effects of silicon incorporation from another angle, we also produced some samples with two layers, one layer being pure polyethylene (PE) with a thickness of 860$\mathring{A}$ and another layer being silicon-incorporated polyethylene (SiPE) with a thickness of 140 $\mathring{A}$. For the two-layer samples, a $SiH_4/C_2H_4$ volume ratio of 0.066 was used for the fabrication of the Si-incorporated polyethylene layers. Since the substrate was p-type silicon, we kept the substrate at positive polarity for the $I$-$V$measurements so that the

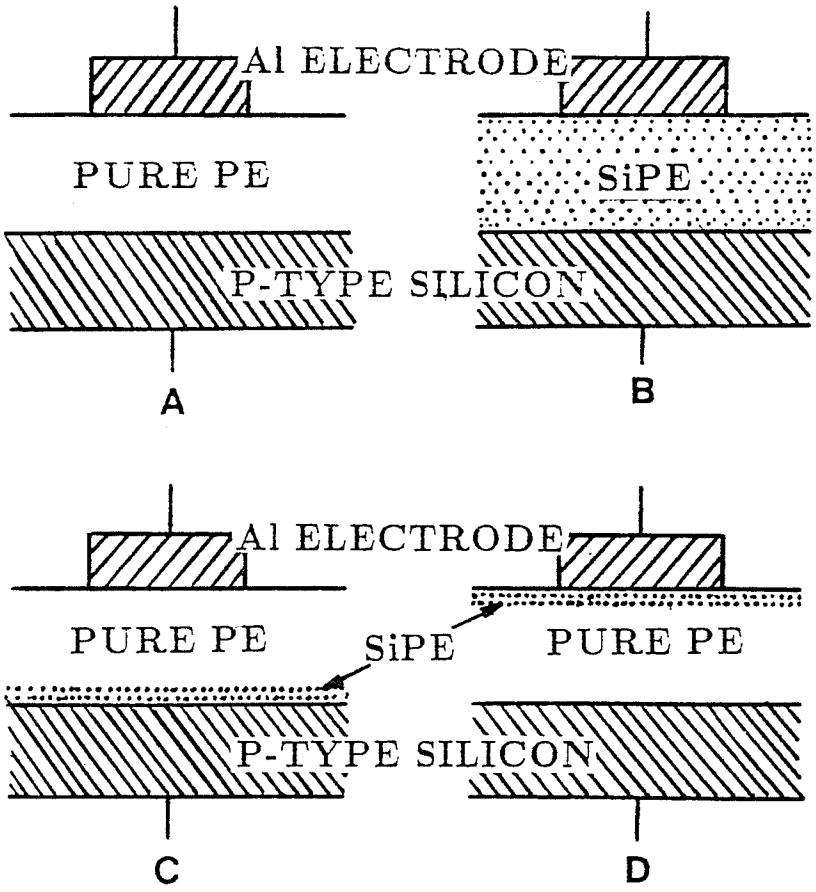


Figure 5.1: *Metal-polymer-semiconductor (MPS) configurations. (A) Al–PE–Si; (B) Al–SiPE–Si; (C) Al–PE–SiPE–Si; and (D) Al–SiPE–PE–Si.*

MPS capacitor was in the accumulation mode. The four sample configurations are shown in Fig. 5.1.

For photoconduction and photo-released current measurements, an aluminum layer was first vacuum-deposited on a glass substrate as the bottom electrode. After that a plasma polymerized polymer film was deposited on the substrate. The top electrode is a gold layer vacuum-deposited on the top surface of the polymer film with a thickness of $100\mathring{A}$. As this electrode served as the illuminated electrode, its thickness had to be controlled by a TM-100

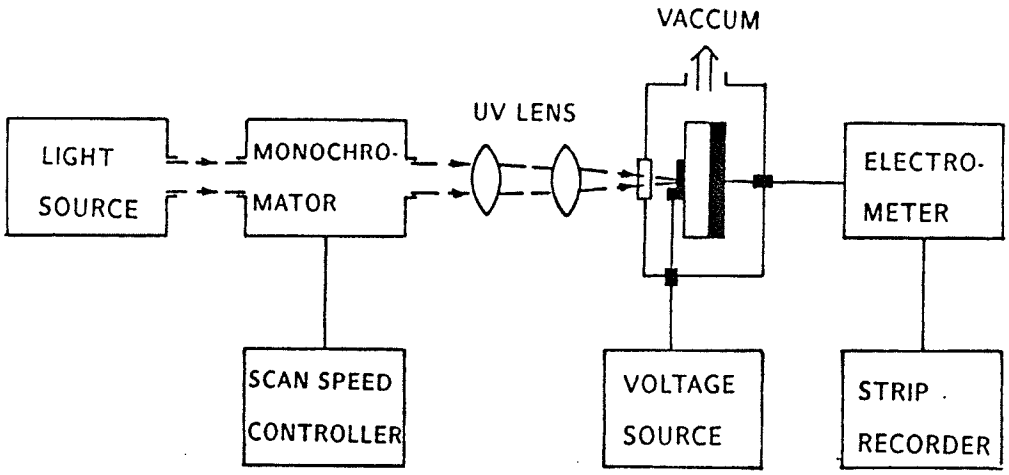


Figure 5.2: *Optical system arrangement for the measurements of photocurrent and photo-released charges.*

thickness monitor. The thickness of the film samples for optical measurement was 3000$\AA$ unless otherwise stated. A small aluminum dot of about 2000$\AA$ in thickness was also vacuum deposited on the edge of this transparent electrode to ensure a good electrical contact. The area of the transparent electrode and the contact dot were $4x10^{-2}cm^2$ and $2x10^{-2}cm^2$, respectively. The experimental arrangement for optical measurements is shown in Fig. 5.2. A 150 W xenon lamp in conjunction with a HR-320 monochrometer was used as the light source. The scanning speed of the monochrometer was set to 35$\AA$/s with a grating of 12000 g/cm. A Keithley 610C electrometer in conjunction with a HP-7132A strip recorder was used for the current measurements. All the measurements were performed in a vacuum chamber of $5x10^{-6}$ Torr at room temperature (22°C).

## 5.2 Results and Discussion

In Chapter 4, we have used different electrode materials and the polarity effect as well as the shifts of the $I$-$V$ and $C$-$V$ characteristics to demonstrate that for pure polyethylene the high-field conduction is due to the Fowler-Nordheim type tunneling injection of holes from the anode (the hole-injecting contact). For Si-incorporated polyethylene films we used first two-layer samples to see how a thin SiPE layer affects the hole injection current. It can be seen from Fig. 5.3 that with the SiPE layer in contact with the Al electrode which is biased at the negative polarity, the $I$-$F_g$ curve (where $F_g$ is the average field equal to the applied gate voltage divided by the film thickness) shifts very little from that of the pure polyethylene. But with the SiPE layer in contact with the $p$-Si substrate which is biased at the positive polarity, the $I$-$F_g$ curve shifts a great deal toward higher fields from that of the pure polyethylene. From these results we extract the following information.

(i) The SiPE layer increases the threshold field for the onset of hole injection. The SiPE layer acts as an emission shield [30] suppressing hole injection from the $p$-Si. The Si-incorporated polyethylene has a higher permittivity than that of pure polyethylene so that it tends to reduce the effective electric field at the hole-injecting contact as well as to suppress the image effect on lowering the tunneling barrier, thus increasing the apparent average field for the onset of hole injection.

(ii) The shift of curve C from curve A is much larger than that of curve B, indicating that the incorporation of Si in the polyethylene creates more hole traps. It is the trapped hole space charge that suppresses the hole injection

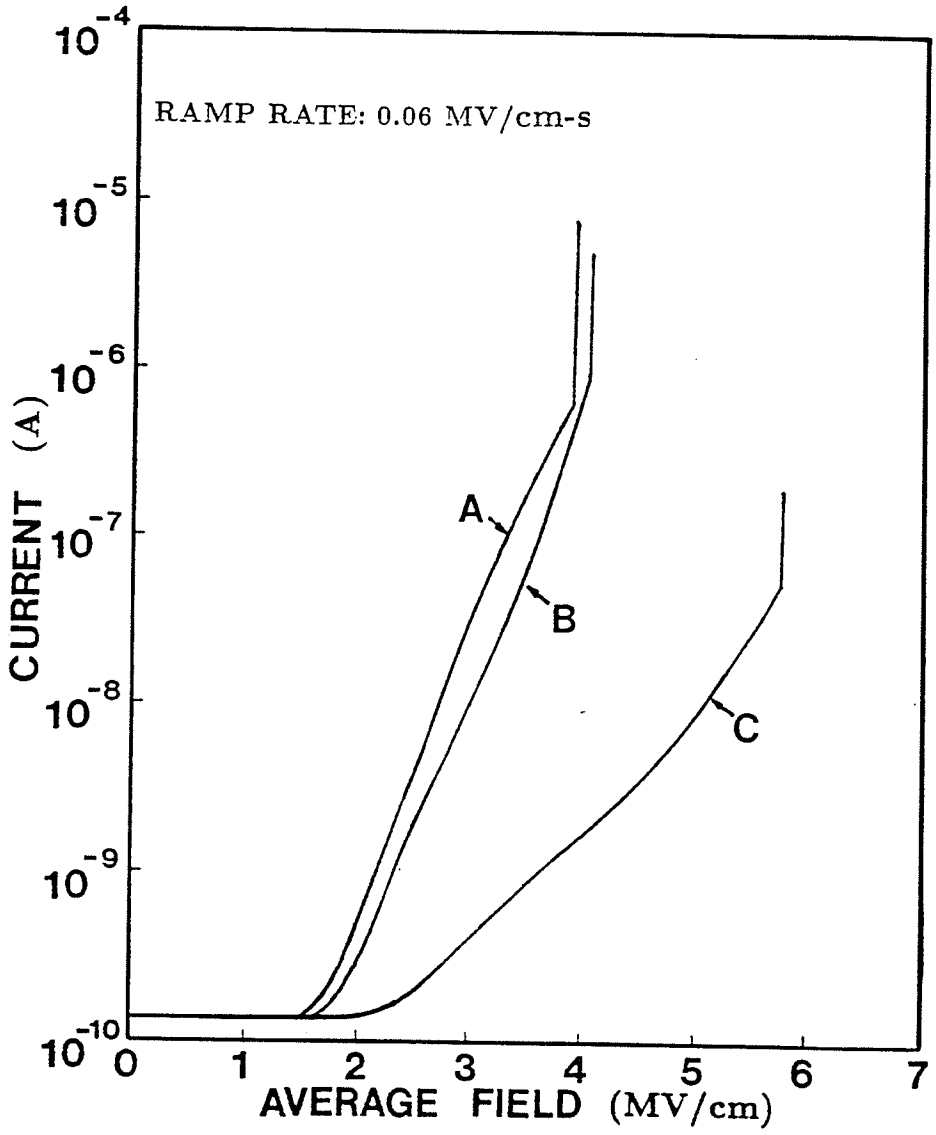


Figure 5.3: *Current-average field ($I$-$F_g$) characteristics for the structures: (A) Al–PE–Si; (B) Al–SiPE–PE–Si; and (C) Al–PE–SiPE–Si. The SiPE layer was deposited at the $SiH_4/C_2H_4$ volume ratio of 0.066. Gate electrode: Al; gate bias: $-V_g$; ramp rate: 0.06 MV/cm s.*

and makes the $I$-$F_g$curve shift to higher fields. The centroid of the trapped hole space charge for the SiPE layer in contact with the $p$-Si is much nearer the $p$-Si (the hole-injecting contact) than that for the SiPE layer in contact with the Al electrode. The closer the centroid to the hole-injecting contact, the more effective is the trapped hole space charge in suppressing the hole injection [183]. This is why at a fixed average field the current is much smaller for the case with the SiPE layer in contact with the $p$-Si as shown in curve C in Fig. 5.3.

(iii) The two-layer sample with the SiPE layer in contact with the $p$-Si exhibits a much higher breakdown strength. This can be considered as evidence that breakdown is initiated by thermal instability rather than by impact ionization. It is reasonable to assume that both the pure polyethylene layer and the SiPE layer are nearly-perfect dielectrics, and that the thermally generated carrier concentration in them is negligible as compared with the injected hole concentration. Based on this assumption, the average field in the pure polyethylene layer is higher than that in the SiPE layer because the permittivity of the former is lower than that of the latter. If breakdown is initiated by impact ionization, breakdown should occur as soon as the critical field for the onset of impact ionization is reached. Our experimental results do not follow this trend. Instead, the breakdown strength depends on the current magnitude at the field close to the breakdown strength. The lower the current magnitude, the higher is the breakdown strength as shown in Fig. 5.3 and Fig. 5.4. Also the breakdown strength depends on the ramp rate of the applied voltage as shown in Fig. 5.5. This dependence means that at fields close to the breakdown strength, the longer the electrical stressing time, the

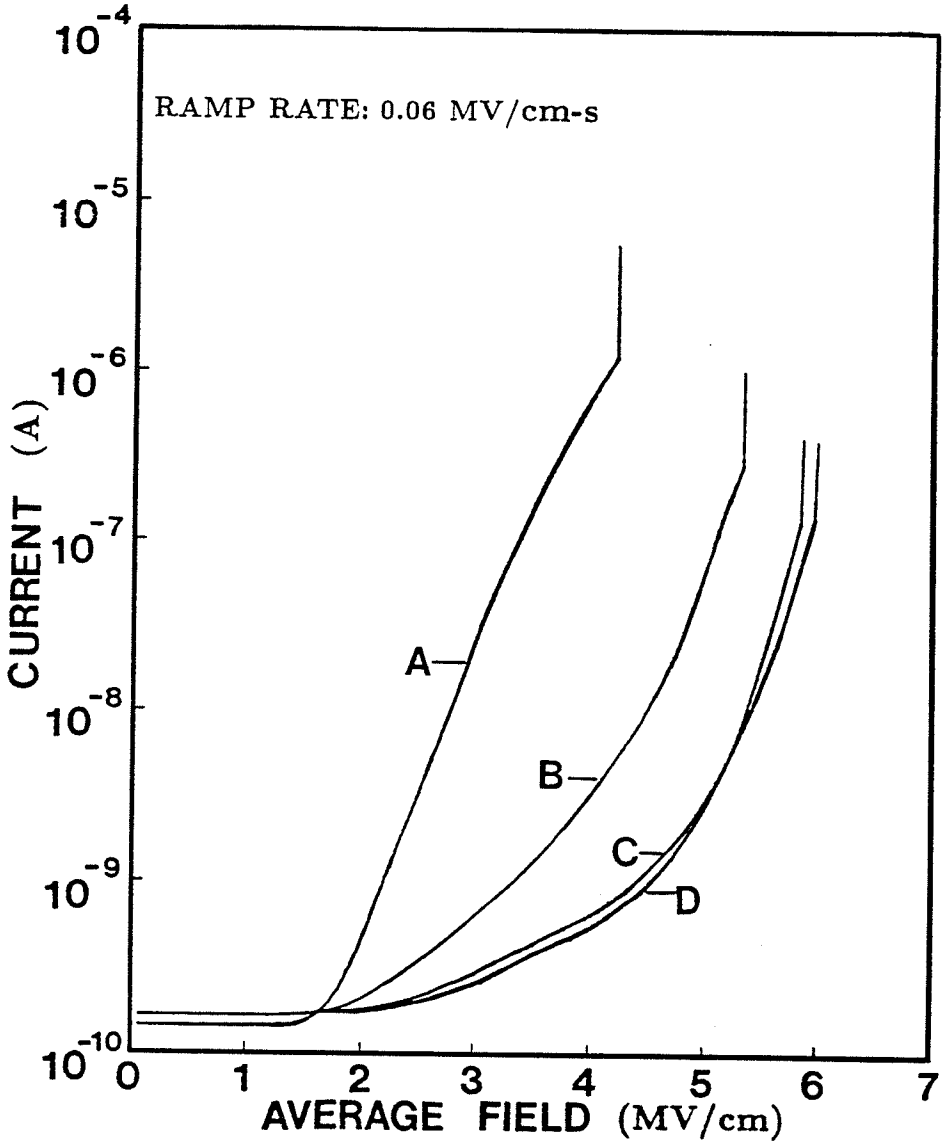


Figure 5.4: *Current—average field (I-$F_g$) characteristics of plasma-polymerized films deposited in a gas mixture with volume ratio of $SiH_4/C_2H_4$ of: (A) 0; (B) 0.022; (C) 0.066; and (D) 0.110. Gate electrode: Al; gate bias: -$V_g$; ramp rate: 0.06 MV/cm s.*

lower is the breakdown strength. This implies that when the energy stored in the current filament reaches a value sufficient to raise the local temperature to a critical level, thermal instability will occur.

(iv) At average fields higher than 3~4 MV/cm, the slope of the I-$F_g$ curves of the Si-incorporated polyethylene tends to change to a higher value, indicating that there is another mechanism becoming operative to contribute to the total current. It is most likely that this mechanism is double injection owing to an increase of the electron injection resulting from the enhancement of the effective field at the cathode by the continuous build-up of trapped hole space charge. This occurs in the Si-incorporated polyethylene but not in pure polyethylene, indicating that the incorporation of Si creates a large quantity of hole traps. The sharp increase in current at breakdown is the result of current runaway leading to final destructive breakdown. We believe that once thermal instability is initiated by Joule heating in a major current filament, low-density domains will be created there leading to long mean free paths for subsequent impact ionization and to an abrupt increase in conduction current and final breakdown along the major filament[119]. It should be noted that this abrupt change in current is not the change in slope signifying the onset of double injection though it may involve double injection as well as impact ionization.

Figure 5.4 shows the typical $I$-$F_g$characteristics for Si-incorporated polyethylene of various Si contents. It can be seen that the incorporation of Si shifts the $I$-$F_g$curves toward higher fields, indicating clearly that the incorporation of Si introduces more hole traps in the polyethylene. The higher the hole trap concentration, the greater is the trapped hole space charge at a

given applied field, and hence the lower is the hole injection current. However, while the trapped hole space charge suppresses the effective field at the hole-injecting contact and hence the hole injection current, it enhances the effective field at the electron-injecting contact and hence the electron injection current. Although the electron mobility is much smaller than the hole mobility, the electron injection could make a significant contribution to the total current when the injected electron concentration reaches a certain critical value. This is in fact the case of double injection because both types of carriers (electrons and holes) injected from both contacts play equally important roles in contributing to the total current. In Fig. 5.4, we can see that at a certain critical field such as at 3.5 MV/cm for the samples with the $SiH_4/C_2H_4$ volume ratio of 0.022 and at 4.5 MV/cm for the samples with the $SiH_4/C_2H_4$ volume ratio of 0.066, the slope of the $I$-$F_g$curve changes to a much higher value indicating that this is the field for the onset of double injection. This means that at this critical field the one-carrier (holes) dominant current changes to a two-carrier (electrons and holes) current. After the onset of double injection, the injected holes tend to enhance the electron injection, and the injected electrons tend to enhance the hole injection. Such a mutual enhancement process makes the current increase very rapidly with the applied field.

The conduction current at a given field decreases and the breakdown strength increases with increasing silicon content as shown in Fig. 5.4. For the $SiH_4/C_2H_4$ volume ratios up to 0.066, the $I$-$F_g$curve shifts toward higher fields as the $SiH_4/C_2H_4$ volume ratio is increased. However, when the ratio is higher than 0.066, (e.g., 0.11), the I–$F_g$ curve crosses over that for the ratio of 0.066 at a critical field, indicating that electron injection begins to play a

significant role in suppressing the trapped hole space charge, thus enhancing the hole injection and lowering the breakdown strength.

The build-up of the trapped hole space charge depends on both the magnitude and the duration of the applied field. The $I$-$F_g$curves depend on the ramp rate of the applied voltage as shown in Fig. 5.5. At a fixed field after the onset of hole injection, the lower the ramp rate, the more the trapped hole space charge is formed and hence the smaller is the hole conduction current. As the applied field is further increased, the electron injection becomes so important that electron space charge starts to suppress the effect of the trapped hole space charge, or in other words, it tends to reduce the total positive space charge. In this case, at a field higher than a certain critical value, such as at 6 MV/cm, the conduction current for the lower ramp rate becomes larger than that for the higher ramp rate for Si-incorporated polyethylene as shown in Fig. 5.5. We have also measured the steady state $I$-$F_g$characteristics under dc fields. In this case, the dc $I$-$F_g$curve crosses over the ramp $I$-$F_g$curves at a critical field ($\sim$ 5.6 MV/cm) for the Si-incorporated polyethylene. At fields lower than this critical field the injected hole current is smaller under a dc voltage than that under a ramp voltage. This implies that under a dc voltage the trapped hole space charge is fully built up to a dynamic equilibrium value at a fixed field, but under a ramp voltage it may not because there may not be enough time at that particularly fixed field for the hole space charge to fully build up.

The typical high frequency (1 MHz) $C$-$F_g$characteristics measured by using the linear voltage ramp to sweep from the inversion mode to the accumulation mode (between $F_g$=+2 MV/cm to $F_g$=−2 MV/cm) at the ramp rate

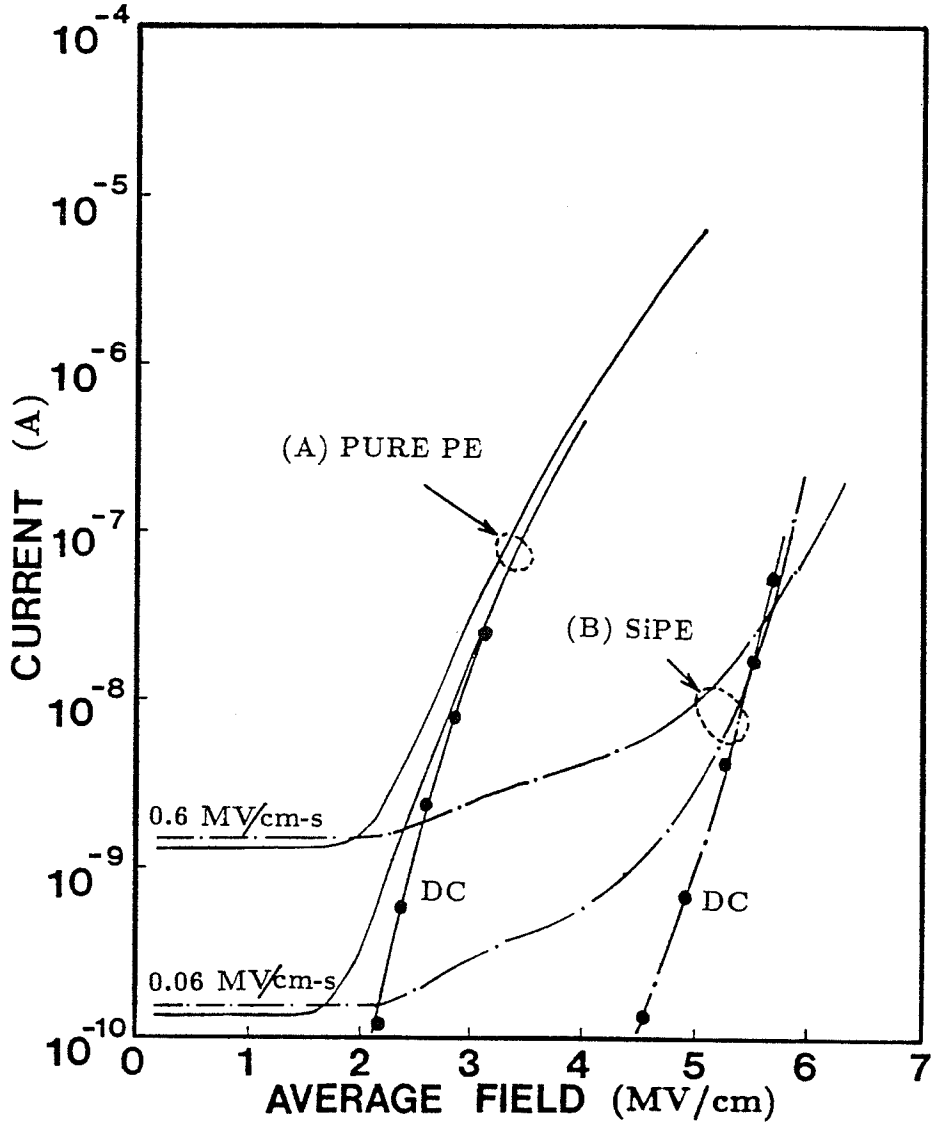


Figure 5.5: *Effect of the ramp rate on the current-average field (I-$F_g$) characteristics for (A) pure polyethylene and (B) Si-incorporated polyethylene with the $SiH_4/C_2H_4$ volume ratio of 0.066. Curves with • measured using dc voltages. Gate electrode: Al; gate bias: $-V_g$.*

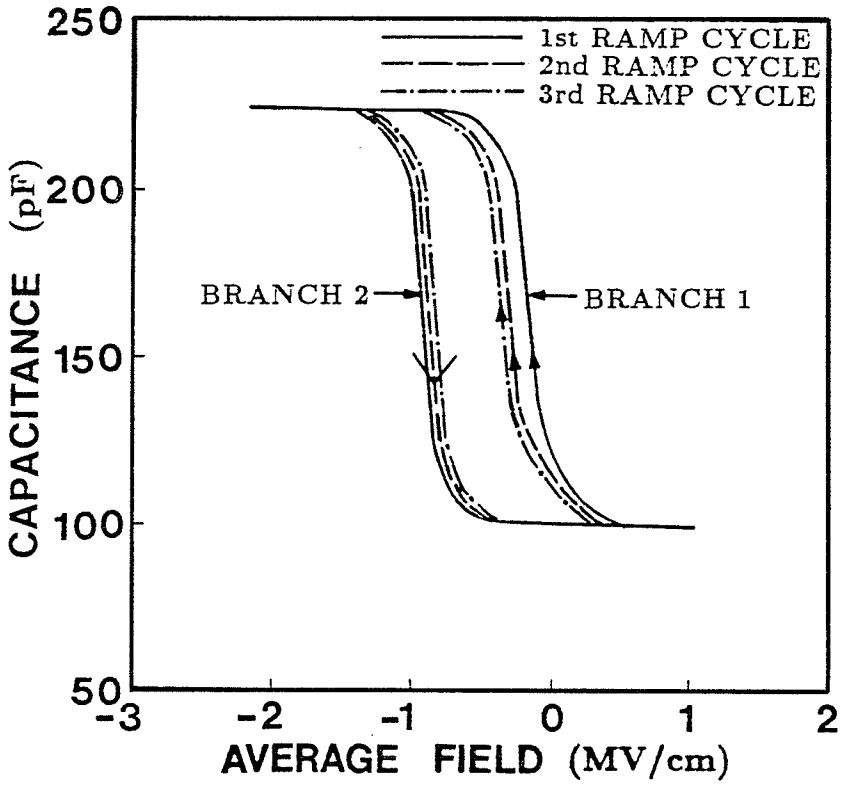


Figure 5.6: *Typical capacitance-average field ($C$-$F_g$) curves for Si-incorporated polyethylene with the $SiH_4/C_2H_4$ volume ratio of 0.066. Gate electrode: Al; ramp rate: 0.06 MV/cm s.*

of 0.06 MV/cm s are shown in Fig. 5.6. In the first cycle of sweeping, the $C$-$F_g$curves (branch 1 and 2) form a hysteresis loop, indicating that there are some positive charges (holes) introduced into the bulk during branch 1 by hole injection at $F_g \geq |-2|$ MV/cm. After the first cycle, $F_g$ becomes positive again, the electron injection reduces the effect of the hole space charge, and so on, so that the width of the second hysteresis loop is smaller than that of the first hysteresis loop. We have also tested how the ramp voltage stressing affects the $C$-$F_g$curves. We first measured the $C$-$F_g$curve on a virgin MPS capacitor (with

$SiH_4/C_2H_4$ volume ratio of 0.066), sweeping from $F_g$=0.5 MV/cm to $F_g$=−1.5 MV/cm, and then from $F_g$=−1.5 MV/cm to $F_g$=1.0 MV/cm. The results are shown in Fig. 5.7(b). After the first cycle of $C$-$F_g$measurements, the MPS capacitor was then stressed with a first cycle of voltage ramp at 0.06 MV/cm s as shown in Fig. 5.7(a). Then a second $C$-$F_g$hysteresis loop was measured right after that and also immediately followed with a second cycle of voltage ramp stressing. This procedure was repeated several times. The $I$-$F_g$and the corresponding $C$-$F_g$curves are shown in Fig. 5.7. The ramp-voltage stressing shifts both the $I$-$F_g$and the $C$-$F_g$curves in the direction corresponding to the build-up of positive space charge in the bulk.

In order to study the nature of the trapped space charge under various fields in some detail, we have also used the following procedure to reveal the build-up of the trapped space charge through the effect of the applied high electric stress on the $I$-$F_g$and the $C$-$F_g$characteristics. First a high-frequency $C$-$F_g$curve for a virgin MPS capacitor was taken and then the capacitor was stressed with first cycle of voltage ramp at a rate of 0.06 MV/cm s until it reached a predetermined level and then held there for 10 seconds. The stress was then released and the $C$-$F_g$curve was immediately measured right after that, and then followed with second cycle of voltage ramp at the same ramp rate but with the stress held for the same 10 seconds at a higher field. This procedure was repeated several times. The typical $I$-$F_g$and the corresponding $C$-$F_g$characteristics for pure PE films are shown in Fig.5.8 and those for SiPE films are shown in Fig.5.9. For pure PE, the current decreases with time during the holding time at 3.5 MV/cm, indicating that the trapped hole space charge and hence the internal field build-up at 3.5 MV/cm with time. In the

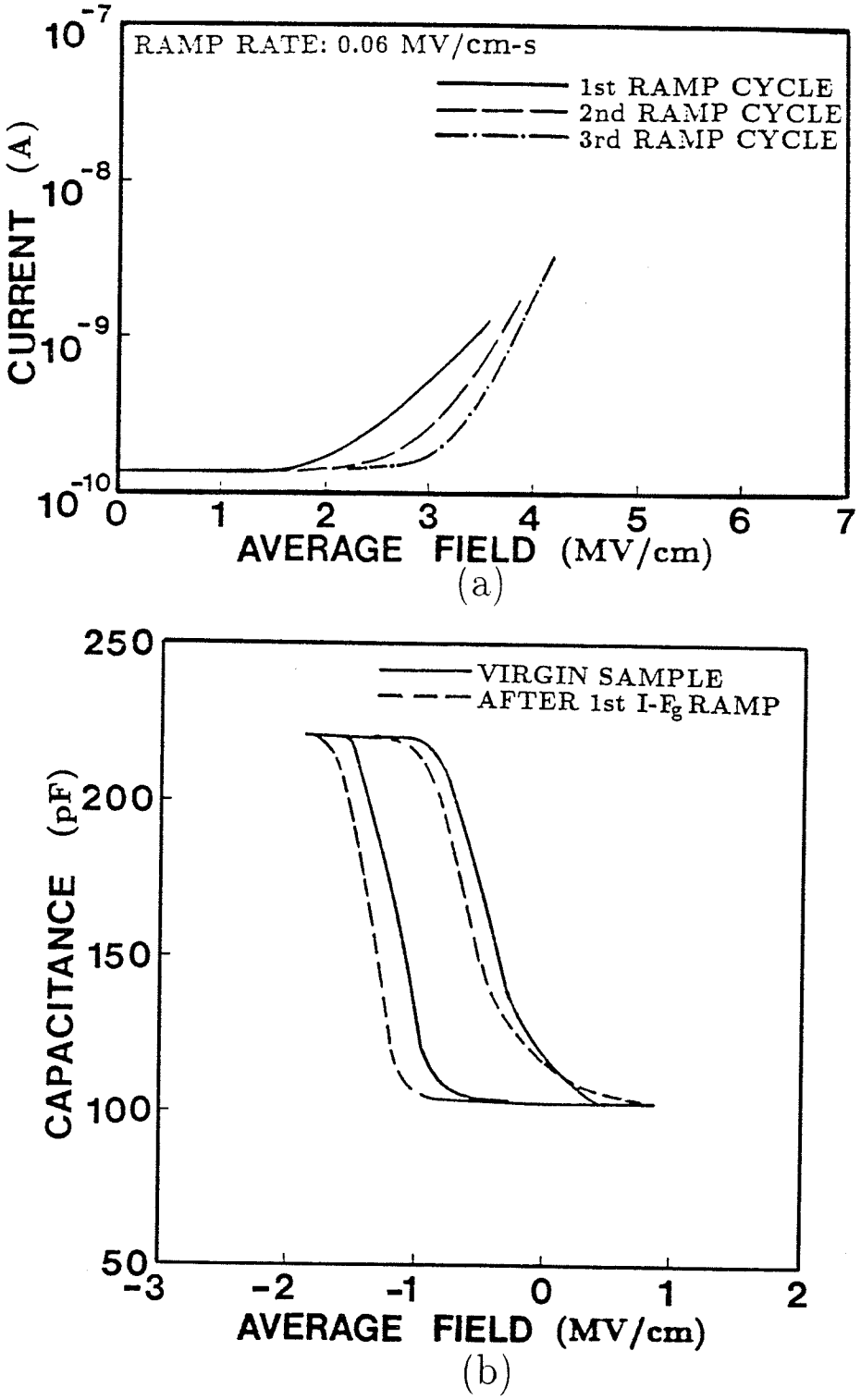


Figure 5.7: *Effects of the ramp voltage stressing on (a) the current-average field ($I$–$F_g$) characteristics and (b) the corresponding capacitance-average field ($C - F_g$) characteristics. Gate electrode: Al; ramp rate: 0.06 MV/cm s.*

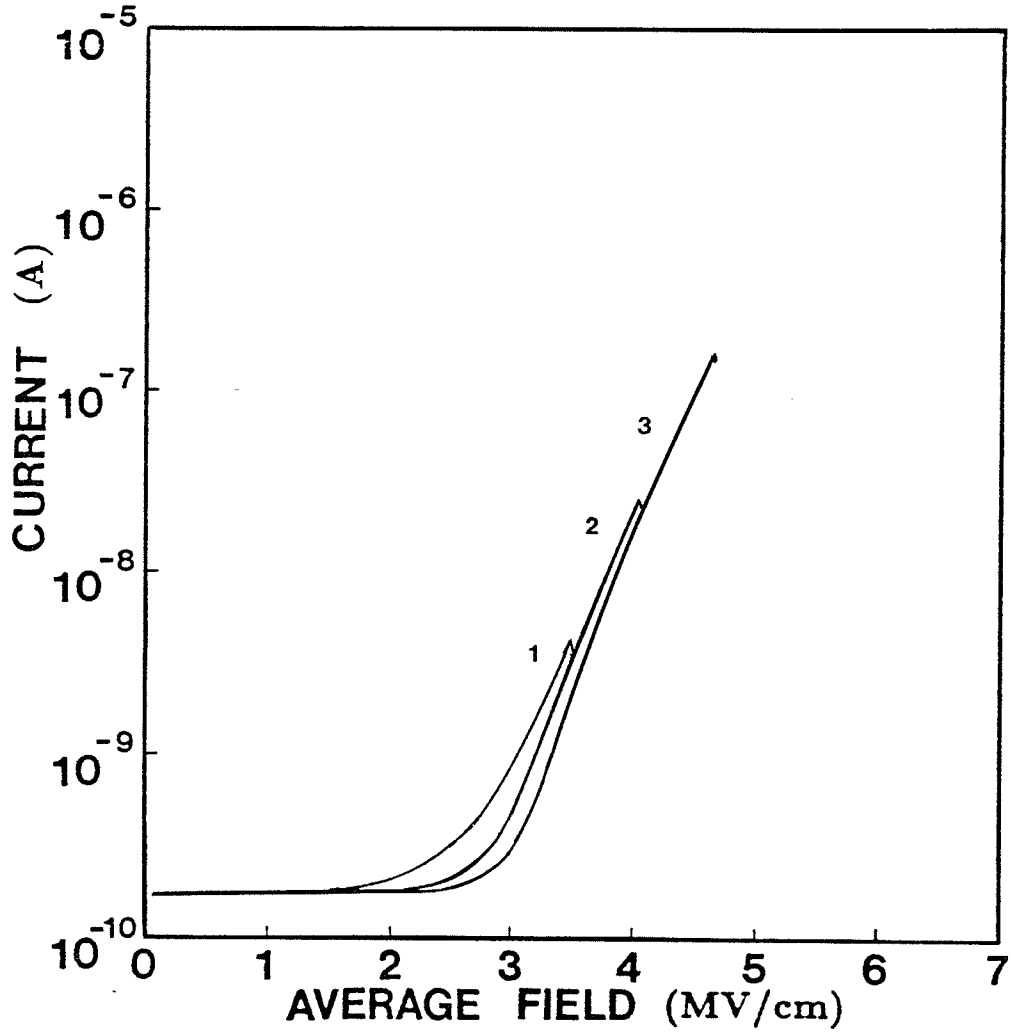


Figure 5.8(a)

Figure 5.8: *Effects of the ramp voltage stressing on (a) the current-average field (I-$F_g$) characteristics and (b) the corresponding capacitance-average field (C-$F_g$) characteristics for a typical pure PE film of 1200Å in thickness for the virgin sample V, and after 1st, 2nd, and 3rd cycle of stressing. After the V, 1st, 2nd and 3rd C-$F_g$ cycle a stress of 3.5MV/cm, 4.0MV/cm and 4.5MV/cm, respectively, was applied to the device for 10 seconds prior to the measurements for the following cycle. Gate electrode: Al; ramp rate: 0.06 MV/cm s.*

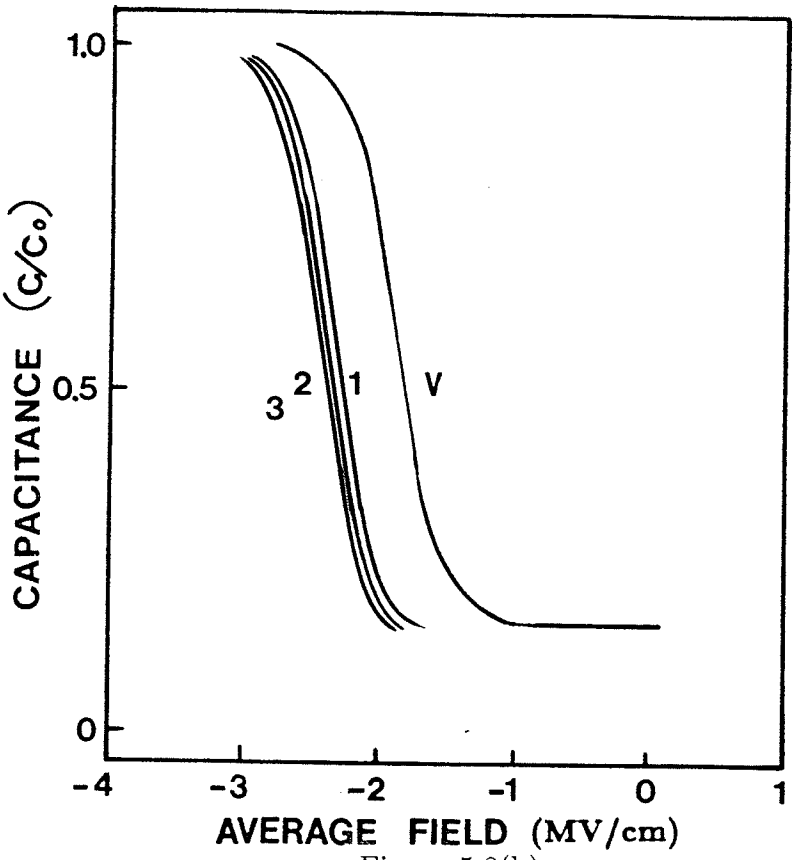


Figure 5.8(b)

second cycle the $I$-$F_g$curve shifts to higher fields, but this shift diminishes in the 3rd and further cycles indicating that most traps may have been filled or the trap filling process may have reached a dynamic equilibrium. This is why during the holding time at 4.0 MV/cm after the 2nd cycle and at 4.5MV/cm after the 3rd cycle the current remains unchanged with time as shown in Fig. 5.8(a). This tendency is also demonstrated in the $C$-$F_g$curves as shown in Fig. 5.8(b). For SiPE films, the behaviour is similar to that for PE films for fields below 4.5MV/cm, except that the current magnitude is generally smaller as compared with that for PE films at a given field, indicating that the incorporation of Si creates a large amount of hole traps. It is this high concentration of hole traps and hence the trapped hole space charge that

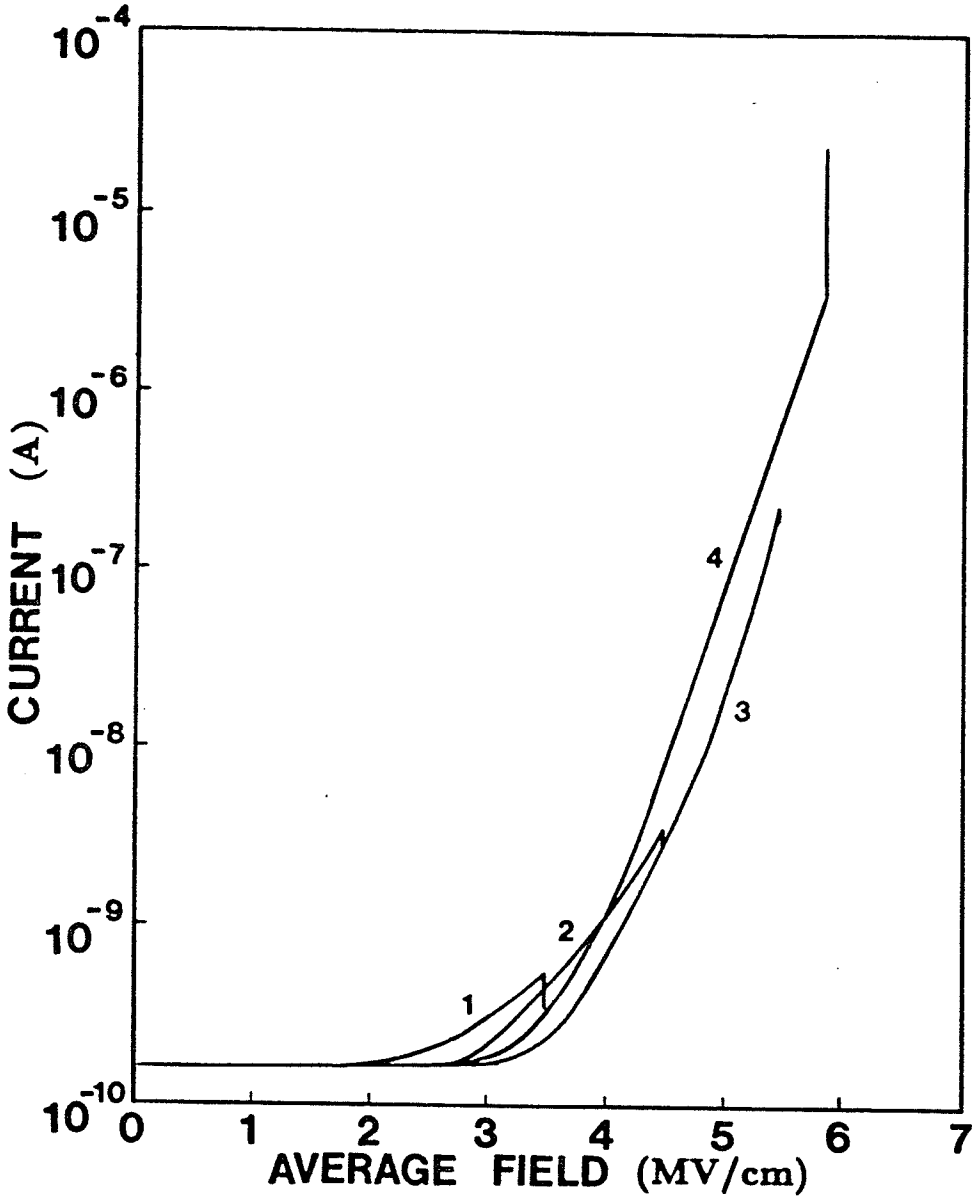


Figure 5.9(a)

Figure 5.9: *Effects of the ramp voltage stressing on* **(a)** *the current- average field (I-$F_g$) characteristics and* **(b)** *the corresponding capacitance- average field (C-$F_g$) characteristics for a typical SiPE film of 1200Å in thickness for the virgin sample V, and after 1st, 2nd, and 3rd cycle of stressing. After the V, 1st, 2nd and 3rd C-$F_g$ cycle a stress of 3.5MV/cm, 4.5MV/cm and 5.0MV/cm, respectively, was applied to the device for 10 seconds prior to the measurements for the following cycle. Gate electrode: Al; ramp rate: 0.06 MV/cm s.*

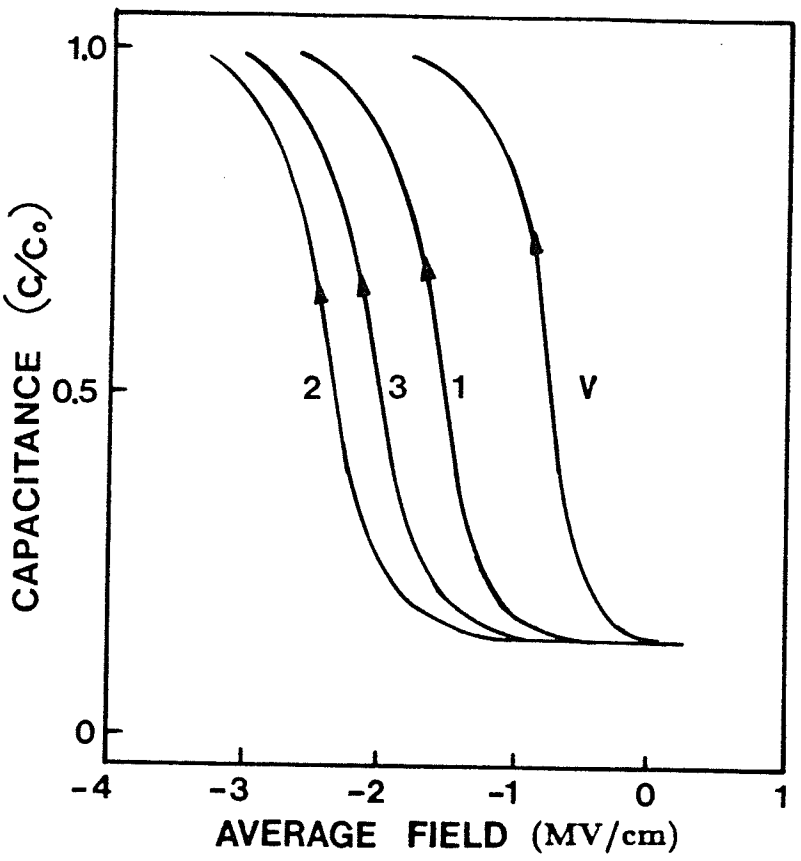


Figure 5.9(b)

enhances the field toward the cathode (the electron-injecting contact) and causes the onset of double injection. It can be seen that after the 3rd cycle of stressing up to 5MV/cm and with this stress held for 10 second, the $I$-$F_g$curve for the 4th cycle shifts toward opposite direction, i.e., toward lower fields as shown in Fig. 5.9(a). This implies that during the 3rd cycle the concentration of the positive trapped hole space charge is reduced, possibly due to a large quantity of electrons injected from the cathode. These results are consistent with the $C$-$F_g$characteristics. After the 3 cycle of stressing the $C$-$F_g$curve shifts backward as shown in Fig. 5.9(b).

We have also measured the $I$-$F_g$characteristics for both the PE and the SiPE films as functions of film thickness using linear voltage ramp at the rate of 0.06MV/cm s with the aluminum gate electrode biased at negative polarity. For pure PE films, the current is practically independent of film thickness at a fixed average field below 3.5 MV/cm, as shown in Fig. 5.10. At fields higher than this, the current increases slightly with increasing film thickness at a fixed average field, but the critical field for the occurrence of thermal instability leading to final breakdown (not shown in Fig.5.10) decreases slightly with increasing film thickness. This phenomenon suggests that the motion of the injected holes in the pure PE bulk is mainly controlled by their interaction with the lattice rather than with the traps in the forbidden gap. This also implies that the injected holes may travel quite a distance before being effectively trapped, and that the traps are first filled by holes at a region between the cathode and the anode and possibly at quite a distance from the hole-injecting anode. The bulk traps in PE are gradually filled starting from that region toward the anode. This is why the trapped hole space charge is more effective in suppressing the hole injection for thin samples than that for thick ones. This explains the increase in current with film thickness at high fields as shown in Fig. 5.10. With the incorporation of silicon in polyethylene, a large amount of new traps are created. These new traps not only produce more trapped hole space charge, but also enhance the interaction between holes and traps. The former tends to reduce the field toward the hole-injecting contact and to increase the field toward the electron-injecting contact, while the latter tends to reduce the hole mobility. This action causes the current to decrease with increasing film thickness as shown in Fig. 5.10. As the trapped hole space

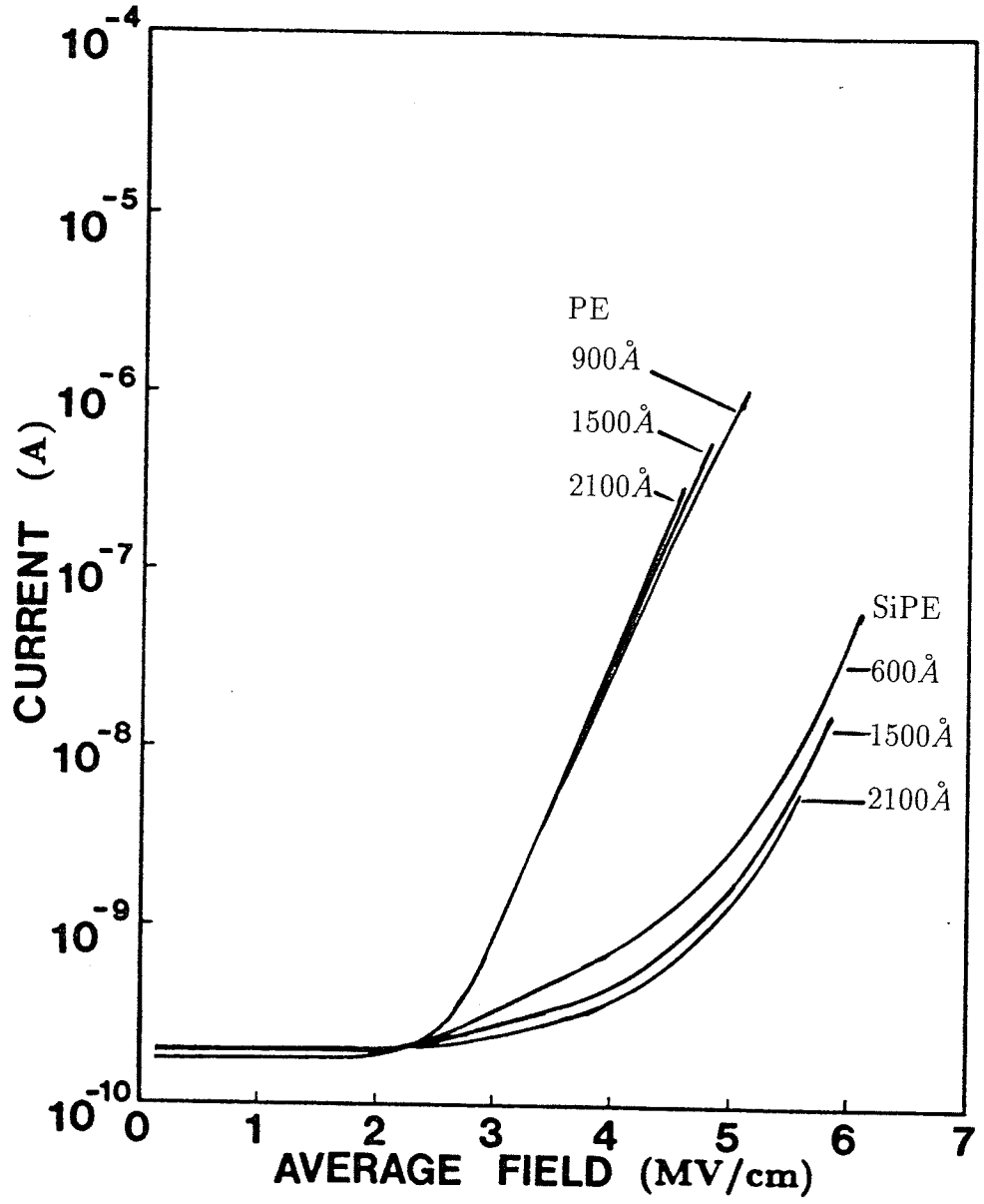


Figure 5.10: *Current-average field characteristics (I-$F_g$) as functions of film thickness for PE films and SiPE films. Gate electrode: Al; ramp rate: 0.06 MV/cm-s.*

charge reaches a certain critical value, the electron injection becomes to play a significant role in the electrical conduction. Since the electron mobility is much smaller than the hole mobility, it is likely that the major role played by the electron injection is to form a negative trapped electron space charge to counteract the already formed positive trapped hole space charge, thus indirectly enhancing the injection of highly mobile holes which contribute more effectively to the conduction current.

We consider the breakdown occurring at the field at which the current increases sharply to an enormous value leading to destructive breakdown as shown in Fig. 5.4. The distributions of such breakdown measurements are shown in Fig. 5.11. The breakdown strength with the highest probability of occurrence is taken as the normal breakdown strength. The values of the normal breakdown strength for pure polyethylene, SiPE($SiH_4/C_2H_4$=0.022), SiPE($SiH_4/C_2H_4$=0.066), and SiPE($SiH_4/C_2H_4$=0.110) are 5.5 MV/cm, 6.5 MV/cm, 6.9 MV/cm, and 6.7 MV/cm, respectively. The breakdown strength for the two-layer samples with the thin SiPE layer at the *p*-Si substrate (the positive electrode) is 6.7 MV/cm and is higher than that for the case with this thin SiPE layer at the Al gate (the negative electrode) which is, 5.8 MV/cm, slightly higher than that for pure polyethylene. For homogeneous samples, the breakdown strength increases with increasing Si content. But for Si contents higher than a certain critical value, such as a value corresponding to the $SiH_4/C_2H_4$ volume ratios higher than 0.066, the breakdown strength starts to decrease, possibly due to the mutual enhancement of double injection.

The incorporation of Si into polyethylene creates $SiH_2$ elements to replace some of the $CH_2$ elements in the main chain of the polyethylene. This

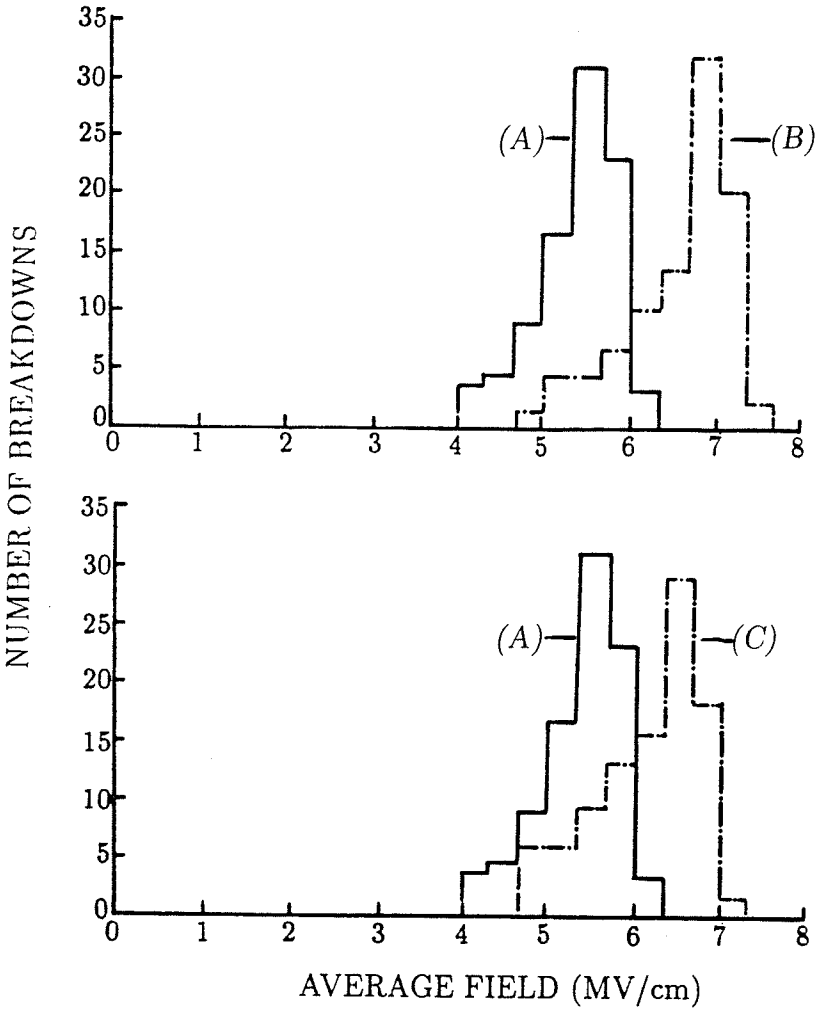


Figure 5.11: *Histograms of the breakdown measurements. (A) pure polyethylene film; (B) Si-incorporated polyethylene with the $SiH_4/C_2H_4$ volume ratio of 0.066; and (C) two-layer samples of Al-PE-SiPE-Si configuration with the SiPE layer deposited at the $SiH_4/C_2H_4$ volume ratio of 0.066. Ramp rate: 0.06 MV/cm s.*

will make the polyethylene chain irregular and hence result in a decrease of the valence band width and an increase in hole scattering, thus reducing the hole mobility. The incorporation of Si creates also side groups which involves $SiH_2$ as well as $SiH_3$. These elements perturb the polyethylene structure, resulting in the formation of structural defects and possibly hole traps. Silicon atoms may also be located in empty vacancies without chemical bonding and act as traps there. The present work provides sufficient evidence that the incorporation of silicon in polyethylene creates new hole traps and reduces the hole mobility.

We have also measured the photoconduction current at an average field of 0.33 MV/cm and the short-circuited photo-released current as functions of photon energy. The photoconduction current was measured after the dark current had reached its steady state value. Figure 5.12 shows that the photoconduction current in both pure PE and SiPE samples for the illuminated electrode at the negative polarity is generally higher than that for illuminated electrode at the positive polarity, and that the photoconduction current in SiPE samples is generally higher than that in pure PE samples. Although the dark current, which is considered to be mainly electron current under this field, is small, and about $10^{-13}$A, the electrons trapped in the bulk during electric stress may be quite a quantity. These trapped electrons may act as hole traps when the illuminated electrode is negative in polarity. The light may generate electrons due to photoemission, as well as electrons and holes via trapping states because the light photon energy is smaller than the energy band gap in this case. The photoconduction current has two components, one due to photoemission of electrons and the other due to photogeneration

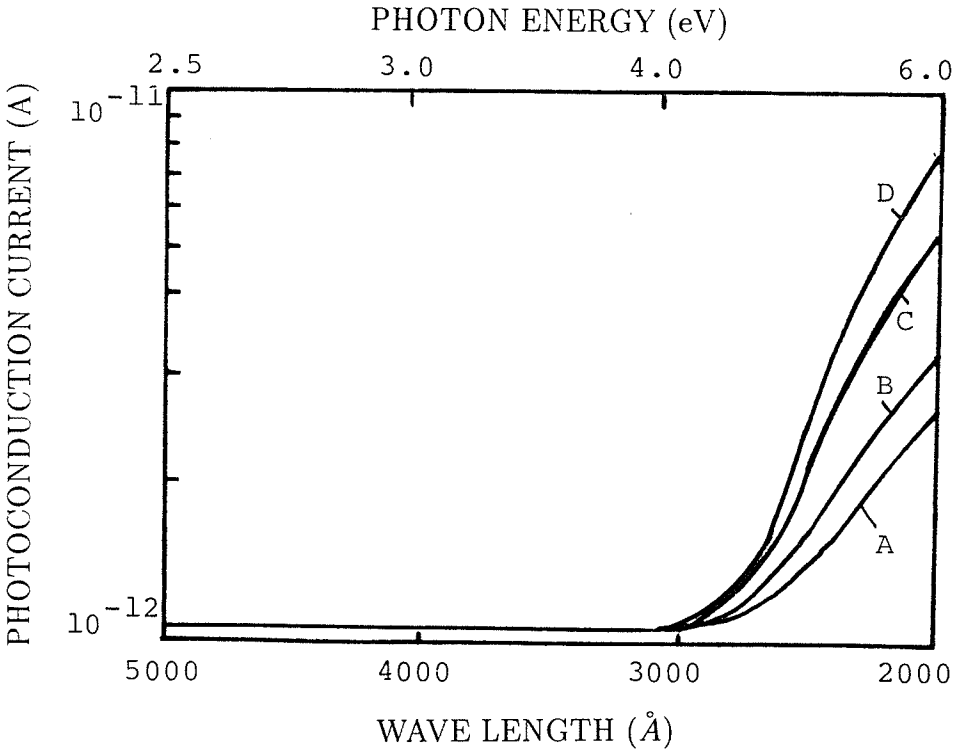


Figure 5.12: *Photoconduction current of (A) the pure polyethylene with the illuminated electrode at the positive polarity; (B) the pure polyethylene with the illuminated electrode at the negative polarity; (C) the Si-incorporated polyethylene with the illuminated electrode at the positive polarity; and (D) the Si incorporated polyethylene with the illuminated electrode at the negative polarity.*

of carriers in the bulk. When the illuminated electrode is positive in polarity, the photoemission of holes is not important because the barrier height for hole emission is much larger than that for electron emission. That the photoconduction current is practically independent of the illuminated electrode material when it is in positive polarity supports this speculation. So in this case the photoconduction current is mainly due to photogeneration of carriers in the bulk.

The introduction of Si into polyethylene creates both electron and hole traps. As these traps act as step-stones for photogeneration of both holes and electrons in the bulk. This may be why the photoconduction current in the SiPE samples is much higher than that in the pure PE samples. Traps tend to capture thermally generated carriers and to reduce carrier mobilities, thus the presence of Si in polyethylene enhances the photocurrent but suppresses the dark current as expected [142].

For photo-released current measurements, the film sample was first charged by ultra-violet (UV) light radiation upon the illuminated electrode which was biased at $-10$ V corresponding to an average field of 0.33 MV/cm in the film sample for 10 or 30 minutes. After such a dc charging process, the sample was short-circuited and the photo-released short-circuited current was measured as a function of photon energy. Figure 5.13 shows that there are two peaks in the photo-released current. During the charging process, it is expected that carriers injected due to photoemission and photogeneration in the bulk will fill most of traps. After the removal of the UV light and the bias voltage, the short-circuited current is due to the photo-induced detrapping process. There are two peaks in the spectra. For pure PE samples, one is located at 3.3

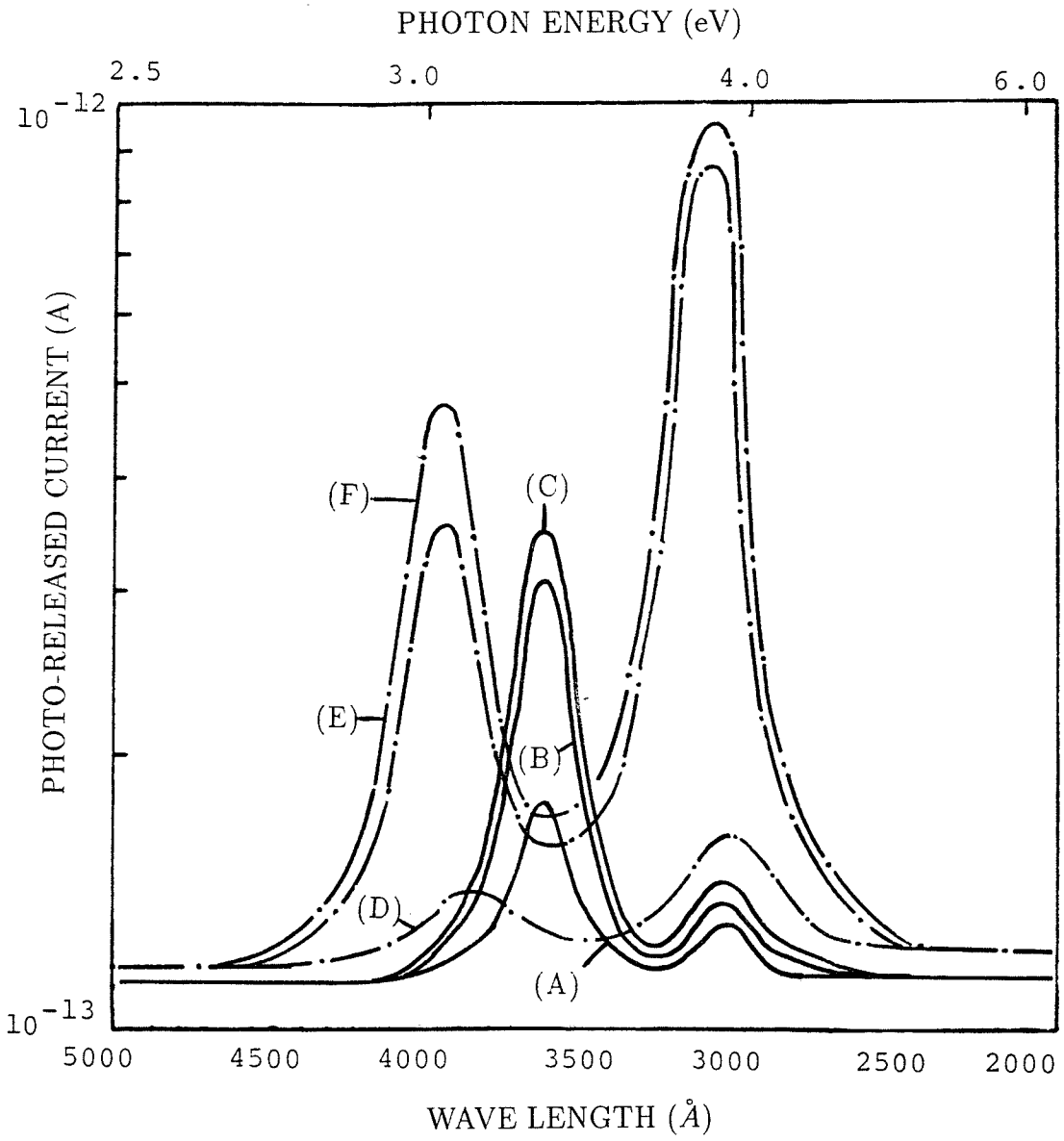


Figure 5.13: *Photo-released current of polyethylene (Solid lines) and Si-incorporated polyethylene (dashed lines) under various charging conditions: (A) Virgin PE sample without charging; (B) PE sample after charging for 10 mintues; (C) PE sample after charging for 30 mintues; (D) Virgin SiPE sample without charging; (E) SiPE sample after charging for 10 mintues; and (F) SiPE sample after charging for 30 mintues.*

eV and the other at 4.15 eV. A good deal of experimental work [30, 33, 43, 114] has indicated that in pure polyethylene there are electron and hole traps, and that the electron trap concentration is higher than the hole trap concentration, but the energy level of the latter is deeper than that of the former. We believe that the traps at 3.3 eV below the conduction band are likely to be electron traps, and those at the 4.15 eV above the valence band be hole traps. The incorporation of Si in polyethylene shifts the energy level of the electron traps to a lower level at 3.1 eV and increases the hole trap concentration by about 10 times. This change in trap parameters due to the incorporation of Si is consistent with our experimental results on photoconduction currents as well as high field conduction and breakdown phenomena.

In summary, high field conduction in Si-incorporated polyethylene is due mainly to Fowler-Nordheim type tunneling injection of holes from the anode (the $p$-Si substrate). The incorporation of silicon in polyethylene creates deep hole traps. The shift of the $I$-$F_g$characteristics from that of pure polyethylene is due to the high concentration of the trapped hole space charge in SiPE. This internal field created by the trapped hole space charge on the one hand reduces the effective field at the hole-injecting contact thus suppressing the hole injection, but on the other hand, enhances the effective field at the electron-injecting contact and hence the electron injection. Depending on the trapped hole charge density, the one-carrier (holes) dominant conduction may be changed to a two-carrier conduction when the electron injection becomes significant. A thin SiPE layer inserted between the pure polyethylene and the hole-injecting contact acts as an efficient emission shield suppressing the hole injection and increasing the breakdown strength. Electrical breakdown is ini-

tiated by thermal instability caused by local high current density in one major conduction filament, and followed with the provision of large mean free paths for subsequent impact ionization, leading to a rapid increase of the current and final breakdown. No impact ionization has been observed prior to the occurrence of thermal instability. Photoconduction and photo-released current measurements confirm also that the incorporation of Si introduce more hole traps into polyethylene.

# Chapter 6

# High Field Electrical Conduction in Polypropylene and Emission Shield Effects

In Chapter 4, the high field conduction processes in plasma-polymerized polyethylene films have been discussed. The films used were thin, about $0.1\mu$m (or $1000\mathring{A}$) in thickness. To examine whether the same conduction processes would apply to chemically polymerized polymers of similar structure and thick samples, we chose chemically polymerized polypropylene films (commercial films) with thickness of $15\mu$m (or $150000\mathring{A}$) for this investigation. As carrier injection from electrical contacts is the prelude for all high-field conduction and breakdown processes. Suppression of this process by an emission shield should improve the dielectric behavior of insulation systems at high fields. In fact, several investigators[29, 30] have reported the effect of emission shields. Plasma processing is an efficient technique for thin film deposition on the surface of any materials. We have therefore used this technique to deposit pure PE, SiPE and $SiO_2$ films on the insulating polymer surface and studied

the effect of these films as emission shields.

## 6.1 Experimental Procedures

The samples used for this investigation were chemically polymerized polypropylene the thickness of 15 $\mu$m, which were used in industry as the insulating material for capacitors. To study the effect of emission shields, we used plasma-polymerized polyethylene films without silicon incorporation (PE) and with silicon incorporation (SiPE) deposited on one surface of the polypropylene samples. The technique for the deposition of PE and SiPE films is similar to that described in Chapter 3 and 4. The thicknesses of the thin films used were from 350$\AA$ to 12000$\AA$. After deposition, the samples were kept in the vacuum chamber under a vacuum of $10^{-6}$ Torr for a heat treatment at 100°C for about 2 hours in order to anneal out any nonequilibrium structural stress. For comparison purposes, the polypropylene samples without deposited films were also subjected to the same heat treatment. For electrical measurements, aluminum ( or gold, or silver, or copper) counter electrodes of 1000$\AA$ in thickness and each of 3.14x$10^{-2}$cm$^2$ in area were vacuum-deposited on both surfaces of the samples to form a sandwich structure. The sample was placed in a specially designed holder with a spring to give an appropriate pressure on the top electrode to ensure good electrical contacts as shown in Fig.6.1. The sample and its holder were immersed in a Silicon oil-filled cell to avoid surface discharges, and the guard electrode on the samples was used to eliminate surface leakage current, if any. A thicker polypropylene film of 150$\mu$m in thickness with the same electrode configuration was used to test the surface leakage current. The result shows that the surface leakage current is

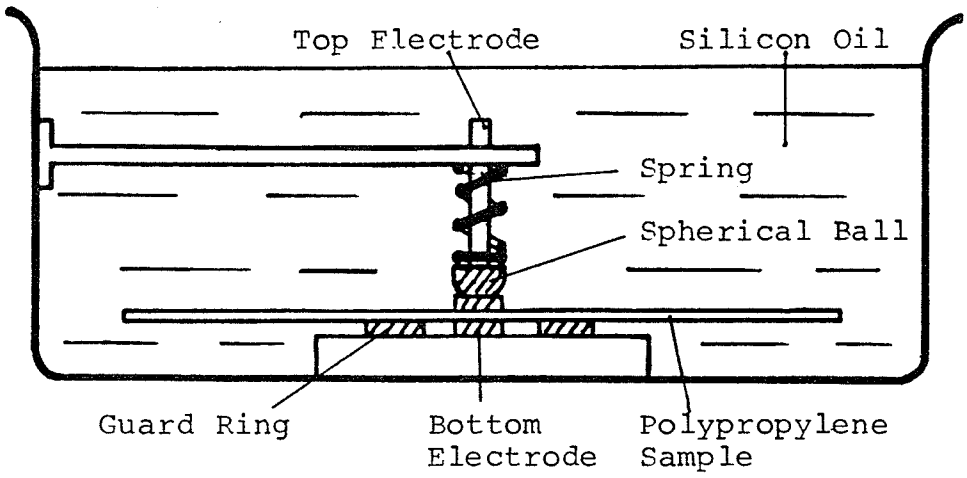


Figure 6.1: *Sample holder for electrical measurements.*

less than $10^{-13}$ A at a dc voltage of 12 kV, which is the highest voltage used in $I$-$V$ measurements for the 15$\mu$m polypropylene samples.

A dc voltage source in conjunction with a ramp rate controller was used to provide a ramp voltage with the rate of 90V/s. (or 0.06MV/cm s) as shown in Fig. 6.2. The conduction current was measured by a logarithmic microammeter in conjunction with a XY recorder. A resistor of 50x$10^6$ $\Omega$ was used to limit the current. The meter response time was less than 1 second to reach the current level of $10^{-6}$A from $10^{-10}$A, which was fast enough for our $I$-$V$ measurements.

We have also studied the effect of a $SiO_2$ film deposited on a plasma-polymerized polyethylene on the properties of polyethylene. In this case, a silicon dioxide layer of 100$\mathring{A}$ was first deposited on a silicon substrate, and

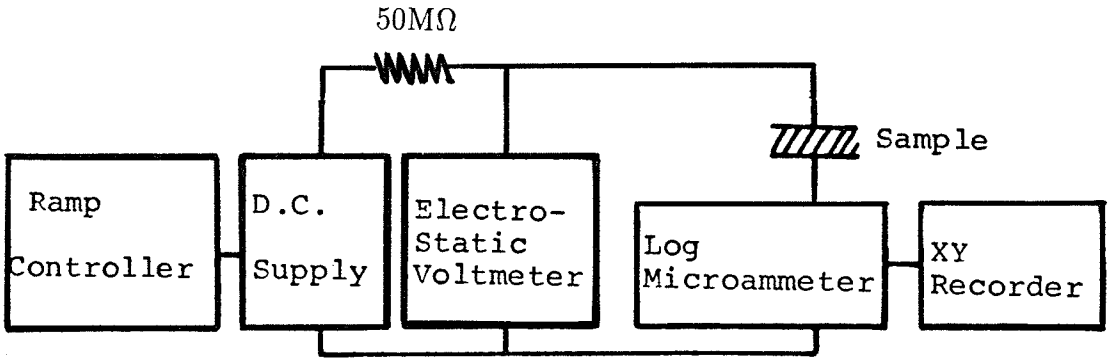


Figure 6.2: *Experimental setup for the measurement of current-voltage (I-V) characteristics.*

followed with a plasma-polymerized polyethylene film of 1000$\AA$ deposited on the top surface of the $SiO_2$ film to form a two-layer structure.

## 6.2 Results and Discussion

Figure 6.3 shows the typical ramp *I-V* characteristics of the polypropylene sample. The threshold field for carrier injection is about 3 MV/cm for the first ramp cycle as indicated in curve (A). After a pause for 1 min, a second ramp cycle was applied, which results in the *I-V* curve (B). In this case the threshold field for carrier injection has shifted to 3.8 MV/cm, indicating that a space charge has built-up near the carrier-injecting contact. Table 6.1 shows that both the threshold field for carrier injection and the breakdown strength of polypropylene depend only on the anode material and are relatively inde-

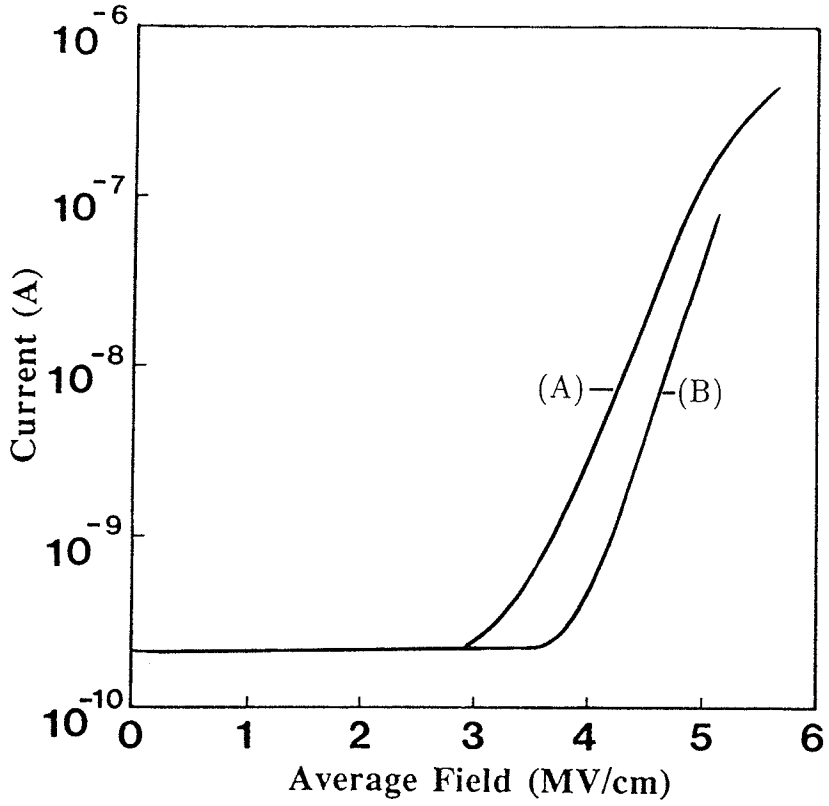


Figure 6.3: *Typical current-average field characteristics of the polypropylene sample. (A) The first ramp cycle; (B) The second ramp cycle; Al electrode at positive polarity; Ramp rate: 0.06MV/cm s; Sample thickness: 15 $\mu$m.*

Table 6.1: The Threshold Field for Carrier Injection and the Breakdown Strength of Polypropylene for Various Combinations of Electrode Materials. (Ramp rate: 0.06 MV/cm-s.)

| Electrode materials | Anode / Cathode | | | | | | | |
|---|---|---|---|---|---|---|---|---|
| | | Au / Cu | Ag / Cu | Cu / Cu | Al / Cu | Cu / Ag | Cu / Au | Cu / Al |
| Threshold field for carrier injection (MV/cm) | | 2.4 | 2.6 | 2.7 | 3.2 | 2.7 | 2.7 | 2.7 |
| Average breakdown strength (MV/cm) | | 5.4 | --- | --- | 6.1 | --- | 5.4 | 5.4 |

pendent of the cathode material, implying that the dominant carriers injected at high fields are holes. Polypropylene is similar to polyethylene in structure, both have a linear and saturated structure. We would therefore expect that the high field conduction and breakdown processes in polypropylene are similar to these in polyethylene described in Chapter 4. There is no evidence of impact ionization at fields close to the breakdown strength. High field conduction is filamentary and governed by the trapped hole space charge. Electrical breakdown is initiated by thermal instability within the high current density regions of the main conduction filaments and then followed by the creation of low-density domains for subsequent impact ionization which lead to final destruction of the material inside the filaments.

The effect of the thin SiPE film deposited on the polypropylene surface to form a hole-emission-shield depends on its thickness as shown in Fig. 6.4. Only when the electrode on the SiPE is positive in polarity, the effect of the emission shield can be observed. The threshold increases with increasing SiPE thickness. The average field is the apparent average field which is equal to the applied voltage divided by the sum of the polypropylene sample thickness and the SiPE film thickness. However, it can be seen that the effect of the emission shield becomes saturated for the film thicknesses larger than $3000\mathring{A}$. The SiPE film has both the permittivity and the hole-trap concentration higher than those for polypropylene. Both of these two parameters tend to reduce the effective field at the hole-injecting contact. It is interesting to note that a plasma-polymerized PE film, whose permittivity is similar to that of polypropylene, also behaves as a hole emission shield as shown in Fig. 6.5. The hole trap concentration in plasma-polymerized polyethylene

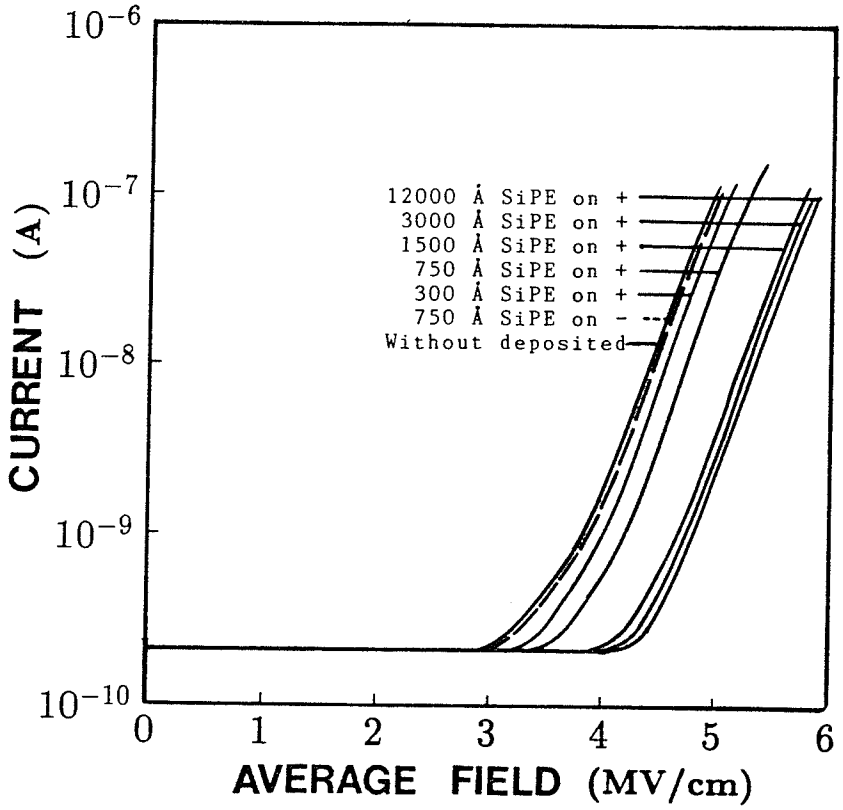


Figure 6.4: *Current-average field characteristics of polypropylene with a plasma-polymerized SiPE layer of various thicknesses as the emission shield. Al anode; Ramp rate: 0.06 MV/cm s.*

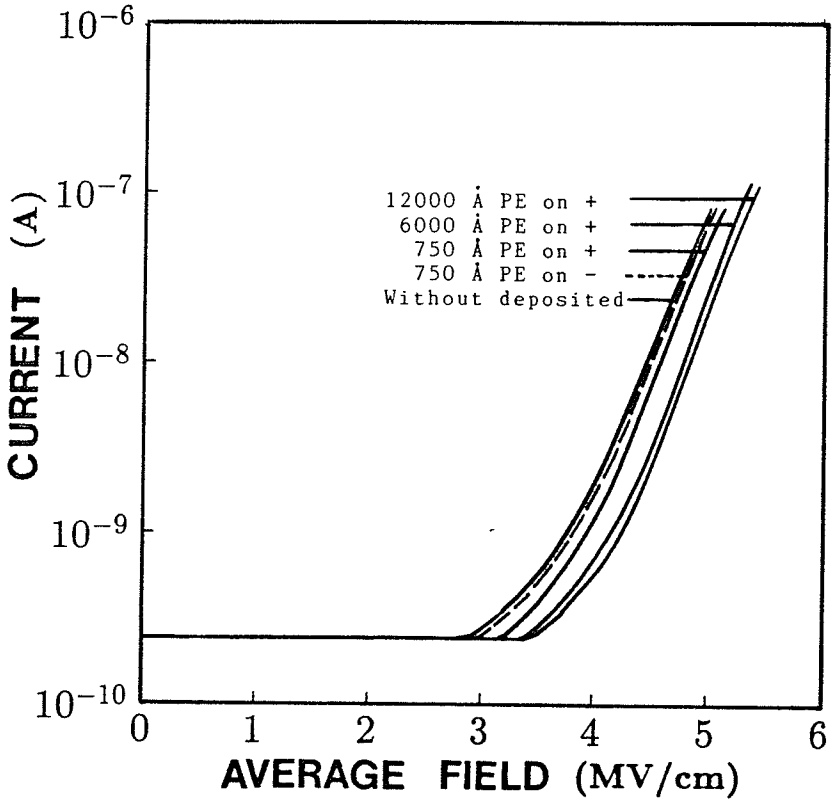


Figure 6.5: *Current-average field characteristics of polypropylene with a plasma-polymerized PE layer of various thicknesses as the emission shield. Al anode; Ramp rate: 0.06 MV/cm s.*

is not expected to be higher than that in polypropylene. We believe that the interface between the PE layer and the polypropylene may have a higher concentration of hole traps. The injected holes trapped there may be sufficient to reduce the effective field at the hole-injecting contact to suppress hole injection. We can conclude that a thin SiPE film inserted between the pure polypropylene and the hole-injecting contact acts as an efficient emission shield suppressing the hole injection and increasing the breakdown strength. A similar emission-shield effect has also been observed by DiMaria et al. [184] who used an electron-trapping layer to suppress electron injection and to improve the breakdown strength of silicon dioxide films.

Figure 6.6 shows that the average field to cause breakdown increases with increasing thickness of the emission-shield layer, and becomes saturated at the thickness of 3000$\mathring{A}$ for the SiPE layer and 6000$\mathring{A}$ for the PE layer. In the case of the SiPE layer, the bulk hole traps may be more important than the interface hole traps. Obviously, the thicker the layer, the larger is the quantity of the trapped hole space charge and hence more effective in suppressing the hole injection. In the case of the PE layer, the interface traps may be more important than the bulk traps. However, the interface traps may act as a barrier blocking the injected holes from penetrating to the polypropylene, making the quantity of the positive space charge including free and trapped holes in the PE layer increases with increasing layer thickness. When the density of space charge reaches a dynamic equilibrium state, further increase in the emission shield layer may not enhance its effect on the effective field at the injecting contact. Under this condition the effect of the emission shield becomes saturated.

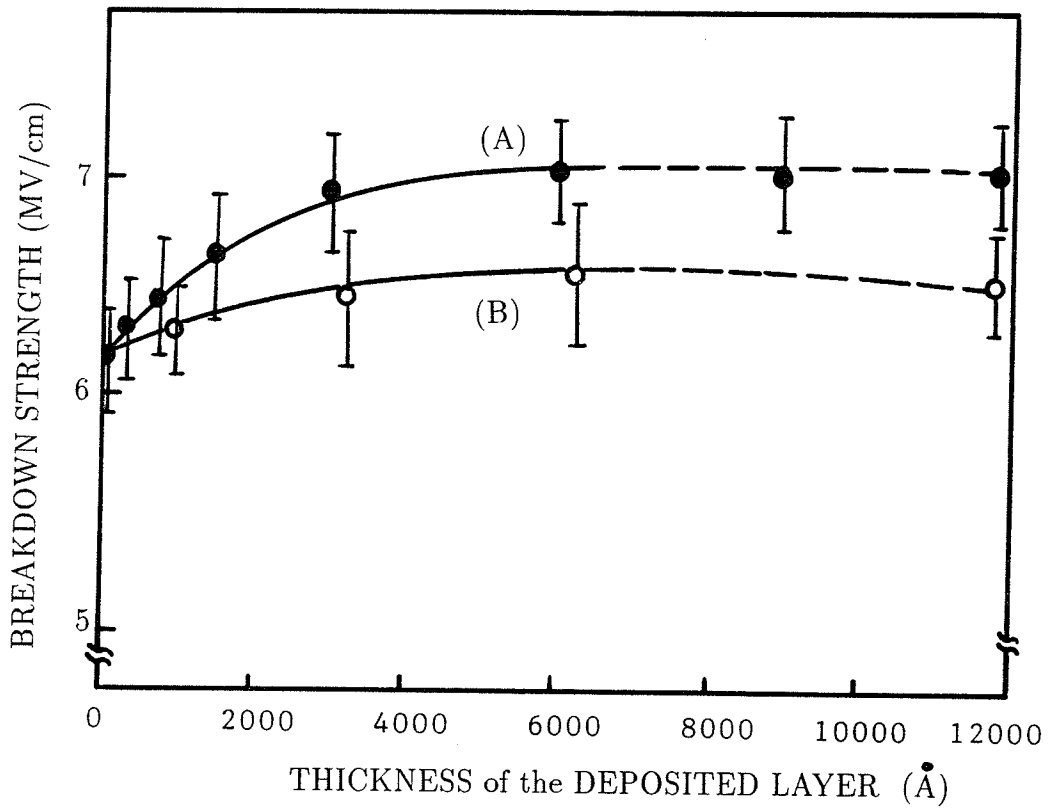


Figure 6.6: *Average field to cause breakdown in polypropylene as a function of the thickness of the emission shield layer. (A) SiPE layer and (B) PE layer.*

We have also studied the $SiO_2$ film used as emission shield for plasma-polymerized polyethylene . Figure 6.7 shows that the $I$-$V$ characteristics shifts to higher fields for polyethylene with a $SiO_2$ emission shield layer. It is well known that at high fields electron conduction is dominant in $SiO_2$, implying that not only the electron mobility is higher than the hole mobility, but also the efficiency for electron injection is much higher than that for hole injection into $SiO_2$. This is why the $SiO_2$ layer used as hole emission shield is much more efficient than that used as an electron emission shield as shown in Fig.6.7. The breakdown process for this structure is expected to be similar to that discussed in Chapter 5.

Figure 6.8 shows the distribution of breakdown measurements. We consider the breakdown occurring at the field at which the current increases rapidly to an enormous value leading to destructive breakdown. The field with the highest probability for the occurrence of breakdown is taken as the normal breakdown strength. The normal breakdown strengths for the pure polypropylene films with and without a plasma-deposited PE layer or a plasma-deposited SiPE layer as emission shield, the plasma-polymerized PE films alone, the plasma-polymerized PE films with a $SiO_2$ layer adjacent to the anode, and the plasma-polymerized PE films with a $SiO_2$ layer adjacent to the cathode, are summarized in Table 6.2. A very thin emission shield layer of about 5% of the thickness of the host material could increase the breakdown strength of the host material up to more than 50%, indicating the significant role played by the emission shield in improving the breakdown strength of the insulating polymers.

In summary, the high field conduction in the polypropylene is due to the

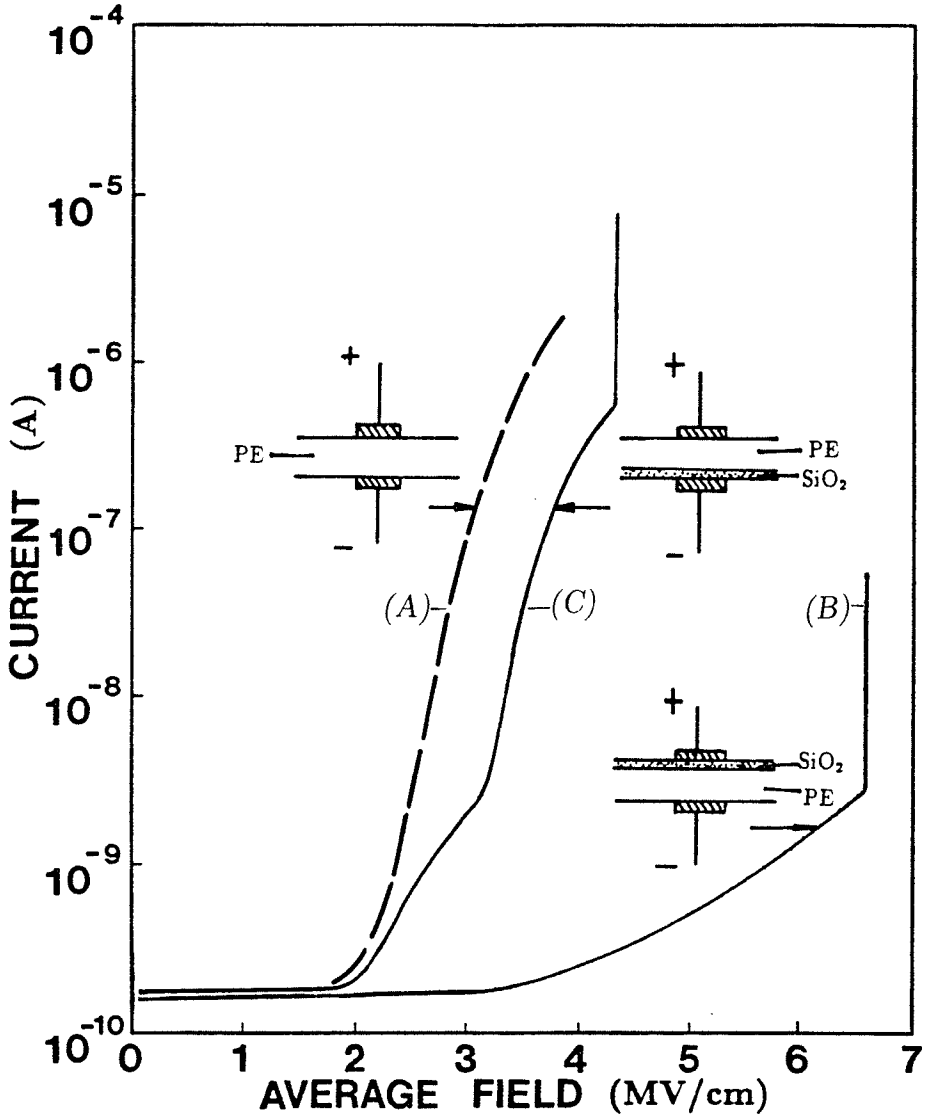


Figure 6.7: *Current-average field characteristics of the plasma-polymerized polyethylene films with a thin $SiO_2$ layer deposited on one surface as the emission shield. (A) Without $SiO_2$ layer; (B) with the $SiO_2$ layer adjacent to the anode and (C) with the $SiO_2$ layer adjacent to the cathode.*

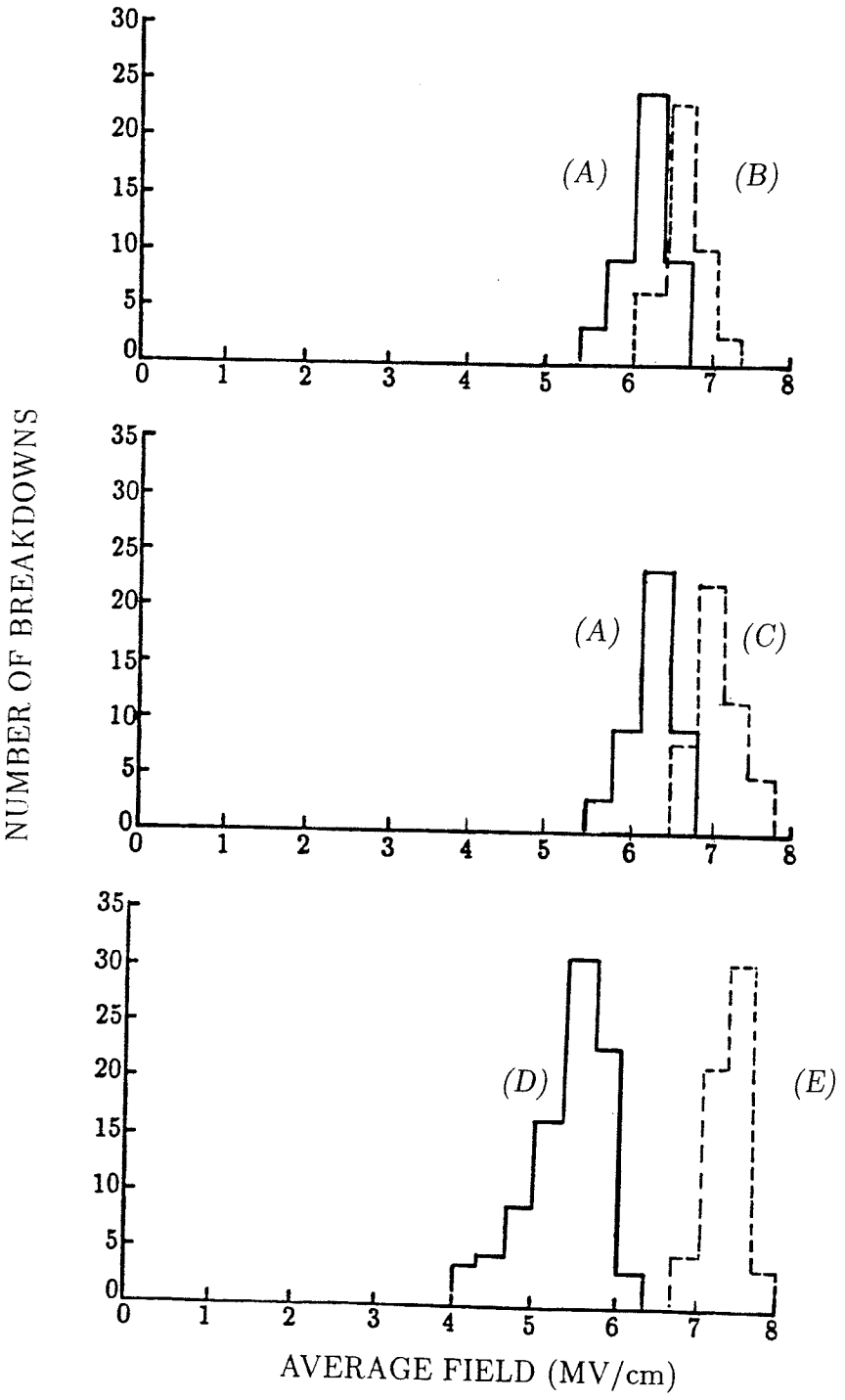


Figure 6.8: *Histograms of the breakdown measurements. (A) Polypropylene films alone. (B) Polypropylene with a 3000Å plasma deposited PE layer as hole emission shield. (C) Polypropylene with a 3000Å plasma deposited SiPE layer as hole emission shield. (D) Plasma-polymerized PE films alone. (E) Plasma-polymerized PE films with a $SiO_2$ layer as hole emission shield.*

Table 6.2: Normal Breakdown Strengths for Various Samples

| Materials and structures | Breakdown strengths MV/cm |
|---|---|
| Pure polypropylene films | 6.1 |
| Polypropylene with PE(+) | 6.5 |
| Polypropylene with SiPE(+) | 7.1 |
| Plasma-polymerized PE | 5.5 |
| Plasma-polymerized PE with $SiO_2$ on (+) | 7.5 |
| Plasma-polymerized PE with $SiO_2$ on (−) | 5.6 |

the hole tunneling injection. A thin SiPE, PE or $SiO_2$ layer deposited on the insulating polymer surface adjacent to the hole-injecting contact suppresses the hole injection.

# Chapter 7

# Conclusions

On the basis of the experimental results described above, the following conclusions are drawn.

(1) The high-field conduction in plasma-polymerized polyethylene with and without Si incorporation as well as chemically polymerized polypropylene is due to holes injected by Fowler-Nordheim type of tunneling from the injecting contact to the material through a potential barrier.

(2) The deviation of the experimental $I$-$V$ characteristics from the trap-free FN relation is due to the trapped hole space charge which creates an internal field opposite to the applied field.

(3) The high hole current density at high fields implies that the valence band is wide and the hole mobility is high in the chains, and that holes migrate from chain to chain by tunneling.

(4) The high-field conduction is filamentary. Electrical breakdown is initiated by thermal instability caused by local high current density, and followed with the provision of large mean free paths for subsequent impact ion-

ization, leading to a rapid increase of the current and final breakdown.

(5) The incorporation of silicon in polyethylene creates deep hole traps. The shift of the $I$-$F_g$characteristics from that of pure polyethylene is due to the trapped hole space charge which creates an internal field. This internal field on the one hand reduces the effective field at the hole-injecting contact thus suppressing the hole injection, but on the other hand, enhances the effective field at the electron-injecting contact and hence the electron injection. Depending on the trapped hole charge density, the one-carrier (holes) dominant conduction may be changed to a two-carrier conduction when the electron injection becomes significant.

(6) A thin SiPE, PE, and $SiO_2$ layer inserted between the polymer and the hole-injecting contact acts as an efficient emission shield suppressing the hole injection and increasing the breakdown strength.

(7) The structure of the plasma-polymerized polyethylene films is similar to that of chemically polymerized polyethylene with long $CH_2$ chains but also with some CH and $CH_3$ elements. The incorporation of silicon into the plasma-polymerized polyethylene introduces SiH, $SiH_2$ and $SiH_3$ elements into the structure. The structures of these films are proposed on the basis of infra-red spectroscopy.

# References


[1] Goodman, J., *"The Formations of Thin Polymer Films in the Gas Discharge"*, J. Polym. Sci. 44, pp.551-552, (1960).

[2] Bradley,A., Hammes,J.P., *"Photoconductivity in thin organic films"*, J. Electrochem. Soc. Vol.110, pp.543-548, (1963).

[3] Stuart,M., *"Dielectric properties of cross-linked polystyrene film formed in the glow discharge"*, Nature, Vol. 199, pp.59-60, (1963).

[4] Stuart,M., *"Dielectric losses in polymer films formd by a discharge"*, Proc. IEE Vol.112, pp.1614-1616, (1965).

[5] Ozawa,P.J., *"Organic thin film capacitor"*, IEEE Trans. Parts. Mater. Package. PMP-5, pp.112-122, (1969).

[6] Bashara,N.M., Doty, C.T., *"Electrical conduction in very thin polybutadiene film formed in a glow discharge"*, J. Appl. Phys. Vol.35, pp.3498-3507, (1964).

[7] Gregor,L.V., *"Electrical conductivity of polydivinylbenzene films"*, Thin Solid Films, Vol.2, pp.235-246, (1968).

[8] Hirai,T., Nakada,O., *"Formation of thin polyactryonitrile films and their electrical properties"*, Jap. J. Appl. Phys. Vol.7, pp.112-121, (1968).

[9] Hozumi,N., Takao,T., Ohki,Y., *"Dielectric loss measurement of plasma polymerized ethylene films in vacuo and effect of hydrogen treatment"*, Jap. J. Appl. Phys. Vol.21, pp.L195-L196, (1982).

[10] Hudis,M., Wydeven,T., *"Plasma polymerization of an ethylene nitrogen gas mixture"*, J. Polym. Sci.: Let.Ed. Vol. 13, pp.549-557, (1975).

[11] Bowden,M.J., Turner,S.R., Ed. *"Electric and photonic Applications of Polymers"*, American chemical Society, Washington, DC (1988).

[12] Ramu,T.S., and Wertheimer,M.R., *"Dielectric properties of plasma polymerized hexamethyldisilioxane films: 2 Dielectric Breakdown"*, IEEE Trans. Elec. Insul. Vol.12, pp.557-562, (1986).

[13] Mearns,A.M., *"Insulator Thin Films Formed by Glow Discharge and Radiation Techniques"*, Thin Solid Films, Vol.3, pp.201-228, (1969).

[14] Gazicki,M., Yasuda,H., *"Electrical Properties of Plasma Polymerized thin organic films"*, Plasma Chemistry and Plasma Processing, Vol. 3, pp.279-327, (1983).

[15] Yasuda,H., *"Glow discharge Polymerization"*, J. Polym. Sci. Macrond. Rev. 16, 199, (1981).

[16] Yasuda, H.,in *Thin Film Processes*, Ed by Vossen,J. L., and Kern,W., (Academic, New York, 1978), Chap. IV.

[17] Kobayashi,H., Bell,A.T., and Shen,M., *"Formation of an amorphous powder during the polymerization of ethylene in radio-frequency discharge"*, J. Appl. Polymer Science Vol. 17, pp.885-892, (1973).

[18] O'Dwyer,J.J., *"The theory of electrical conduction and breakdown in solid dielectrics"*, Clarendon Press, Oxford, (1973).

[19] Klein,N., *"Electrical breakdown mechanisms in thin insulators"*, Thin Solid Films, Vol.50, pp.223-232, (1978).

[20] Ieda,M., *"Dielectric breakdown process of polymers"*, IEEE Trans. Elec. Insul. Vol.15, pp.206-224, (1980).

[21] Gill,W. D., *"Transient photocurrent for field-dependent mobilities"*, J. Appl. Phys. Vol.43, pp.529-539, (1972).

[22] Anderson,D. A., and Spear,W. E., *"Electrical and optical properties of amorphous silicon carbide silicon nitride and germanium carbide prepared by the glow discharge technique"*, Philos. Mag. Vol.35, pp.1-16, (1977).

[23] Hudis,M., in *Techniques and Applications of Plasma Chemistry"*, edited by J. R. Hollahan and A. T. Bell (Wiley, New York, 1974), Chap.3.

[24] Clark,D. T., and Dilks,A., *"ESCA applied to polymers. XV. RF Glow discharge modification of polymers, studied by means of ESCA in terms of a direct and radiative energy-transfer model"*, J. Polym. Sci.: Polym. Chem. Ed. Vol.15, pp. 2321-2345, (1977).

[25] Clark,D. T., and Abrahman,M.Z., *"Plasma polymerization VII. An ESCA investigation of the RF Plasma polymerization of Perfluorobenzene/Hydrogen mixtures"*, J. Polym. Sci. Vol.20, pp.1717-1728, (1982).

[26] Morosoff,N., Newton,W., and Yasuda,H., *"Plasma polymerization of ethylene by magnetron discharge"*, J. Vac. Sci. Technol. Vol.15, pp.1815-1822, (1978).

[27] Ikeda,M., and Ohki,Y., *"Copolymers of ethylene and aromatic monomers their electrical properties and a possibility of developing a new insulating material"*, Proceedings of the 2nd Int. Conf. on Conduction and Breakdown in Solid Dielectrics, pp.71-75, (1986).

[28] Liu,F.Y., Kim,S.H., Liu,D., and Kao,K.C., *"Plasma implantation technique for incorporation of foreign element into polymer films"*, Rev. Sci. Instrum., Vol.57(5), pp.986-988, (1986).

[29] Bahder,G., Eager, G.S.Jr., and Silver,D.A., *"High voltage solid extruded insulated power cables"*, U.S. Patent Specification No. 3.885.085, May, 1975.

[30] Tu,D.M., Liu,W.B., Zhuang,G.P., Liu,Z.Y., Kao,K.C., *"Electric breakdown under quasi-uniform field conditions and effect of emission shields in polyethylene"*, IEEE Trans. Elec. Insul. Vol.24, pp. 581-590, (1989).

[31] Nakano,T., Kihira,T., and Ohki,Y., *"Plasma polymer coating for suppression of charge injection into polyethylene"*, Conf. on Elec. Insul. and Dielec. Phenomena, Annual Report, pp.245-250, (1987).

[32] Mott,N.F., and Davis,E.A., *"Electronic Process in Non-Crystalline Materials"*, Clarendon Press, Oxford, (1979).

[33] Tanaka, T., *"Optical absorption and electrical conduction in polyethylene"*, J. Appl. Phys. Vol.44, pp.2430-2432, (1973).

[34] Partridge, R.H., *"Vacuum-Ultraviolet absorption of polyethylene"*, J. Chem. Phys. Vol.45, pp.1685-1690, (1966).

[35] McCubbin,W.L., and Gurney,I.D.C., *"Conduction in paraffinic polymers"*, J. Chem. Phys. Vol.43, pp.983-986, (1965).

[36] Mizutani,T., Suzuoki,Y., and Ieda,M., *"Thermally stimulated currents in polyethylene and ethylene-vinyl-acetate copolymers"*, J. Appl. Phys. Vol.48, pp.2408-2413, (1977).

[37] Mizutani,T., Suzuoki,Y., Hanai,M., and Ieda,M., *"Determination of trapping parameters from TSC in polyethylene"*, Jap. J. Appl. Phys. Vol.21, pp.1639-1641, (1982).

[38] Lewis, T.J., *"Charge transport in polymers"*, Conf. on Elec. Insul. and Dielec. Phenomena, Annual Report, pp.533-561, (1976).

[39] Wintle, H.J., *"Absorption currents and steady currents in polymer dielectrics"*, J. Non-Cryst. Solids. Vol.15 pp.471-486, (1973).

[40] Wintle, H.J., *"Reversals in electrical current and other anomalies in insulating polymers"*, IEEE Trans. Elec. Insul. Vol.21, pp.747-762, (1986).

[41] Mizutani,T., Kaneko,K., and Ieda,M., *"Anomalous discharging currents duo to space charge"*, Jap. J. Appl. Phys. Vol.20, pp.1443-1448, (1981).

[42] Walden, R.H., *"A method for the determination of high-field conduction laws in insulating films"*, J. Appl. Phys. Vol.43, pp.1178-1187, (1972).

[43] Tahira,K., and Kao,K.C., *"Anomalous photocurrent transient in polyethylene"*, J. Phys. D: Appl. Phys., Vol.18, pp.2249-2259, (1985).

[44] Legyel, G., *"Schottky emission and conduction in some organic insulating materials"*, J. Appl. Phys. Vol.37, pp.807-813, (1966).

[45] Taylor, D.M., and Lewis, T.J., *"Electrical conduction in polyethylene terephthalate and polyethylene films"*, J. Phys. D: Appl. Phys., Vol.4, pp.1346-1358, (1971).

[46] Cole, K.S., and Cole, R.H., *"Dispersion and absorption in dielectrics II: direct current characteristics"*, J. Chem. Phys. Vol.10, pp.98-105, (1942).

[47] Davies,D.K., *"Carrier transport in polyethylene"*, J. Phy. D: Appl. Phys., Vol. 5, pp.162-168, (1972).

[48] Davies,D.K. and Look,P.J., *"Charge trapping in polymers"*, J. Electrochem. Soc. Sol. State Sci. Tech., Vol. 120 pp. 216-270, (1973).

[49] Davies,D.K., *"Field stimulates interfacial electron transfer"*, IEE Proc. Vol. 128, Pt. A, pp. 153-158, (1981).

[50] Fabish, T.J., Saltsburg, H.M., and Hair,M.L., *"Charge Transfer in Metal/Atactic Polystryene contacts"*, J. Appl. Phys. Vol.47, pp.930-939, (1976).

[51] Davies, D.K., *"Charge Generation on dielectric surfaces"*, Brit. J. Appl. Phys. (J. Phys. D.) Vol.2, pp. 1533-1537, (1969).

[52] Murata, Y., *"Photoelectric emission and contact charging of some synthetic high polymers"*, Jap. J. Appl. Phys. Vol.18, pp.1-8, (1979).

[53] Duke, C.B. and Fabish, T.J., *"Contact electrification of Polymers: A Quantitative Model"*, J. Appl. Phys. Vol.49, pp. 315-321, (1978).

[54] Lewis, T.J., *"The role of electrodes in conduction and breakdown phenomena in solid dielectrics"*, IEEE Trans. Elec. Insul. Vol.19, pp.210-216, (1984).

[55] Toomer, R., and Lewis, T.J., *"Charge effects at aluminium electrodes on insulating films"*, Inst. Phys. Conf. Ser. No.48, pp.225-232, (1979).

[56] Tanaka,T., and Greenwood,A., *"Effect of charge injection and extraction on tree initiation in polyethylene"*, IEEE Trans on PAS, Vol. PAS-97, pp.1749-1757, (1978).

[57] Khalil,M.S., and Zaky,A.A., *"The effect of cable structure on space charge"*, IEEE Trans. Elec. Insul. Vol.23, pp.1043-1046. (1988).

[58] Barnes, C., Lederer, P.G., Lewis, T.J., and Toomer, R., *"Electron and ion transfer processes at insulator surfaces"*, J. Electrostatics, Vol. 10, pp.107-114, (1981).

[59] Ferris-prabhu, A.V., *"Charge transfer in layered insulators"*, Solid State Electron., Vol.16, pp.1086-1087, (1973).

[60] St-Onge,H., *"Electrical conduction in 3-percent carbon -filled polyethylene, part II: high field results"*, IEEE Trans. Elec. Insul. Vol.15, pp.350-358, (1980).

[61] Yahagi,K., *" Dielectric properties and morphology in polyethylene"*, IEEE Trans. Elect. Insul. Vol.EI-15, pp.241-250 (1980).

[62] Kosaki,M., Yoda,M., and Ieda,M., *"First order transition and electrical conduction of polyethylene"*, J. Phys. Soc. Japan, Vol.31, pp.1598-1598, (1971).

[63] Binks.A.E., and Sharples, A., *"Electrical conduction in Olefin Oxide Polymers"*, J. Polymer Science Pat.A-2, Vol. 6, pp.407-420, (1968).

[64] Lawson,W.G., *"High field conduction and breakdown in polythene"*, Brit. J. Appl. Phys. Vol. 16, pp.1805-1812, (1968).

[65] Das Gupta, D.K., and Barbarez, M.K., *"On electronic conduction in polyethylene films"*, J. Phys. D: Appl. Phys., Vol.6, pp.867-871, (1973).

[66] Ieda,M., Sawa,G., and Kato,S., *"A consideration of Poole-Frenkel effect on electric conduction in insulators"*, J. Appl. Phys. Vol.42, pp.3737-3740, (1968).

[67] Hill, R.M., *"Poole-Frenkel conduction in amorphous solids"*, Phil. Mag. Vol. 23, pp. 59-86, (1971).

[68] Adamec, V., and Calderwood, J.H., *"Electric conduction in dielectrics in high fields"*, J. Phys. D: Appl. Phys., Vol.8, pp.551-560, (1975).

[69] Adamec, V., and Calderwood, J.H., *"Electric Field enhanced conductivity in dielectrics"*, J. Phys. D: Appl. Phys., Vol.10, pp. L79-81, (1977).

[70] Paracchini, C., Dallacasa, V., and Romano, L., *"The role of the internal field on the electronic transport in insulators"*, IEEE Trans. Elec. Insul. Vol.26 pp.222-227, (1991).

[71] Nath, R., Kaura, T., and Perlman, M.M., *"Steady-state conduction in linear low-density polyethylene with Poole-lowered trap depth"*, IEEE Trans. Elec. Insul. Vol.25, pp.419-425, (1990).

[72] Kao, K.C., *"Double injection in solids with non-ohmic contacts: I. Solids without defects "*, J. Phys. D: Appl. Phys., Vol.17, pp. 1433-1448, (1984).

[73] Kao, K.C., *"Double injection in solids with non-ohmic contacts: II. Solids with defects "*, J. Phys. D: Appl. Phys., Vol.17, pp.1449-1467, (1984).

[74] Kao,K.C., and Hwang,W., *"Electrical Transport in solids"*, Pergamon Press, (1981).

[75] Ishii, K., Ohki, Y., and Nakao, T., *"Dielectric breakdown due to hole avalanche"*, Conf. Record 1990 IEEE Int. Sympo. on Elec. Insu. Toronto, Canada, pp. 76-79, (1990).

[76] Mizutani,T., Mori,T., Takai,T., and Ieda,M., *"High field conduction in poly-p-xylylene thin film"*, Conf. Record 1988 IEEE Int. Sympo. on Elec. Insu. Cambridge, Massachusetts, USA, pp.154-157, (1988).

[77] Takai,Y., Hayase,Y., Mizutani,T., and Ieda,M., *"Avalanche in poly-p-xylylene thin polymer films"*, J. Phys. D: Appl. Phys., Vol.19, pp.115-125, (1986).

[78] Pfluger,P., Cartier, E., and Dersch, H., *"Electron Transport in thin insulating films: Physics and effects on dielectric aging"*, Conf. Record 1988 IEEE Int. Sympo. on Elec. Insu. Cambridge, Massachusetts, USA, pp.135-140, (1988).

[79] Van Roggen, A., *"Electronic conduction of polymer single crystals"*, Physical Review Letters, Vol. 9, pp.368-370, (1962).

[80] Senecal, G., and Ham, J.S., *"Electronic conduction through single crystals of polyethylene"*, J. Appl. Phys. Vol.42, pp.2714-2718, (1971).

[81] Miyoshi, Y., and Chino,K., *"Electrical properties of polyethylene single crystals"*, Jap. J. Appl. Phys. Vol.6, pp.181-190, (1967).

[82] Watson,D.B., Heyes,D., Kao,K.C., and Calderwood,J.H., *" Some aspects of dielectric breakdown of solids"*, IEEE Trans. Elec. Insul. Vol.1, pp. 30-37, (1965).

[83] Mizutani,T., Kanno,I., Hikita,M., Ieda,M., *"Pre-breakdown current due to filamentary thermal breakdown in polyimide films"*, IEEE Trans. Elec. Insul. Vol.22, pp.473-477, (1987).

[84] Inuishi,Y., and Powers,D.A., *"Conduction and breakdown through Mylar Films"*, J. IEE of Japan, Vol. 77, pp.1072-1078, (1957).

[85] Nagao,M., Kimura,T., Mizuno,Y., Kosaki,M., and Ieda,M., *"Detection of Joule heating before dielectric breakdown in polyethylene films"*, IEEE Trans. Elec. Insul. Vol.25, pp.715-722, (1990).

[86] Xie,H.K., Kao, K.C., *"A study of the low density developed in liquefied polyethylene under high electric fields"*, IEEE Trans. Elec. Insul. Vol.20, pp. 293-297, (1985).

[87] Sueda,H., and Kao,K.C., *" Prebreakdown phenomena in high-viscosity dielectric liquids"*, IEEE Trans. Elec. Insul. Vol.17, pp. 221-227, (1982).

[88] Murooka,Y., *"Observation on the intermittent electron emission in liquid nitrogen"*, J. Appl. Phys. Vol.48, pp.136-142, (1977).

[89] Kao,K.C., Xie,H.K., and Tu,D.M., *" Electrical treeing in polyethylene under hydrostatic pressures"*, J. Electrostatics, Vol. 16, pp. 115-121, (1984).

[90] Smith,C.W., Kao,K.C., Calderwood,J.H., and McGee,J.D., *"Light emission in n-hexane under high electric stress"*, Nature, Vol. 210, pp.192-193. (1966).

[91] Cooper,R., and Elliot,C.T., *"Formative processes in the electric breakdown of potassium bromide"*, Brit. J. Appl. Phys., Vol.17 pp.481-488, (1966).

[92] Bamji,S.S., Bulinski,A.T., Densley,R.J., Matsuki,M., *"Degradation mechanism at LXPE/Semicon interface subjected to high electrical stress"*, IEEE Trans. Elec. Insul. Vol.26, pp.278-284, (1991).

[93] Kosaki,M., Shimizu,N., and Horii,K., *" Treeing of polyethylene at 77K"*, IEEE Trans. Elec. Insul. Vol.12, pp.40-45, (1977).

[94] Shimizu,N., Kosaki,M., and Horii,K., *" Space charge effect on local electric breakdown of polyethylene at 77 K"*, J. Appl. Phys. Vol.48, pp.2191-2195, (1977).

[95] Shimizu,N., Katsukawa,H., Miyachi,M., Kosaki,M., and Horii,K., " *The space charge behavior and luminescence phenomena in polymers at 77K*", IEEE Trans. Elec. Insul. Vol.14, pp.256-263, (1979).

[96] Bamji,S., Bulinski,A., Densley,J., and Shimizu,N., *"Light emission from polyethylene subjected to high divergent fields"*, Conf. on Elec. Insul. and Dielec. Phenomena, Annual Report, pp.592-597, (1982).

[97] Laurent,C., Mayoux,C., and Noel,S., *"Dielectric breakdown in polyethylene in divergent fields: Role of dissolved gases in electroluminescence"*, J. Appl. Phys. Vol.54, pp.1532-1539, (1983).

[98] Kao,K.C., and Rashwan, M.M., *"Pressure dependence of electroluminescence in dielectric liquids"*, Proc. IEEE June 1974, pp.856-857, (1974).

[99] Vahlstrom,W., Paper presented at IEEE Conference on under ground distribution, Detroit, Mich, Sept. (1971).

[100] Olyphant,M., *"Corona and treeing breakdown of insulation "*, The lake publishing Company Vol. 9, No. 2,3, and 4, (1963).

[101] McMahon,E.T., and Perkins,J.R., *"Surface and volume phenomena in dielectric breakdown of polyethylene"*, IEEE Trans. PAS. Vol.82, pp. 1106-1112, (1963).

[102] Lawson,J.H., and Vahlstrom,W., " *Investigation of insulation in 15 kV and 22 kV polyethylene cable removed from service–part II"*, IEEE Trans. PAS. 92, pp.824-835, (1973).

[103] Kitchin,D.W., Pratt,O.S., *"Treeing in polyethylene as a prelude to breakdown"*, AIEE Transaction, pt. III, (PAS) Vol.77, pp.180-186, (1958).

[104] McMahon,E.T. and Perkins,J.R., *"Evaluation of high-voltage insulating compounds; dendrite(tree) formation under highly divergent fields"*, IEEE Trans. PAS. Vol.83, pp.1253-1261, (1964).

[105] Mason,J.H., *"Breakdown of Solid dielectrics in divergent fields"*, Proc. IEE Vol. 102, Pt. C, pp.254-264, (1955).

[106] Eichhorn,R.M., *"Treeing in solid extruded electrical insulation"*, IEEE Trans. Elec. Insul. Vol.12, pp.2-18, (1976).

[107] Kitchin,D.W., and Pratt,O.S., *"An accelerated screening test for polyethylene high voltage insulation"*, AIEE Trnas. Paper 62-54. (1962).

[108] Shaw,M.T., and Shaw,S.H., *"Water treeing in solid dielectrics"*, IEEE Trans. Elec. Insul. Vol.19, pp.419-452, (1984).

[109] Gluchowski,S., and Juchniewicz,J., *" A new approach to treeing inception tests"*, IEEE Trans. Elec. Insul. Vol.22, pp.81-86, (1987).

[110] Shimizu,N., Mori,J., Kosaki,M., Horii,K., *" The effect of absorbed oxygen on treeing in polymers"*, 1982 IEEE Intern. Symp. on Elect. Insul. Philadelphia, (1982).

[111] Noto,F., *"Tree initiation in polyethylene by application of DC and Impulse voltage"*, IEEE Trans. Elec. Insul. Vol.12, pp.26-30, (1977).

[112] Saito,Y., Fukuzawa, Nakamura,H., *"On the mechanism of the tree initiation"*, IEEE Trans. Elec. Insul. Vol.12, pp.31-34, (1977).

[113] Ieda,M., and Nawata,M., *"DC treeing breakdown associated with space charge formation in polyethylene"*, IEEE Trans. Elec. Insul. Vol.12, pp.19-25, (1977).

[114] Liu,D., Tu,D.M., and Kao,K.C., *" The influence of an oxide layer at the metal polymer interface on electrical treeing properties of polyethylene"*, Proc. of Intern. Conf. on Properties and Appl. of Dielec. Mat. held in Xi'an, China, pp.84-87, (1985).

[115] McLeod,R.D., Liu, D., Pries,W., Kao,K.C., and Card,H.C., *"Polarity dependence of fractal geometry in partial discharge in dielectrics"*, Solid State Comm. Vol.56, No.2, pp.197-199, (1985).

[116] Bamji,S.S., Bulinski,A.T., and Densley,R.J., *"Degradation of polymeric insulation due to photoemission caused by high electric fields"*, IEEE Trans. Elec. Insul. Vol.24, pp.91-98, (1989).

[117] Ranby,B., and Rabek,J.F., *Photodegradation, photooxidation and photostabilization,* Wiley Pub. N.Y., (1975).

[118] Kao,K.C., Tu, D.M., Wu,L.H., Wu,X.Z., and Cheng,C.K., *"On the mechanism of tree initiation in polymer"*, IEEE conf. Rec. of 1982 IEEE Int. Sympo. on Elect. Insul. pp.300-304, (1982).

[119] Kao,K.C., *"New theory of electrical discharge and breakdown in low-mobility condensed insulators"*, J. Appl. Phys. Vol.55, pp.752-755, (1984).

[120] Shibuya,Y., Zoledziowski,S., and Calderwood,J.H., *"Void formation and electrical breakdown in epoxy resin"*, IEEE Trans. PAS. Vol.96, pp.198-207, (1977).

[121] Densley,R.J., *"An investigation into the growth of electrical trees in XLPE cable insulation"*, IEEE Trans. Elec. Insul. Vol.14, pp.148-158, (1979).

[122] Fujita,H., Nakanishi,T., and Yamaguchi,K., *"Acoustic emission distribution and types of electric trees"*, IEEE Trans. Elec. Insul. Vol.18, pp.520-527, (1983).

[123] Laurent,C. and Mayoux,C., *"Analysis of the propagation of electrical treeing using optical and electrical method"*, IEEE Trans. Elec. Insul. Vol.15, pp.33-42, (1980).

[124] Laurent,C., Mayoux,C., Noel,S., Sinisuka,N.I., *" A study of emission lines from electrical tree"*, IEEE Trans. Elec. Insul. Vol.18, pp.125-130.

[125] Wolter,K.D., Tanaka,J., Johnson,J.F., *"A study of the the gaseous degradation products of corona exposed polyethylene"*, IEEE Trans. Elec. Insul. Vol.17, pp.248-252, (1982).

[126] Laurent,C., Mayoux,C., *"Light detection during the initiation of electrical treeing at room temperature"*, J. Phys. D. Appl. Phys. 14 (1981).

[127] Tu,D.M., Wu,L.H., Wu,X.Z., Cheng,C.K., and Kao,K.C., *"On the mechanism of treeing inhibition by additives in polyethylene"*, IEEE Trans. Elec. Insul. Vol.17, pp.539-544, (1982).

[128] Patsch,R., *"On tree-inhibition in polyethylene"*, IEEE Trans. Elec. Insul. Vol.14, pp.200-203, (1979).

[129] McMahon,E.J., *"A tree growth inhibiting insulation"*, IEEE Trans. Elec. Insul. Vol.16, pp.304-318, (1981).

[130] Oakes,W.G., *"The electric strength of some synthetic polymers"*, Proc. IEE, Vol.96, pp.37-43, (1949).

[131] Pelissou,S., St-Onge,H., and Wertheimer,M.R., *"Dielectric breakdown on polyethylene at elevated temperatures"*, IEEE Trans. Elec. Insul. Vol.19, pp.241-244, (1984).

[132] Amakawa,K., Moriuchi,T., Yoshida,T., and Inuishi,Y., *"Electric conduction and dielectric breakdown of polyethylene films"*, J. IEE. of Japan, Vol.84, pp.129-135, (1964).

[133] Miyauchi,H., and Yahagi,K., *"Electronic breakdown in polyethylene film in room temperature region"*, Trans. IEE of Japan, Vol.97-A, pp.617-622, (1972).

[134] Kolesov,S.N., *"The influence of morphology on the electric strength of polymer insulation"*, IEEE Trans. Elec. Insul. Vol.15, pp.382-388, (1980).

[135] Kitagawa,K., Sawa,G., and Ieda,M., *"Self-healing breakdown at spherulite boundaries of polyethylene thin films"*, Japan. J. Appl. Phys. Vol.20, pp.87-94, (1981).

[136] Park,C.H., Hara,M., and Akazaki,M., *"Effects of mechanical stresses on the dielectric breakdown strength of PET and FRP"*, IEEE Trans. Elec. Insul. Vol.17, pp.234-240, (1982).

[137] Park,C.H., Okajima,K., Hara,M., and Akazaki,M., *"Effect of heat treatment on dielectric strength of polyethylene terephthalate under compressed stress"*, IEEE Trans. Elec. Insul. Vol.18, pp.380-398, (1983).

[138] Hara,M., Park,C.H., and Akazaki,M., *"Effect of heat treatment and mechanical stresses on the dielectric strength of uniaxially drawn PET film"*, IEEE Trans. Elec. Insul. Vol.19, pp.273-280, (1984).

[139] Fendley, J.J., and Parkman,N., *"Effect of impregnation, compression and temperature on electric strength of polyethylene and polypropylene"*, IEE Proc., Vol. 129, Pt.A, pp.113-118, (1982).

[140] Bradwell,A., Cooper,R., and Varlow,B., *"Conduction in polyethylene with strong electric fields and the effect of prestressing on the electric strength"*, Proc. IEE, Vol.118, pp.247-254, (1971).

[141] Mizutani,T., Susuoki,Y., Hikita,M., Yoo,K.M., and Ieda,M., *" High field conduction and carrier traps in polyethylene copolymerized with various*

*monomers"*, Annual Report, 1986 IEEE Conference on Electrical Insulation and Dielectric Phenomena, pp.37-42, (1986).
Ieda,M., *"In pursuit of better electrical insulating solid polymers–Present status and future trends"*, Annual Report, 1986 IEEE Conference on Electrical Insulation and Dielectric Phenomena, pp.13-30, (1986).

[142] Liu,D., Liu,F.Y., Kim,S.H., Xu,C.X., and Kao,K.C., *"Trapping states created by inorganic impurities incorporated in organic dielectric polymer"*, 2nd international conference on conduction and breakdown in Solid Dielectrics" Erlangen, Germany July 7 - 19, 1986, pp 507 - 511, (1986).

[143] Bahder,G., Katz,C., Eager,G.S.,Jr., and D.A. Silver, *" Development of technology for the manufacture of crosslinked polyethylene insulated cables rated 138 through 345 kV"*, IEEE Trans. PAS. Vol.96, pp.1741-1747, (1977).

[144] Ball,E.H., Holdup,H.W., Skipper,D.J., and Vecellio,B., *"Development of Crosslinked polyethylene insulation for high voltage cables"*, CIGRE paper 21-01, (1984).

[145] O'Dwyer,J.J., *"Theory of high field conduction in dielectric"*, J. Appl. Phys. Vol.40, pp.3887-3890, (1969).

[146] DiStefano,T.H., and Shatkzes,M., *"Dielectric instability and breakdown in wide bandgap insulators"*, J. Vac. Sci. Tech. Vol.12, pp.37-45, (1975).

[147] Klein,N., *"Electrical breakdown of insulators by one-carrier impact ionization"*, J. Appl. Phys. Vol.53, pp.5829-5839, (1982).

[148] Stark,K.H. and Garton,C.G., *"Electric strength of irradiated polythene"*, Nature, Lond. Vol. 176, pp.1225-1226, (1955).

[149] McKeown,J.J., *"Intrinsic electric strengths of organic polymeric dielectrics"*, Proc. IEE Vol.112, p.824, (1965).

[150] Lawson, W.G., *"Effects of temperature and techniques of measurement on the electric strength of polythene"*, Proc. IEE Vol.113, pp.197- (1966).

[151] Budenstein,P.P., *"On the mechanism of dielectric breakdown of solids"*, IEEE Trans. Elec. Insul. Vol.15, pp.225-240, (1980).

[152] Knaur,J., and Budenstein,P.P., *"Impulse breakdown in PMMA under Megavolt, Nanosecond excitation"*, IEEE Trans. Elec. Insul. Vol.15, pp.313-321, (1980).

[153] Zeller,H.R., Pfluger,P., and Bernasconi,J., *" High mobility states and dielectric breakdown in polymeric dielectric"*, IEEE Trans. Elec. Insul. Vol.19, pp.200-204, (1984).

[154] Kim,S.H., Xie,H.K., and Kao,K.C., *"Dielectric and optical properties of Nitrogen-Incorporated polyethylene films fabricated by plasma polymerization"*, J. Appl. Polymer Science, Vol.32, pp.5543-5556 (1986).

[155] Kern,W., and Puotiue,D.A., *"Cleaning Solution Based on Hydrogen Peroxide for use in Silicon Semiconductor Technology"*, RCA review, Vol.31, pp.187-206, (1970).

[156] Kern, W., *"The evolution of silicon wafer cleaning technology"*, J. Electrochem. Soc., Vol.137, pp.1887-1892, (1990).

[157] Simons,W.N., *"The Sadtle Handbook of Infrared Spectra"*, Published by Sadtler Research Lab. Inc. (1978).

[158] Kendall,D., Ed. *"Applied Infrared Spectroscope"*, New York. Reinbold, Publishing Corporation Chapman and Hall, Ltd. London.

[159] Dischler,B., Bubenzer,A., and Koidl,P., *"Bonding in hydrogenated hard carbon studied by optical spectroscopy"*, Solid State Communications, Vol.48, No.2 pp 105 - 108, (1983).

[160] Tawada,Y., Tsuge,K., Kondo,M., Okamoto,H., and Itamakawa,Y., *Properties and structure of a-SiC:H for high efficiency a-Si solar cell"*, J. Appl. Phys. Vol.Vol.53, pp.5273-5281, (1982).

[161] Launer,P.J., *"Infrared Analysis Of Organic Silicon Compounds: Spectra - Structure Correlations"*, Book Silicon Compounds Register and Review.

[162] *Weast,R.C., Handbook of Chemistry and Physics,* 75th Ed., edited by R.C. Weast, M.J. Astle, and W.H. Beyer, (CRC Press Inc. Boca Raton, 1988), p. F-174.

[163] Nakazaw,K., Ueda,S., Kumeda,M., Morimoto,A., and Shimizu,T., *"NMR and IR Studies on Hydrogenated Amorphous $Si_{1-x}C_x$ Films"*, Jap. J. Appl. Phys. Vol.21, pp. L176-L178. (1982).

[164] Fang,C.J., Cruntz,K.J., Ley,L., and Cardona,M., Demond,F.J., Muller,G., and Kalbitzer, *"The hydrogen content of a-Ge:H and a-Si:H as determined by IR spectroscopy, gas evolution and nuclear reaction techniques"*, J Non-Cryst. Solids. Vol.36, pp.255-260, (1980).

[165] Katayama, Y. and Shimada, T. *"Infra-red spectra of amorphous silicon-fluorine alloys prepared by sputtering in fluorosilane-argon gas mixture"*, Jap. J. Appl. Phys. Vol.19, No.5, pp.L265-L268, (1980).

[166] Brodsky, M.H., Cardona, M. and Cuomo, J.J. *Infra-red and Raman spectra of the silicon -hydrogen bonds in amorphous silicon prepared by glow discharge and sputtering"*, Phys. Rev. B-16, pp.3556-3571, (1977).

[167] LeBlano,O.H., *"Hole and electron drift mobilities in anthracene"*, J. Chem. Phys. Vol.33, pp.626-626, (1960).

[168] McCubbin,W.L., and Manne,R., *"Simple LCAO band calculation for the ideal polyethylene chain"*, Chem. Phys. Lett. Vol. 2, pp.230-232, (1968).

[169] Andre,J.M., Delhale,J., Delhale,S.D, Candano,R., Pireaux,J.J., and Verbist,J.J., *"Comments on comparison of photoelectron spectrum and crystal orbital calculations of polyethylene"*, Chem. Phys. Lett. Vol. 23, pp.206-210, (1973).

[170] Delhale,J., Andre,J.M., Delhale,S.D., Pireaux,J.J., Candano,R., and Verbist,J.J., *"Electronic structure of polyethylene: Theory and ESCA measurements"*, J. Chem. Phys. **60**, 595 (1974).

[171] Barnett,A.M., and Milnes,A.G., *"Filamentary injection in semi-insulating silicon"*, J. Appl. Phys. Vol.37, pp.4215-4223, (1966).

[172] Kao,K.C., *"Theory of high field electric conduction and breakdown in dielectric liquids"*, IEEE Trans. Elec. Insul. Vol.11, pp.121-128, (1976).

[173] Nicollian,E.H., and Brews,J.R., *" MOS Physics and Technology"*, New York, Wiley (1982).

[174] Powell,R.J., and Bergund,C.N., *"Photoinjection studies of charge distribution in oxides of MOS structure"*, Jap. J. Appl. Phys. Vol.42, pp.4390-4397, (1971).

[175] DiMaria,D.J., Weinberg,I.A., and Aitken,J.M., *"Location of positive charges in $SiO_2$ films on Si generated by vuv photons, x-rays, and high field stressing"*, J. Appl. Phys. Vol.48, pp.898-906, (1977).

[176] Ning,T.H. and Yu,H.N., *"Optical inducted injection of hot electrons into $SiO_2$"*, J. Appl. Phys. Vol.45, pp.5373-5378, (1974).

[177] DiMaria,D.J., *"Determination of insulator bulk trapped charge densities and centroids from photocurrent-voltage characteristics of MOS structures"*, J. Appl. Phys. Vol.47, pp.4073-4077, (1976).

[178] DiMaria,D.J., Ghez,R., and Dong,D.W., *"Charge trapping studies in $SiO_2$ using high current injection from Si-rich $SiO_2$ films"*, J. Appl. Phys. Vol.51, pp.4830-4841, (1980).

[179] DiMaria,D.J., *"Correlation of trap creation with electron heating in silicon dioxide"*, Appl. Phys. Lett. Vol.51, pp.655-657, (1987).

[180] Deal,B.E., and Snow,E.H., and Mead,C.A., *"Barrier energies in metal-silicon dioxide-silicon structure"*, J. Phys. Chem. Solids, Vol. 27, pp.1873-1879, (1966).

[181] Lenzlinger,M., and Snow,E.H., *"Fowler-Nordheim tunneling into thermally grown $SiO_2$"*, J. Appl. Phys. Vol.40, pp.278-283, (1969).

[182] Williams,R., *"Photoemission of electrons from silicon into silicon dioxide"*, Phys. Rev. Vol.140, pp.A569-A575, (1965).

[183] Chau,T.T., Mejia,S.R., and Kao,K.C., *"Thickness dependence of the dielectric behavior of $SiO_2$ films fabricated by microwave electron cyclotron resonance plasmas"*, J. Vac. Sci. Technol. Vol. B-9, pp.50-57, (1991).

[184] DiMaria,D.J., Young,D.R., and Ormond,D.W., *"Use of electron-trapping region to reduce leakage currents and improve breakdown characteristics of MOS structures"*, Applied Physics Letters, Vol.31, pp.680-682, (1977).

[185] Liu,D., and Kao,K.C., *"Study of the structure of plasma polymerized ethylene films with and without silicon incorporation by infrared spectroscopy"*, Polymer Communications Vol.32(2), pp.329-331, (1991).

[186] Liu,D., and Kao,K.C., *"High-field hole injection, conduction and breakdown in polyethylene films fabricated by plasma polymerization"*, J. Appl. Phys. Vol.69(4), pp.2489-2496, (1991).

[187] Liu,D., Kan,L., and Kao,K.C., *"High field electric conduction and breakdown in silicon incorporated polyethylene films"*, J. Appl. Phys. Vol.70(2), pp.919-924, (1991).

[188] Liu,D., Kan,L., and Kao,K.C., *"Electrical properties of plasma polymerized silicon incorporated polyethylene films under very high electric fields"*, Presented at the 3rd Int. Conf. on Properties and Applications of Dielectric Materials, held in Tokyo, July 8-12, (1991).